AD-A173 900 FRACTURE BEHAVIOR UNDER IMPACT PART 1(U) 1/1
FRAUNHOFER-INST FUER WERKSTOFFMECHANIK FREIBURG
(GERMANY F R) J F KALTHOFF ET AL. AUG 86 W-10/86-PT-1
UNCLASSIFIED DAJA37-81-C-0013 F/G 20/11 NL

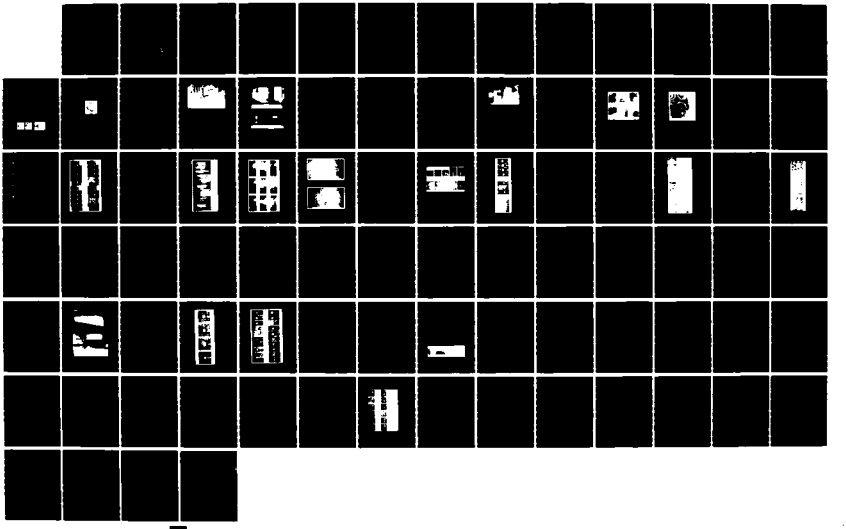

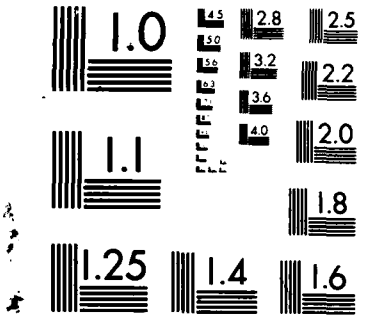

Fraunhofer-Gesellscha

FRACTURE BEHAVIOR UNDER IMPACT

W-10/86

Final Report, Part I

by

J.F. Kalthoff and S. Winkler

Fraunhofer-Institut
für Werkstoffmechanik

(12)

FRACTURE BEHAVIOR UNDER IMPACT

W-10/86
Final Report, Part I

by

J.F. Kalthoff and S. Winkler

Reporting Period:
Feb. 1981 - Feb. 1984, (Feb. 1985)

United States Army
EUROPEAN RESEARCH OFFICE OF THE U.S. Army
London England

CONTRACT NUMBER DAJA 37-81-C-0013

Fraunhofer-Institut für Werkstoffmechanik
Wöhlerstr. 11, 7800 Freiburg/Brsg., West-Germany

R&D 3012-AN

REPORT DOCUMENTATION PAGE		READ INSTRUCTIONS BEFORE COMPLETING FORM
1. REPORT NUMBER	2. GOVT ACCESSION NO.	3. RECIPIENT'S CATALOG NUMBER
4. TITLE (and Subtitle) Fracture Behavior Under Impact		5. TYPE OF REPORT & PERIOD COVERED Final Technical Report Dec 80 - Mar 84 6. PERFORMING ORG. REPORT NUMBER
7. AUTHOR(s) J.F. Kalthoff S. Winkler		8. CONTRACT OR GRANT NUMBER(s) DAJA37-81-C-0013
9. PERFORMING ORGANIZATION NAME AND ADDRESS Fraunhofer-Institut für Werkstoffmechanik Wöhlerstr. 11 7800 Freiburg/Brsg., West Germany		10. PROGRAM ELEMENT, PROJECT, TASK AREA & WORK UNIT NUMBERS 61102A 1L161102BH57-06
11. CONTROLLING OFFICE NAME AND ADDRESS USARDSG-UK Box 65 FPO NY 09510-1500		12. REPORT DATE August 1986 13. NUMBER OF PAGES 133 (Part I & Part II)
14. MONITORING AGENCY NAME & ADDRESS(if different from Controlling Office)		15. SECURITY CLASS. (of this report) Unclassified 15a. DECLASSIFICATION/DOWNGRADING SCHEDULE

16. DISTRIBUTION STATEMENT (of this Report)
Approved for Public Release; distribution unlimited

17. DISTRIBUTION STATEMENT (of the abstract entered in Block 20, if different from Report)

18. SUPPLEMENTARY NOTES

19. KEY WORDS (Continue on reverse side if necessary and identify by block number)
Dynamic fracture, Impact loading, Crack instability, Dynamic stress intensity factor, Impact fracture toughness, Multiple cracks, Mutual crack interaction, Stress optical techniques, Shadow optical method of caustics

20. ABSTRACT (Continue on reverse side if necessary and identify by block number)
The physical behavior of cracks under impact loading is investigated. Single edge cracks or arrays of multiple cracks are considered. The specimens are loaded by time dependent tensile stress pulses moving perpendicular to the crack direction. The specimens are directly loaded by an impinging projectile or by a base plate which is accelerated by a projectile. The specimens are made from a transparent model material, Araldite B, or a high strength steel, X2 NiCoMo 18 9 5. The initial crack lengths and impact velocities are varied

20. Contd.

throughout the experiments. By means of the shadow optical method of caustics in combination with high speed photography, the dynamic stress intensity factors at the tip of the crack are measured as functions of time during the impact event. In particular the critical value of the dynamic stress intensity factor at onset of rapid crack propagation, i.e. the dynamic fracture toughness K_{Ia}, is determined and discussed with regard to the time t_f at which the crack becomes unstable.

With steel specimens crack tip loading rates higher than 10^7 $MNm^{-3/2}s^{-1}$ are observed. The fracture toughness measured with Araldite B does not show a significant dependence on loading rate, but the data measured with high-strength-steel specimens indicate a sharp increase of fracture toughness at loading rates exceeding a certain limit. An attempt is made to explain the observed behavior assuming the existence of an incubation time for a crack to become unstable.

The mutual crack tip interaction of double crack configurations which are loaded by asymmetric stress pulses was found very different and resulted in larger mode II (in-plane shear) components than under equivalent static loading.

Details of the loading arrangements and the shadow optical recording techniques are described. The observed experimental results are presented and discussed with regard to the equivalent static data. Implications on the load carrying capacity of structures under high rate impact conditions are discussed.

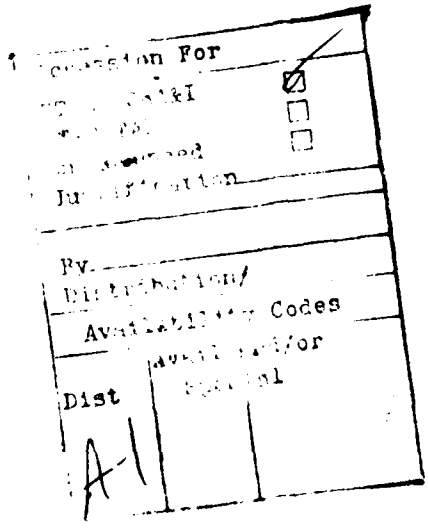

ABSTRACT

The physical behavior of cracks under impact loading is investigated. Single edge cracks or arrays of multiple cracks are considered. The specimens are loaded by time dependent tensile stress pulses moving perpendicular to the crack direction. The specimens are directly loaded by an impinging projectile or by a base plate which is accelerated by a projectile. The specimens are made from a transparent model material, Araldite B, or a high strength steel, X2 NiCoMo 18 9 5. The initial crack lengths and impact velocities are varied throughout the experiments. By means of the shadow optical method of caustics in combination with high speed photography, the dynamic stress intensity factors at the tip of the crack are measured as functions of time during the impact event. In particular the critical value of the dynamic stress intensity factor at onset of rapid crack propagation, i.e. the dynamic fracture toughness K_{Id}, is determined and discussed with regard to the time t_f at which the crack becomes unstable.

With steel specimens crack tip loading rates higher than 10^7 $MNm^{-3/2}s^{-1}$ are observed. The fracture toughness measured with Araldite B does not show a significant dependence on loading rate, but the data measured with high-strength-steel specimens indicate a sharp increase of fracture toughness at loading rates exceeding a certain limit. An attempt is made to explain the observed behavior assuming the existence of an incubation time for a crack to become unstable.

The mutual crack tip interaction of double crack configurations which are loaded by asymmetric stress pulses was found very different and resulted in larger mode II (in-plane shear) components than under equivalent static loading.

Details of the loading arrangements and the shadow optical recording techniques are described. The observed experimental results are presented and discussed with regard to the equivalent static data. Implications on the load carrying capacity of structures under high rate impact conditions are discussed.

KEYWORDS:
dynamic fracture, impact loading, crack instability, dynamic stress intensity factor, impact fracture toughness, multiple cracks, mutual crack interaction, stress optical techniques, shadow optical method of caustics,

CONTENTS:

1 INTRODUCTION

The failure behavior of structures which contain cracks or crack like defects is generally very well understood. The concept of fracture mechanics provides a powerful tool for quantitative safety predictions:

- The stress intensity factor, K, is a measure of the severity or criticality of a crack. The main parameters which determine this mechanical property are the length of the crack and the load which is applied to the crack.

- The fracture toughness, K_{Ic}, i.e. the critical stress intensity factor for onset of rapid crack propagation, is a material property which describes the resistance of the materal to crack extension.

For static or quasistatic loading conditions this concept has been successfully applied to many cases of practical importance:

- Formulas have been established to determine (exactly or at least approximately) the static stress intensity factor K_I^{stat} for almost any crack problem.

- Standardized test procedures have been developed for measuring the static fracture toughness K_{Ic} for different materials.

- Design criteria have been formulated on the basis of these two properties, i.e. K_I^{stat} and K_{Ic}, which allow the assessment of the safety of a structure under the specific service conditions [1,2].

The fracture behavior of cracks subjected to dynamic loading is considerably less well understood. The reason for this situation is the fact that these proclems are far more complicated. The stress intensification at the crack tip becomes a complicated function of time and consequently, the instability event is controlled by a rather complex process which cannot be described by simple means.

Thus, the most commonly used dynamic material strength value still is the Charpy energy, i.e. the energy to break a Charpy V-notch specimen in a pendulum type impact tester. This material property represents only a relative material characterization which cannot be used for quantitative design purposes. Research work is performed to develp a test procedure for measuring the dynamic fracture toughness value under impact loading, i.e. the impact fracture toughness K_{Id}. A currently proposed procedure for measuring this quantity in instrumented impact tests [3], however, is based on a simplified static evaluation procedure which determines the stress intensity factor from load values measured at the tup of the striking hammer via static stress intensity factor fomulas. Fig. 1 compares these static stress intensity factors K_I^{stat} with the actual dynamics stress intensity factors at the crack tip, denoted K_I^{dyn} [4,5]. The differences are quite large, in particular at early times of the impact event. The differences have not vanished even after time of 3τ, where τ is the period of the eigenoscillation of the specimen (see [3]). This procedure, therefore, is only applicable for

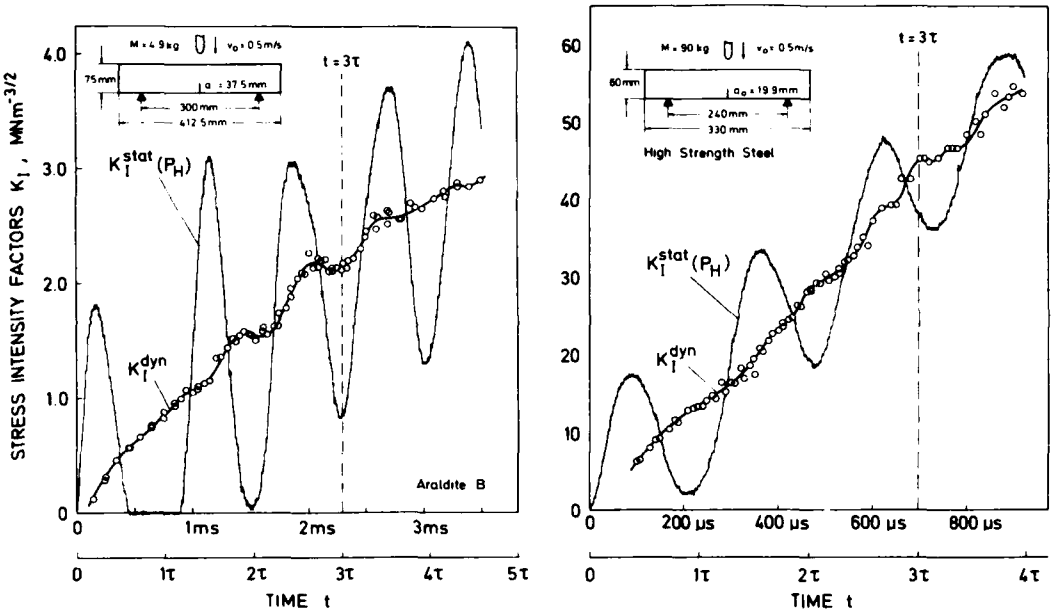

Fig. 1 Stress intensity factors for precracked bend specimens under drop weight loading

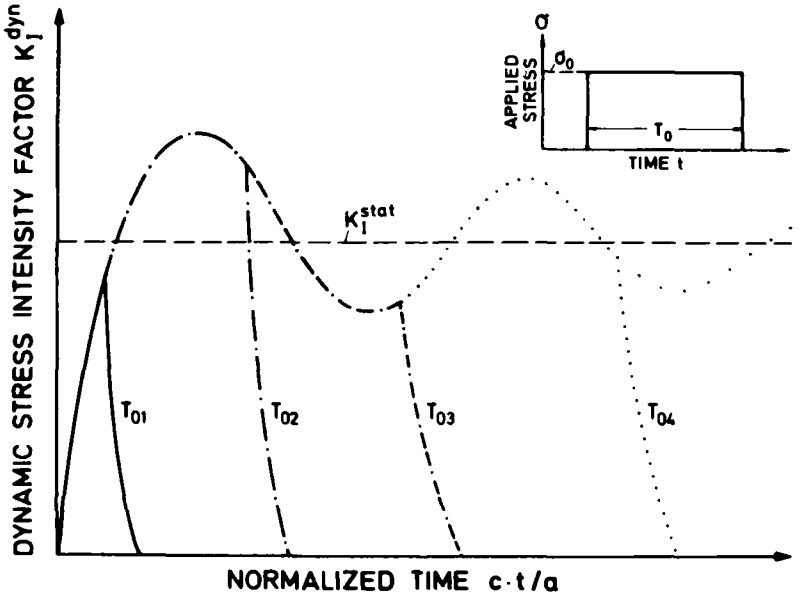

Fig. 2 Dynamic stress intensity factor for a crack under step function loads of durations $T_{01} < T_{02} < T_{03} < T_{04}$, schematically

very large times to fracture which, however, can only be obtained when the impact velocity is reduced to very low values. Depending on the conditions the maximum tolerable impact velocity has to be as low as about 1 m/s [3].

Another example which demonstrates the complex behavior of dynamic stress intensifications is shown in Fig. 2. For a crack of length a under mode-I step function load of duration T_o the dynamic stress intensity factor is plotted as a function of time (see [6-10]). The dimensionless time unit $(c_1 t)/a_o$ is used in this diagram, where c_1 is a wave velocity. K_I^{dyn} increases with time according to a $\sqrt{t}$-dependence, overshoots the equivalent static stress intensity factor K_I^{stat} upto to 30%, and only for larger times approaches K_I^{stat} by an oscillation with a damped amplitude. The duration T_o of the pulse controls the physically valid time interval (see Fig. 2). Because of the complicated $K_I^{dyn}(t)$-behavior, expecially for short pulse durations, conclusions on the effective stress intenstiy factor for the impact event can hardly be made. The maximum value of the $K_I^{dyn}(t)$-curve cannot control the actual instability event, because this value is only active for a very short time and does not allow the crack to make large jumps. On the basis of energy and momentum considerations, Steverding and Lehnigk [11-14] developed a dynamic fracture criterion which correlates the critical crack lengths with the applied pulse durations. A similar but more general criterion was developted later by Kalthoff and Shockey [15-18] denoted as minimum time fracture criterion.

These influences of time effects on the stress condition can have severe influences on procedures for measuring dynamic fracture toughness values [5].

Impact fracture toughness data have been measured at different loading rates. Depending on the strain rate sensitivity of the material, K_{Id} measured in the lower shelf or transition regime decreases more or less strongly with increasing loading rate $\dot{\sigma}_o$, as is indicated in Fig. 3. Most of the dynamic fracture toughness data have been obtained in the lower impact velocity range with Charpy- and drop weight tests. An overview on the results obtained and the problems encountered in measuring these quantitites is given in the papers of Turner, Venzi, Shoemaker, Rolfe, Loss, Ireland, Wullert, and others [19-23]. Data at higher loading rates have been measured for examply by Costin, Duffy, Freund, and Server [24,25] and by Klepaczko [26] with Hopkinson bar experiments, by Shockey, Curran, Homma and Kalthoff [18,27-30] with flyer plate impact experiments, and by Ravi Chandar and Knauss [31] using electromagnetic loading techniques. In their papers Eftis and Krafft [32] and Shockey and Curran [27] discuss the interesting question whether a minimum value of K_{Id} exists, which cannot be reduced even if the loading rate would be increased further (see Fig. 3).

The difficulty in all the measuring procedures consists of establishing a relation between quantities measured externally at the test machine and the actual stress intensity factor existing at the tip of the crack in the specimen. Different approaches are used: Simplyfied static analyses (e.g. with Charpy tests [3]), theoretical analyses which some-

times are based on nonrealistic assumptions (e.g. infinite boundaries or step function loads [6-10]), or numerical analyses which necessarily are very complicated. In this project the problem of deriving the stress intensity factor from secondary quantities measured in an experiment shall be avoided by measuring the actual dynamic stress intensity factor directly at the crack tip by a special optical technique developed at the Fraunhofer-Institut für Werkstoffmechanik, i.e. the shadow optical method of caustics [33,34].

The investigations of this research projekt are aimed to generate basic information on the failure behaviour of precracked specimens with finite boundaries subjected to dynamic tensile stresses. The results are of special importance for the development of improved impact fracture toughness tests and the assessment of the load carrying capacity of structures under dynamic loading conditions in general.

2 GENERAL OUTLINE

2.1 Technical Objectives

The physical behaviour of cracks under impact loading is investigated. Single edge cracks or arrays of multiple cracks in rectangular specimens are considered. The specimens are loaded by time dependent tensile stress pulses p(t) moving perpendicular to the crack direction. The pulses are produced by impinging projectiles. The specimens are made from a transparent model material or a high strength steel. Utilizing the shadow optical method of caustics in combination with high speed photography, the dynamic stress intensity factors, K_I^{dyn}, at the tip of the crack are measured as functions of time during the impact event. The critical value of the dynamic stress intensity factor at onset of rapid crack propagation, i.e. the dynamic fracture toughness K_{Id}, is determined and compared to the corresponding static fracture toughness K_{Ic}. The results are discussed with regard to the times t_f at which the initial cracks become unstable.

Two kinds of impact experiments are envisaged in the research program:

A) Direct impact loading: The precracked specimen is directly impacted by the projectile. After passage of the compressive stress pulse through the specimen and reflection of the pulse at the free end of the specimen, the crack is loaded by tensile stresses (see schematic drawing - Fig. 4a).

B) Base plate loading: The precracked specimen is loaded in tension by a base plate which is accelerated by the impinging projectile (see schematic drawing - Fig. 4b).

Single edge cracks (as shown in the lower specimen of Fig. 4b) ore arrays of multiple cracks (as shown e.g. in the upper specimen of Fig. 4b) are investigated.

2.2 The Shadow Optical Method of Caustics

The method of caustics is an optical tool for measuring stress intensifications. The technique has been introduced by Manogg in 1964 [33,34]. Later on, Theocaris [35] and Rosakis et al. [36] further developed the method. The authors and their coworkers extended and applied Manogg's

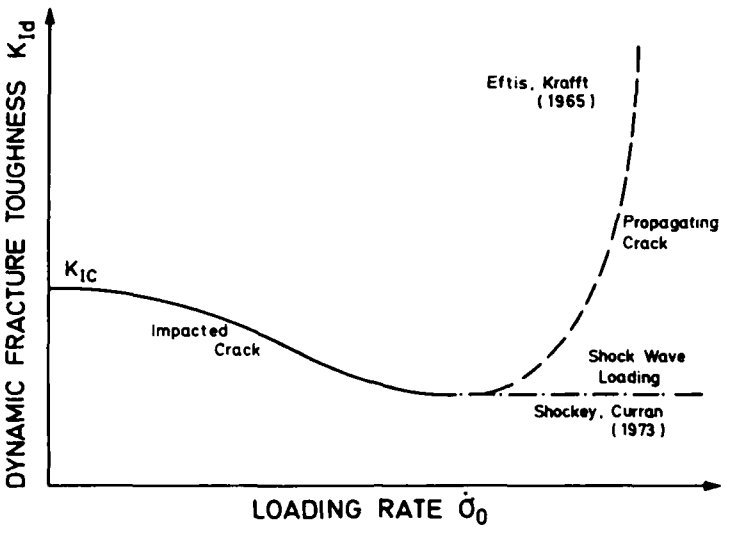

Fig. 3 Dynamic fracture toughness as a function of loading rate, (schematically)

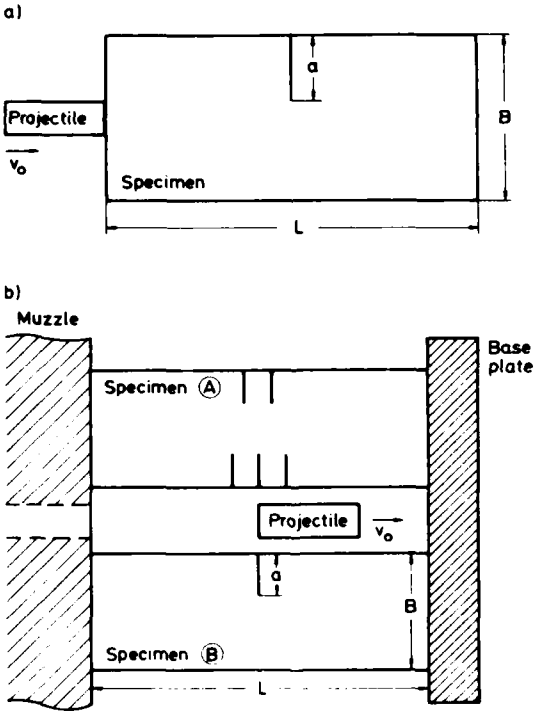

Fig. 4 Loading conditions, a) direct impact loading, b) base plate loading (schematically)

technique for investigating dynamic fracture phenomena [4,5,37-44]. For an overview on the shadow optical technique see Kalthoff [39].

The physical principle of the method is illustrated in Fig. 5. A pre-cracked specimen under load is illuminated by a parallel light beam. A cross-section through the specimen at the crack tip is shown in Fig.5b for a transparent specimen, and in Fig. 5c for a non-transparent steel specimen. Due to the stress concentration the physical conditions at the crack tip are changed. For transparent specimens both the thickness of the specimen and the refractive index of the matrial are reduced.Thus, the area surrounding the crack tip acts as a divergent lens and the light rays are deflected outwards. As a consequence, on a screen (image plane) at a distance z_0 behind the specimen a shadow area is observed which is surrounded by a region of light concentration, the caustic (see Fig. 6). Fig. 5c shows the situation of a non-transparent steel specimen with a mirrored front surface. Due to the surface deformations light rays near the crack tip are reflected towards the center line. An extension of the reflected light rays onto a virtual image plane at the distance z_0 behind the specimen results in a light configuration which is similar to the one obtained in transmission. Consequently a similar caustic is obtained. The mode I shadow pattern was calculated by Manogg [34] from the linear elastic stress strain field around the crack tip. Fig. 6 compares theoretical results with experimentally observed caustics which were photographed in transmission and in reflection with different materials. The single caustic curve obtained for isotropic materials splits up into a double caustic for optically anisotropic materials.

The size of the shadow pattern is related to the stress intensification at the crack tip. The quantitative correlation between the diameter D of the caustic and the stress intensity factor K_I is given by the euqation

$$K_I = M \cdot D^{5/2} \qquad (1)$$

where M is a known numerical factor which depends on the optical arrangement and the material utilized [37,38,39].

A quantitative shadow-optical analysis is also available for cracks subjected to superimposed tensile (mode I) and shear (mode II) loading. With increasing ratio $\mu = K_{II}/K_I$ the caustic becomes asymmetric (see Fig. 7a). Fig. 7b shows the theoretically calculated caustic in comparison to an experimentally observed shadow pattern for the case $\mu=1$ From the minimum and maximum diameters D_{min} and D_{max} of the caustics (defined in Fig. 7b) the absolute values of the stress intensity factors K_I and K_{II} can be determined using the relation

$$K_i = M_{i,k} \cdot D_k^{5/2} \quad (i = I,II;\ k = min, max). \qquad (2)$$

This relation is imilar to eq. (1). The (four possible) factors $M_{i,k}$ which again contain optical and geometrical parameters are known functions [37,39,45,46].

For further details of the shadow optical techniques see [37-39].

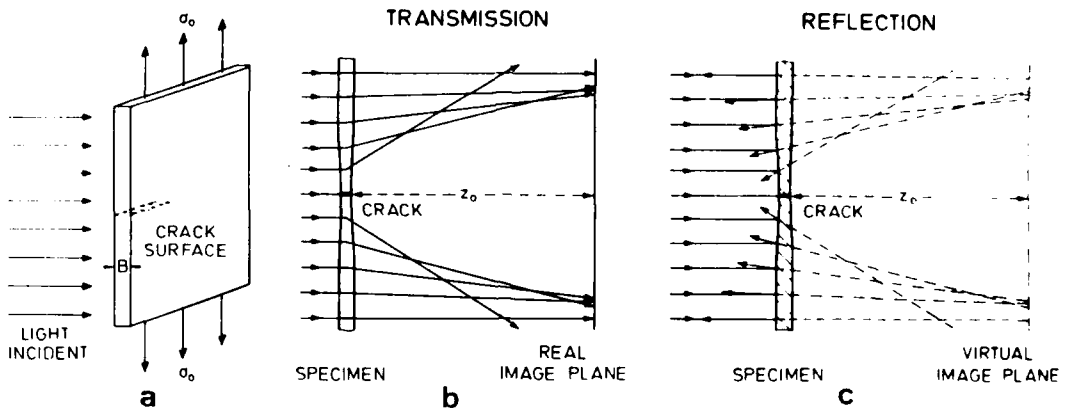

Fig. 7 Physical principles of the shadow optical method of caustics

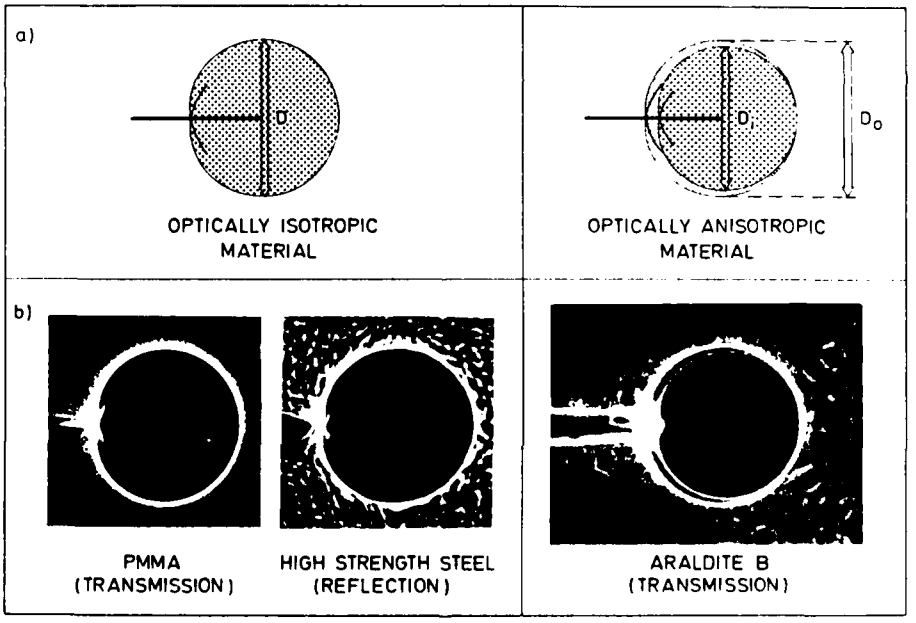

Fig. 8 Mode-I caustics, a) calculated, b) measured

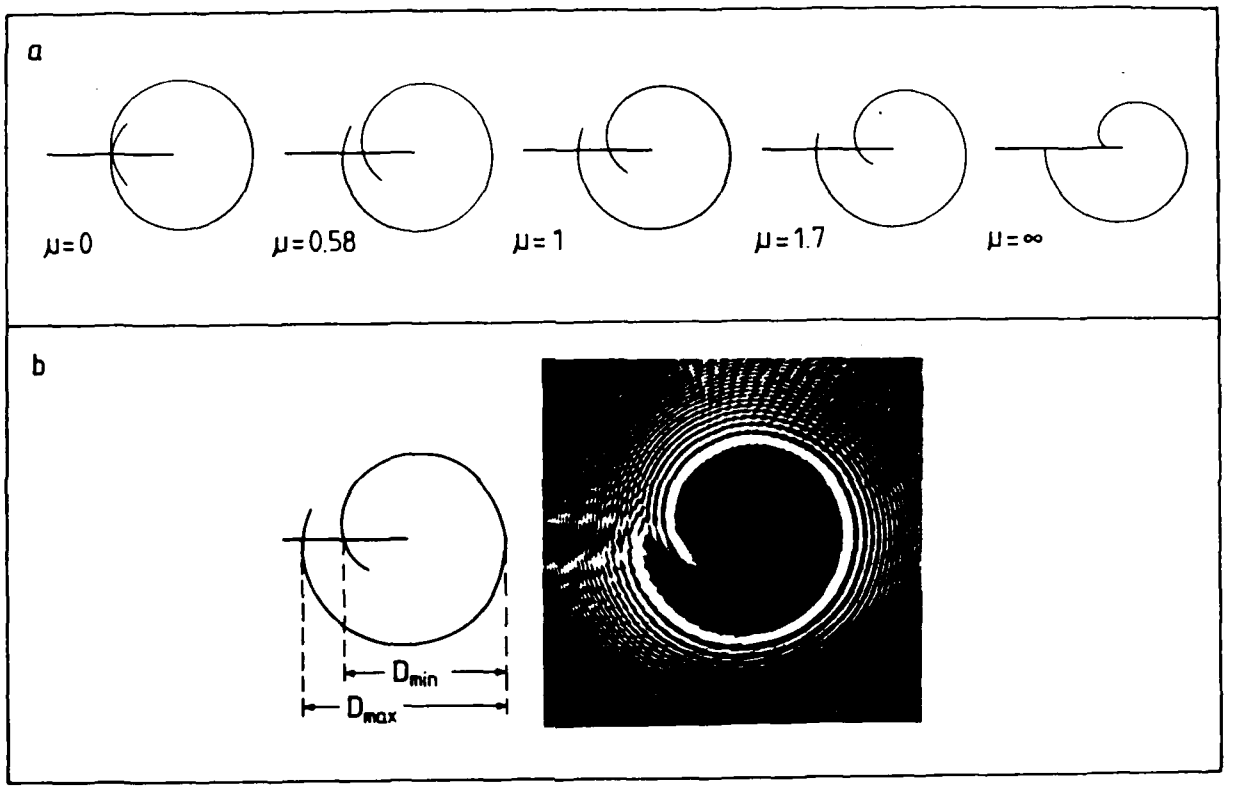

Fig. 7 Mixed (I, II) mode caustics, a) calculated for different ratios $\mu = K_{II}/K_I$, b) definition of diameters and experimentally observed shadow pattern

Crack tip caustics are of a simple form and can easily be evaluated. The technique, therefore, is very well suited for investigating complex phenomena, as e.g. in fracture dynamics, and is used in this work to measure dynamic stress intensity factors under impact loading.

2.3 Research Program

Within the initial phase of the three years' research project the experimental set-up for investigating the fracture behavior under impact loading has been built up (see Chapter 3). The existing IWM gas gun has been modified for this purpose. A Cranz Schardin high speed camera has been aligned to the gas gun. A holding fixture has been designed and built to load the specimens under direct impact - and base plate loading conditions (see Chapter 4). The set-up has been successfully tested under different impact conditions. Several series of experiments have been performed to specify the parameters for the main investigations.In the second and third year the main experiments with a systematic variation of parameters were performed. In particular, the impact fracture toughness K_{Id} was measured at different loading rates (see Chapter 5) and the interaction of multiple crack configurations was studied (see Chapter 6). The investigations during the second year were predominently carried out with Araldite B specimens (see Section 5.1 and Chapter 6). During the third year these investigations were completed and extended to investigations with high strength steel specimens (see Section 5.2). The main findings on the dependence of the impact fracture toughness from loading rate and concluding remarks on the instability behavior of cracks under extremely high loading rates are presented in Section 5.3. Chapter 7 gives a summary of the total achieved research work and the obtained results.

3 DESIGN AND BUILDING OF THE EXPERIMENTAL SET-UP

The IWM gas gun is used for impact loading of the specimens. A schematic drawing and a photograph of the equipment are given in Fig. 8. The high pressure chamber (30 l volume) can be filled with air or helium to a maximum pressure of 200 bar. A barrel of 50 mm diameter and 3 m length is used to accelerate the projectile. A measuring chamber at the muzzle holds the target and the measuring devices. The catcher tank collects the remaining pieces of the experiment and is able to absorb their kinetic energy. The gas gun has been modified and supplemented by special devices in order to meet the specific requirements for the proposed experiments. Shadow optical pictures of the specimen during impact are recorded with a Cranz-Schardin high speed camera. 24 pictures can be taken at a minimum picture interval time of 1 µs. A photograph of the camera is given in Fig. 9. An overview of the complete experimental set-up is given in Fig. 10.

In particular the following work has been performed:

- Design and construction of a holding fixture for the specimens: Special arrangements have been developed to load the specimens in either one of the two loading conditions, i.e. direct impact loading or base plate loading. These arrangements meet the optical requirements for

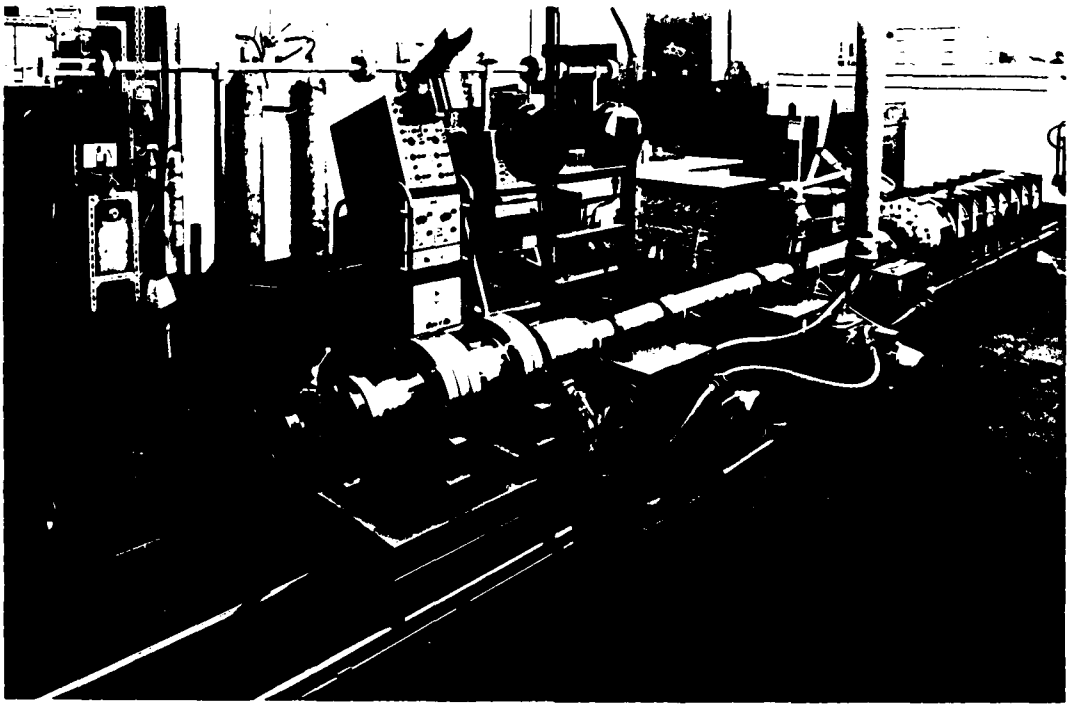

DRUCKKAMMER		LAUF		MESSKAMMER mit AUFFANGER	
Volumen	1 30 l	Lange	3 m	Lange	2 m
p_{max}	200 bar	Kaliber	50 mm	Volumen	120 l
		Volumen	6 l		

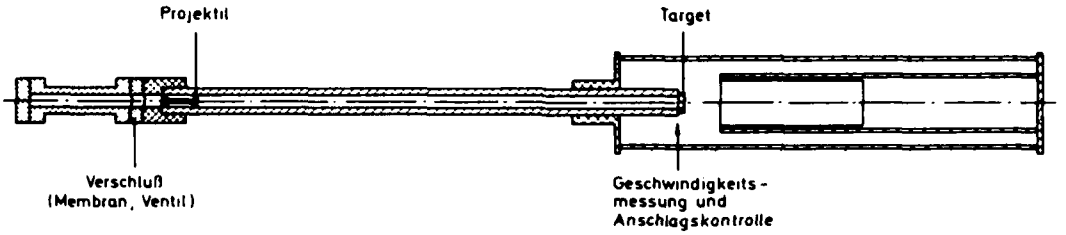

Fig. 8 IWM gas gun

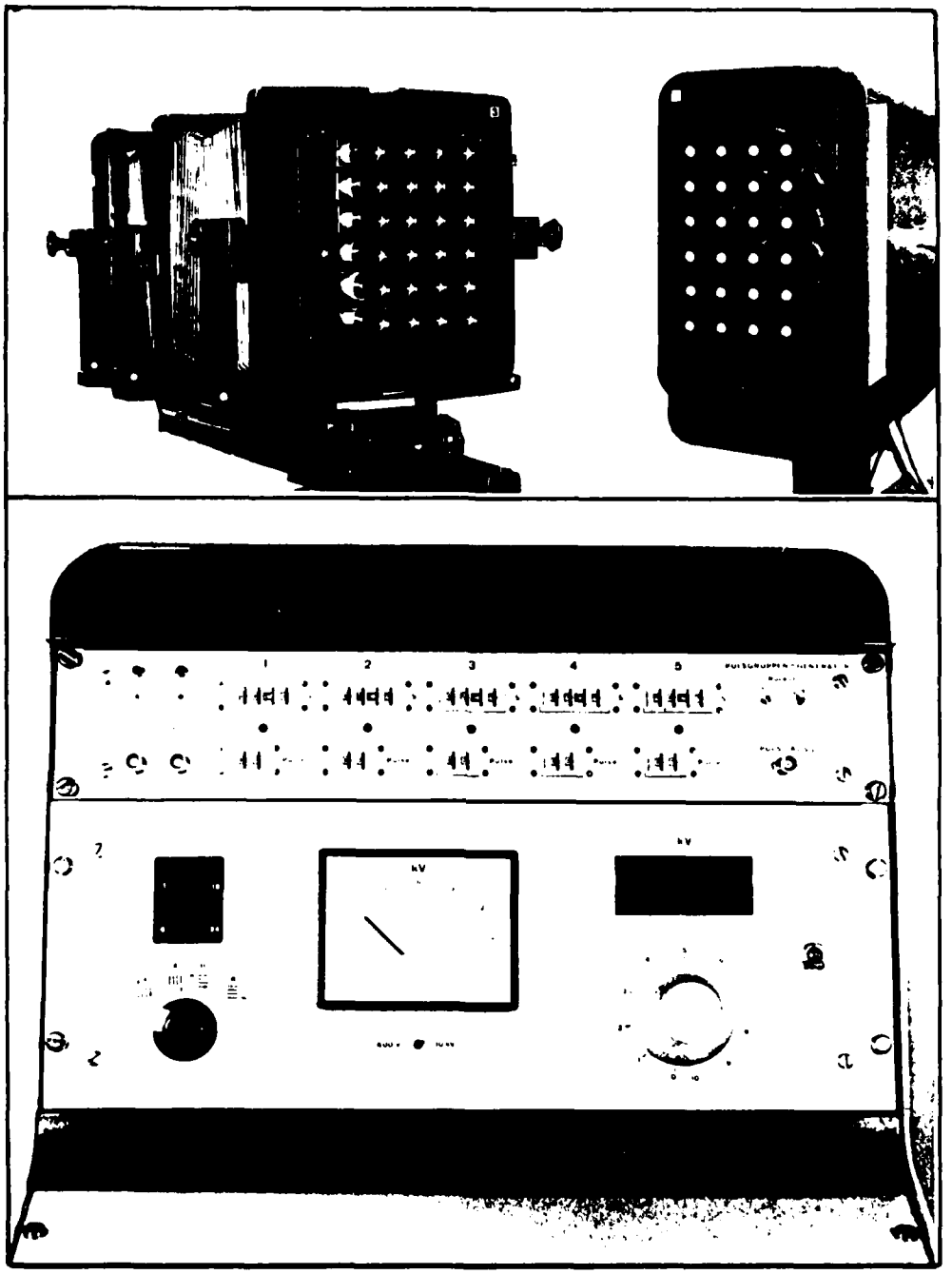

Fig. 9 Cranz-Schardin 24 spark high spead camera

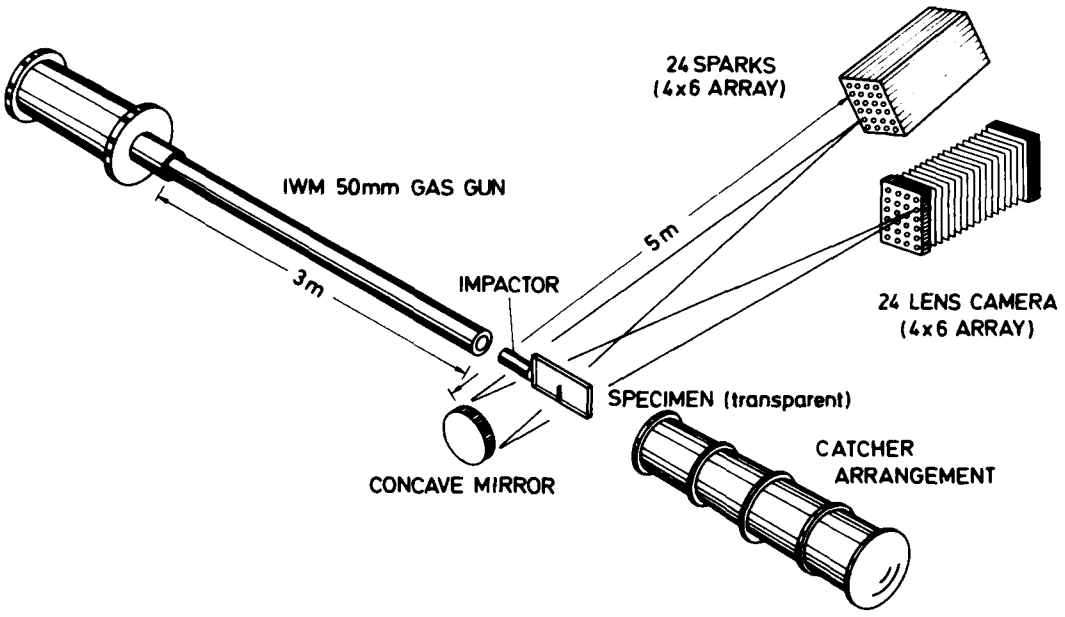

Fig. 10 Experimental set-up, schematically

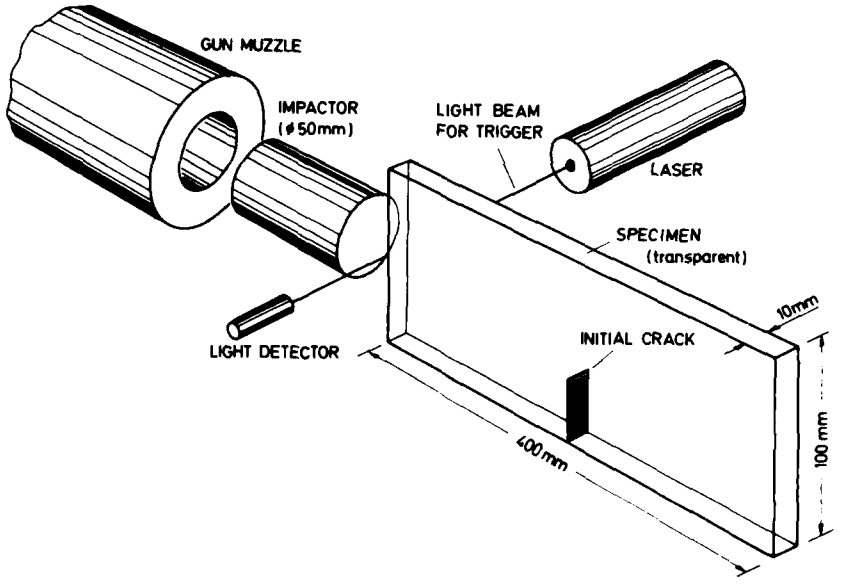

Fig. 11 Illustrative view of the direct impact loading arrangement

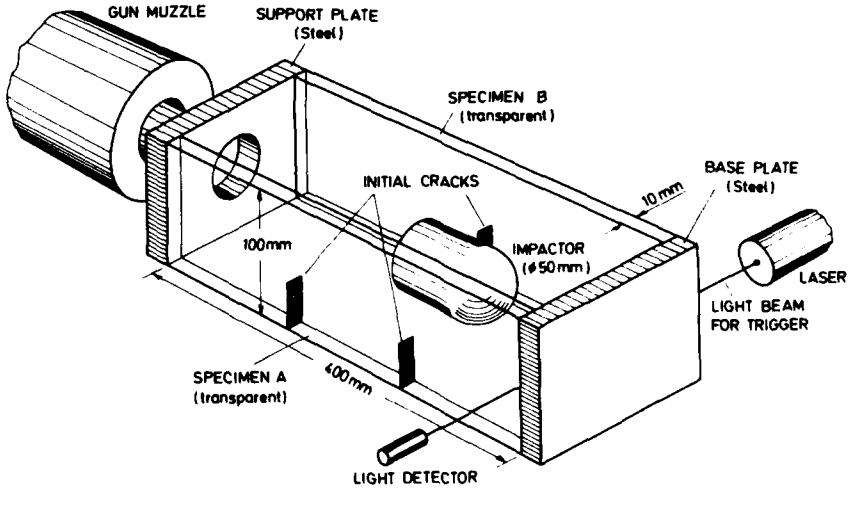

Fig. 12 Illustrative view of the base plate loading arrangement

a photographic recording of the specimen behavior. Illustrative views of the two loading arrangements are given in Figs. 11 and 12.

For the conditions of direct impact loading the specimen is prositioned at the center line of the gas gun. The specimen is almost free and only loosely attached to a support (just to keep it in a definite position). For the conditions of base plate loading an arrangement with two specimens has been developed. The specimens are positioned to the right and to the left hand side of the center line of the gas gun. The front ends of the specimens are attached to a rigid support plate which is kept at a fixed position. The ends of the specimens are fastened to a free base plate which is accelerated by the impinging projectile. The observation direction of the shadow optical measuring system is perpendicular to the surfaces of the specimens. Thus, the two specimens - one lying in front of the other - are simultaneously photographed when the shadow optical system is used in transmission with transparent specimens. The arrangement then has the advantage that two different crack configurations can simultaneously be investigated in the two specimens. Of course, only one specimen is analyzed if the shadow optical system would be used in reflection with steel specimens.

A fixture to hold the specimens according to these two arrangements has been designed and built. A photograph is given in Fig. 13. The fixture consists of two parts: a front part and a rear part which are separately mounted on the supporting I-beam (180 mm high, 3400 mm long). The distance between the two parts can be varied, thus specimens of different length can be utilized in the experiments. The maximum specimen width is limited to 100 mm. The front part of the fixture is adjustable to allow for a straight and plane impact.

- Catcher tank:
An existing catcher tank had been modified and adapted to the loading fixture and the supporting I-beam. The catcher arrangement was necessary in order to collect the moving parts after impact, i.e. the projectil, the base plate, the broken pieces of the specimen etc. Rags absorb the kinetic energy of the moving parts.

- Triggering device for the high speed camera:
An optical device had been designed and built to trigger the Cranz-Schardin high speed camera. A laser beam traverses the path of the flying projectile (see Figs. 11 and 12)
  - directly in front of the specimen (direct impact condition) or
  - directly in front of the base plate (base plate loading condition).

  The laser beam is interrupted by the impinging projectile and thus provides a pulse to trigger the camera via a delay time generator.

- Adaption of the Cranz-Schardin high speed camera:
The 24 spark high speed camera had been adjusted and aligned to the gas gun. Since the camera is normally operated at a height of about 1.4 m, the gas gun, however, at a lower height of only 0.6 m, considerable work was necessary to lower the whole optical arrangement, i.e. the camera, the spark unit, and the mirror. The existing tripods had to be modified by special holding fixtures.

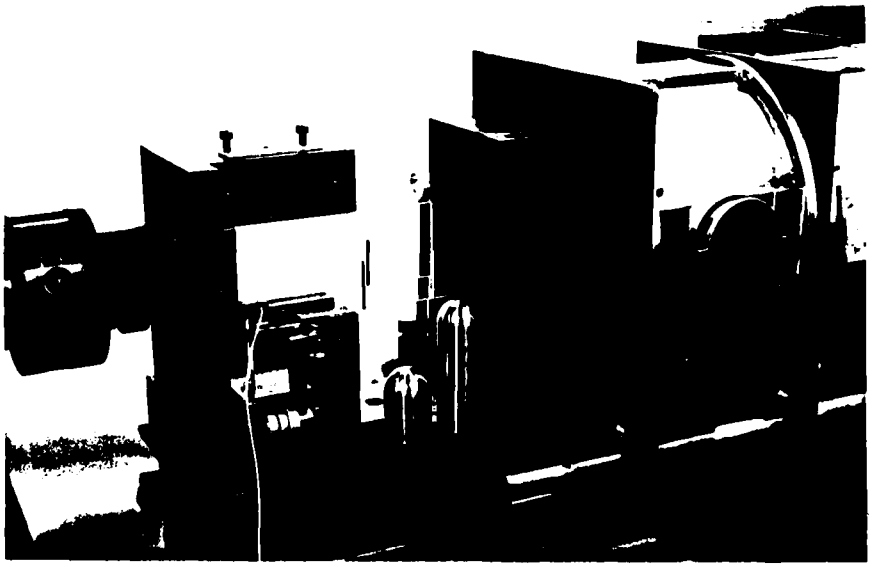

Fig. 13 Holding fixture for specimen

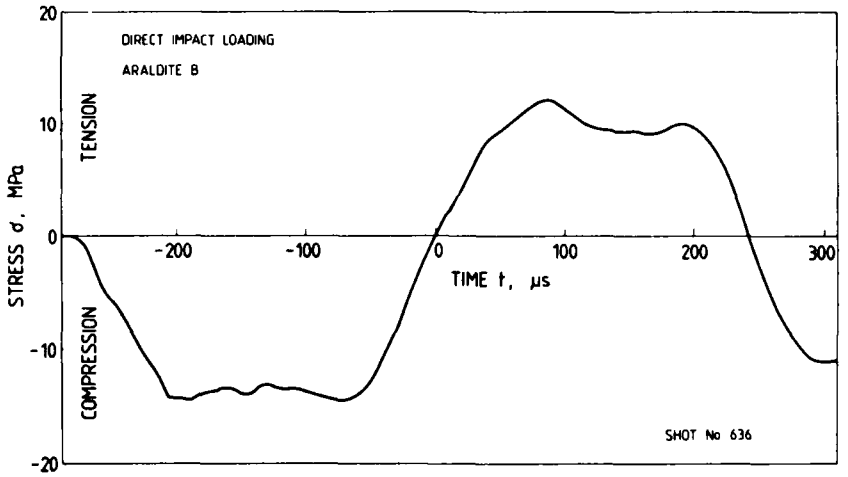

Fig. 14 Stress pulse history

4 TEST OF THE EXPERIMENTAL SET-UP

Several shots were necessary to test the different systems of the experimental set-up, in particular
- the holding fixture and the catcher tank,
- the triggering system, and
- the alignment of the high speed camera.

The information obtained from these preliminary experiments was used to improve the experimental set-up. Modifications to the first design of the holding fixture were necessary in order to achieve an undisturbed tensile loading of the specimens under the two loading conditions. Serious difficulties were encountered with the triggering system. In several cases the air shock wave travelling ahead of the flying projectile provided the first trigger pulse. Consequently the camera was started ahead of time. These problems had been solved by adjusting the trigger threshold to an appropriate level. This level has experimentally been established in a series of test shots. The final alignment of the high speed camera caused no major problems.

Results obtained under the two different types of loading conditions are reported in the following sections. Due to cost reasons, these experiments were performed with specimens made from the model material Araldite B.

4.1 Direct Impact Loading

First, several experiments have been performed to study the load pulse history in the specimen under direct impact loading conditions (see Fig. 11). Data were obtained from strain gage measurements, photoelastic investigations, and shadow optical investigations. Some typical results which give an indication of the loading situation in the specimens are reported.

4.1.1 Load Pulse History

All experiments were performed with specimens 400 mm long and 100 mm wide. The specimen thickness was 10 mm. The specimens were impacted by a projectile of 200 mm length and 50 mm diameter made from the same material as the specimens, i.e. Araldite B. The chosen dimensions were a result of pre-experiments in which the length of the specimen had been varied: with short specimens, i.e. specimens of length 100 mm and 200 mm it was found that the crack did not propagate in a straight manner through the specimen but deviated from its original direction. Test specimens of 400 mm length, however, showed a straight crack propagation in the original crack direction.

- Strain Gage Measurements:

The signal from a strain gage positioned in the middle of a specimen without a crack is shown in Fig. 14. For a period of 280 µs the crack is loaded by compressive stresses, then tensile stresses build up due to the reflection of the compressive waves at the free ends of the specimen

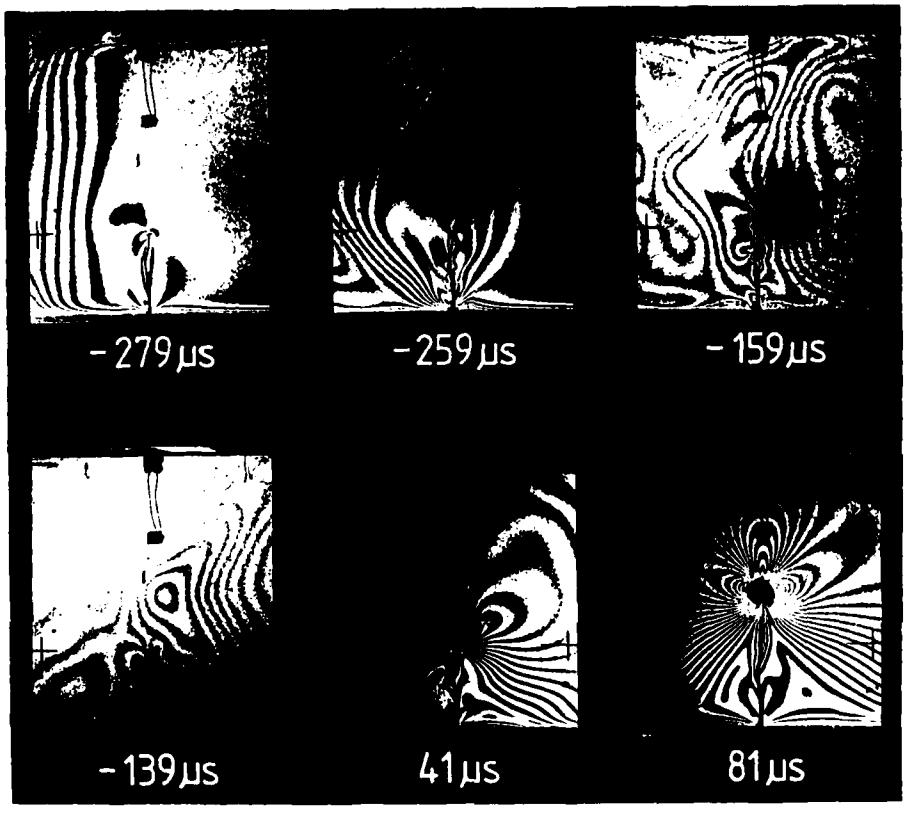

Fig. 15 Photoelastic recording of the passage of the stress pulse through the specimen

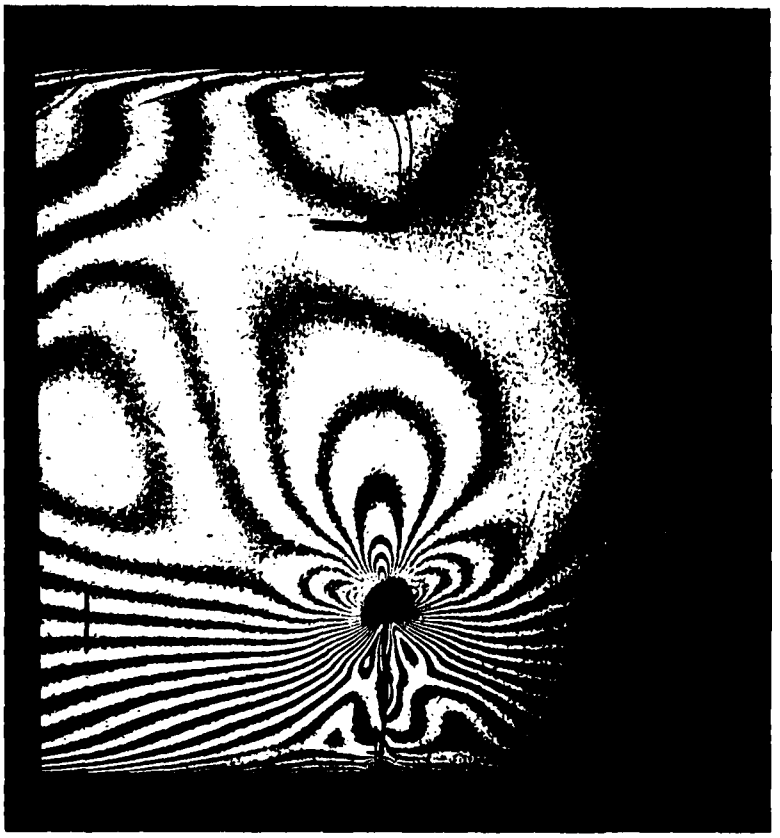

Fig. 16 Photoelastic crack tip fringe pattern

and the projectile. In this diagram and also in the following ones the time at which compression changes into tension has been set equal to zero (0 μs). The tensile stress pulse has a duration of about 240 μs.At later times compressive stresses again build up in the center part of the specimen. The increasing part of the tensile stress pulse would be used in specimens with inital cracks to initate unstable crack propagation.

In order to get information on the stress history not only at the single point where the strain gage is located but over a larger area further investigations have been carried out utilizing photoelastic and shadow optical techniques.

● Photoelastic Measurements:

Photoelastic isochromatic fringe patterns associated with the passage of the stress pulse through the specimen were recorded. The Cranz-Schardin camera was equiped with a photoelastic measuring device and focussed directly onto the specimen. The specimen dimensions and the impact conditions were the same as for the strain gage measurements, but specimens with inital cracks were utilized. Fig. 15 shows six picutres at subsequent times. The passage of the compressive stress pulse into the specimen is visible. Since the crack is closed by the compressive stresses the stress pulse is only slightly disturbed by the crack.After tensile stresses have been built up in the center part of the specimen ($t > 0$ μs), the typical tensile crack tip fringes develop. Fig. 16 shows another photoelastic picture of a tensile crack tip fringe pattern.

No attempts have been made to quantitatively evaluate the rather complex photoelastic fringe patterns; instead a special shadow optical measuring technique was utilized to obtain information on the stress distribution in the specimen.

● Measurement of Shadow Patterns Around Hole Fields:

Shadow patterns around holes which are drilled into a specimen can be used as indicators of the stress field at that point. Fig. 17 shows the shadow pattern around a hole under the influence of a biaxial stress field $\sigma_y = p$, $\sigma_x = q$, with $p > q$ (see [33,39]). The intersection of the shadow pattern is oriented parallel to the larger of the tensile stresses. The diameter of the caustic D in longitudinal direction of the shadow pattern is quantitatively related to the difference of the principle stresses $p - q$,

$$p - q = N \bullet D^4. \qquad (3)$$

N is a known numerical factor which depends on the optical arrangement and the material utilized. Consequently, for a tensile stress field the intersection of the shadow pattern points into the direction of the stresses, for compressive stress fields it points in a direction perpendicular to the stress field. Furthermore, the size of the caustic is an indicator of the magnitude of the stress. Utilizing this technique,a series of experiments has been performed to study the stress distribution in the specimen.

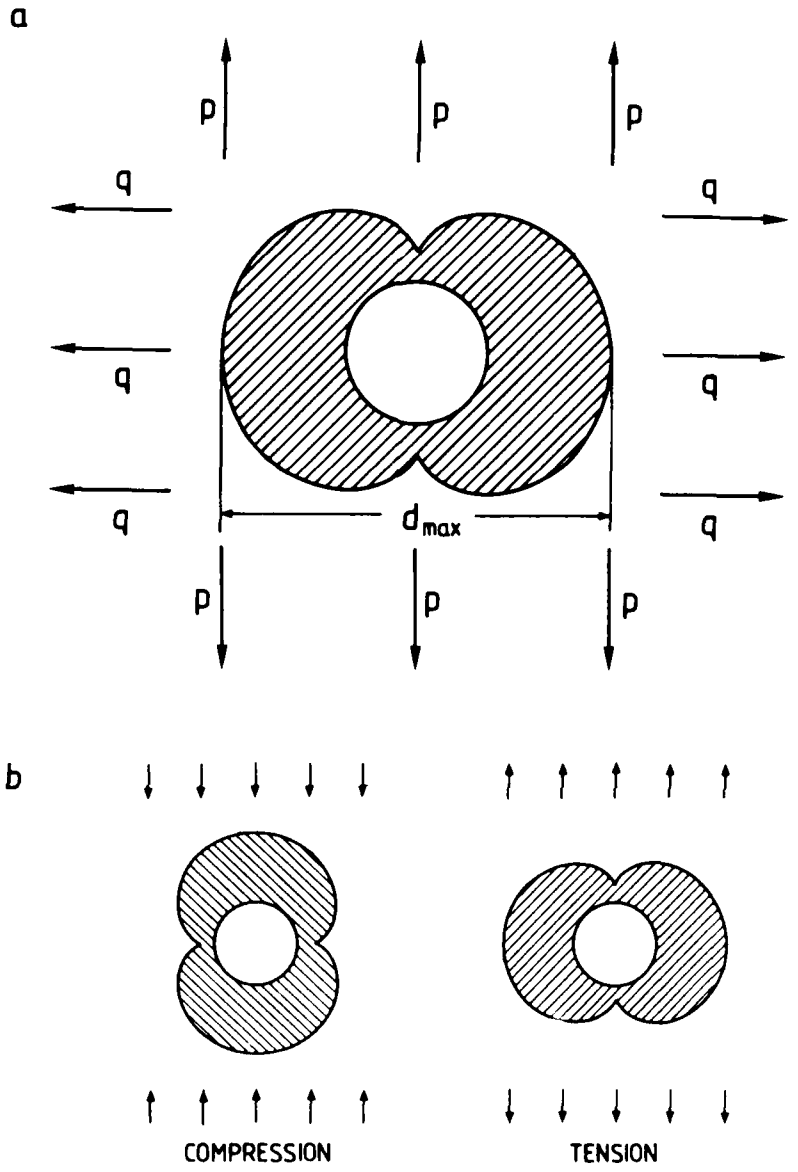

Fig. 17 Caustics around a hole

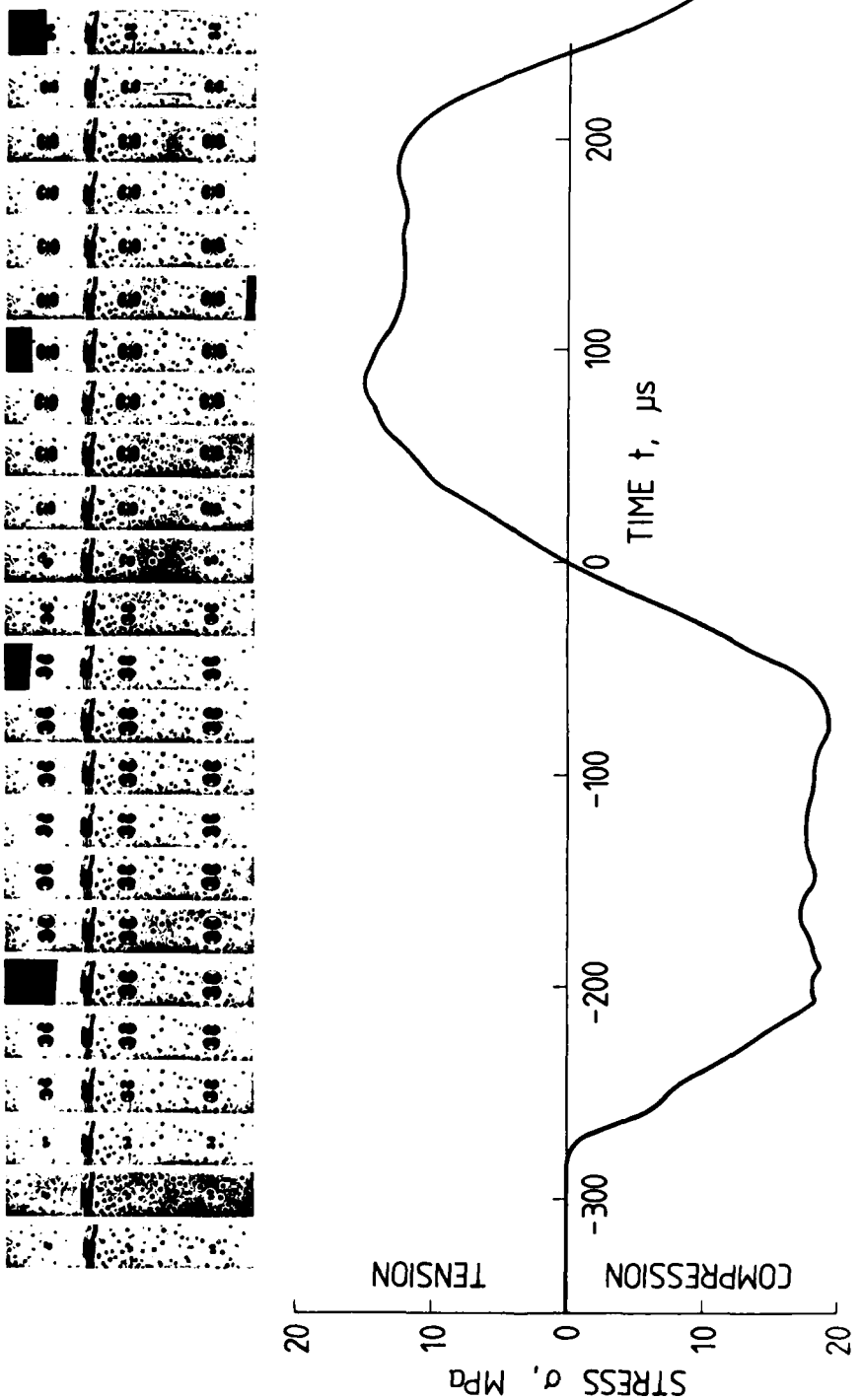

Fig. 18 Shadow optical investigation of the stress pulse history, (arrangement of 3 holes)

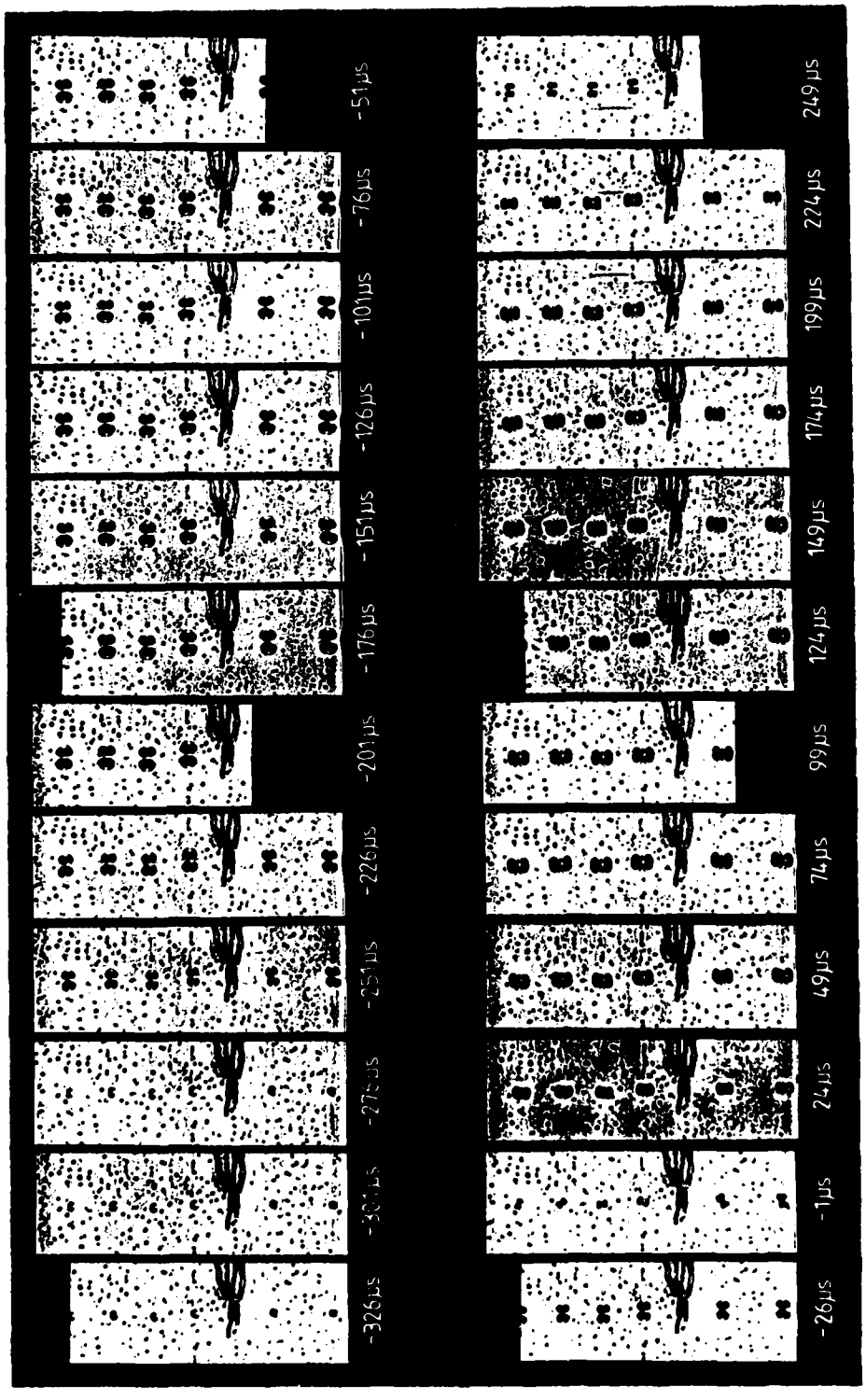

Fig. 19 Shadow optical investigation of the stress pulse history, (arrangement of 6 holes)

First, a row of three holes was drilled in the middle of the specimen at 1/4, 1/2, and 3/4 of the width of the specimen. In addition, the specimen was instrumented by a strain gage located between two of the holes. The insert in Fig. 18 illustrates the geometrical arrangement. The results of both, the strain gage measurements and the shadow optical investigations are given in Fig. 18. The shadow patterns change their direction and their size analogous to the strain gage signal. The size of the patterns varies with the stress amplitude. In frame No. 14 the direction of the patterns change and from frame No. 15 on tensile shadow patterns are recorded. The last pattern at 250 μs again indicates compressive stresses.

More detailed information on the distribution of the stresses along the width of the specimen is obtained from the results in Fig. 19. In this experiment six instead of three holes were used. The picture shows the same general behavior as discussed above. The six shadow optical patterns positioned across the width of the specimen do not vary very much in size, in particular the patterns near the boundary are almost of the same size as the center patterns, indicating a rather even distribution of stresses along the location of the prospective crack.

The passage of the stress pulse through the specimen has been made visible in a specimen with a row of holes positioned in length direction of the specimen. The shadow optical pictures are given in Fig. 20. Frames No. 1 to 13 show the propagation of the compressive stress pulse into the specimen. Between frames No. 13 and 14 the stresses change from compression into tension, and between frames No. 23 and No. 24 they have changed back again into compression. Fig. 21 shows the change from the compressive state of stress to the tensile stresses with higher time resolution. In this case a cross shaped arrangement of holes has been utilized. At the time t = 0 μs zero stresses are observed directly in the center of the specimen, the region around this center still is under compressive stresses. In the next frame, at 18 μs, tensile stresses have already built up in the center.

An overview on the stress distribution in the whole specimen is given in Fig. 22 showing the shadow optical photograph of a specimen with a field of 91 holes. The photograph was taken during the tensile loading phase. The data indicate that the stress field in the center of the specimen, i.e. at the location of the prospective crack, is rather uniform, thus allowing a controlled investigation of the instability behavior of cracks.

In a subsequent experiment the development of the stress intensification at an initial notch has been photographed. A notch of 35 mm length has been machined in a specimen which had been provided with the hole field already. Fig. 23 shows a well developed mode-I caustic around the crack tip. The picture was taken 54 μs after the beginning of the tensile stress field. The shadow patterns around the holes behind the crack tip indicate unloading of the specimen in this area. The other patterns in the near crack tip region show a disturbed stress field due to interactions with the crack tip stress field.

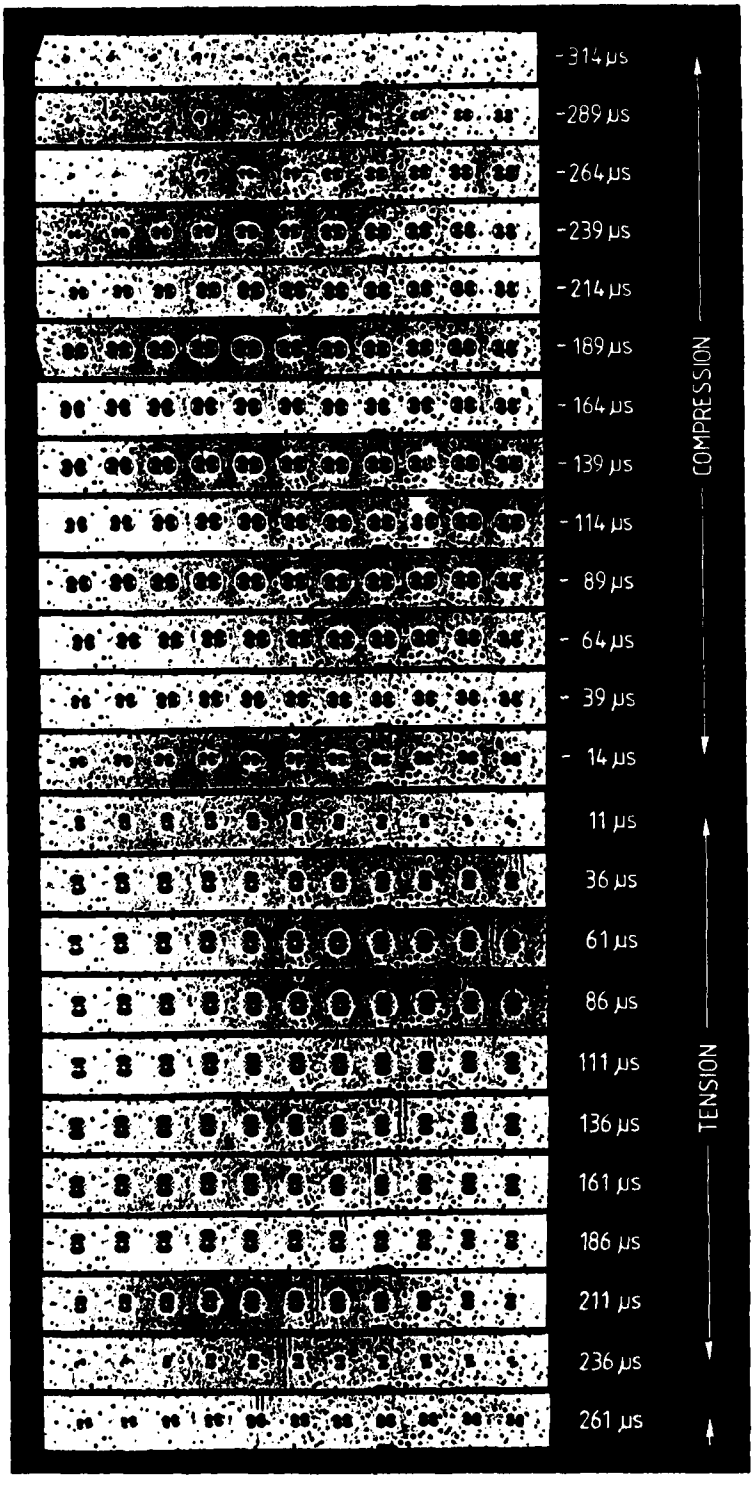

Fig. 20 Shadow optical investigation of the stress pulse history, (arrangement of holes in length direction of the specimen)

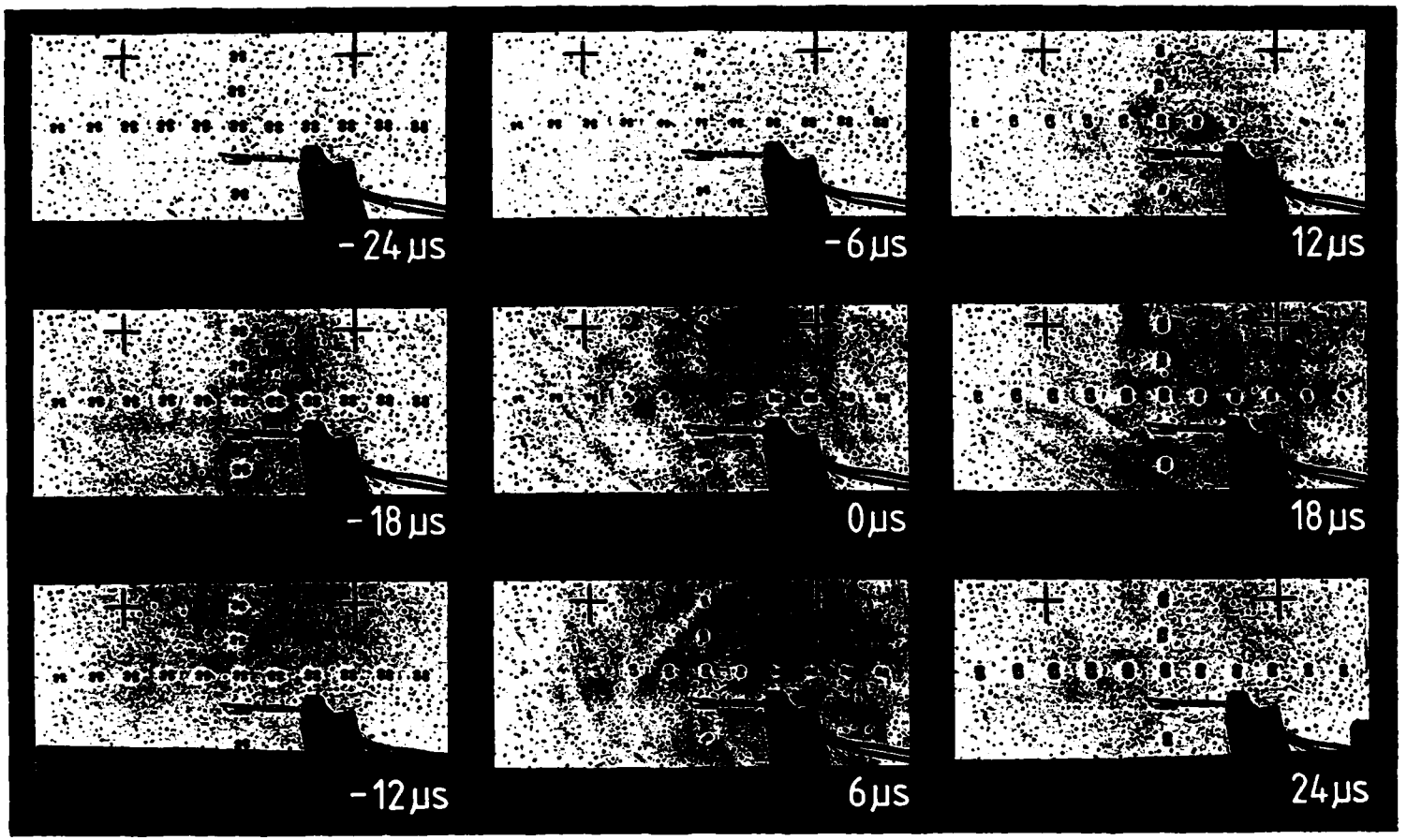

Fig. 21 Change from compressive to tensile stresses (shadow optical investigation with a cross shaped arrangement of holes)

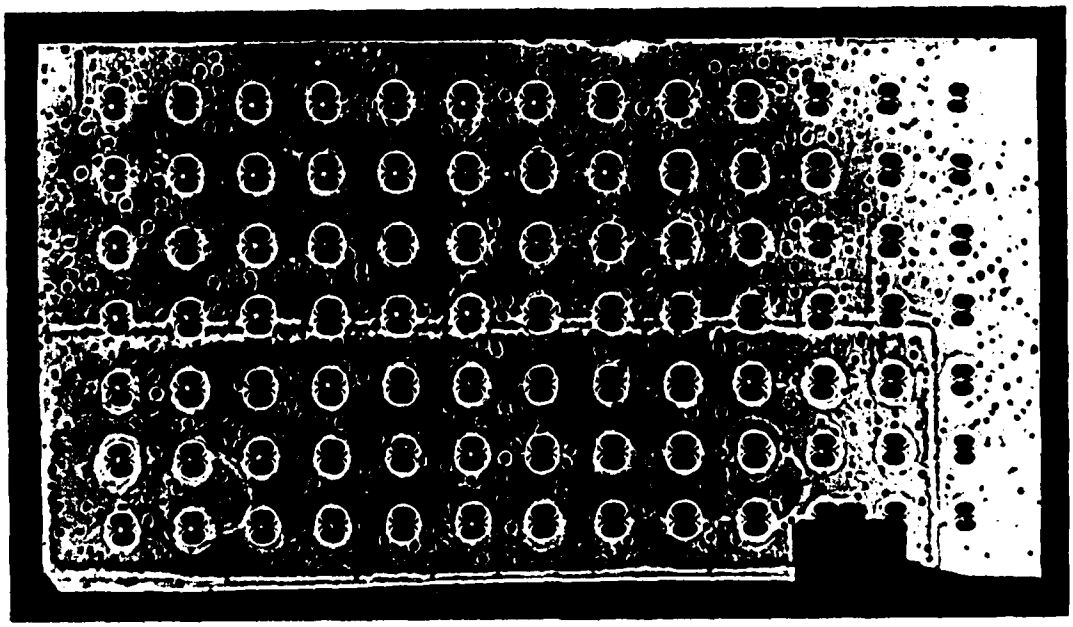

Fig. 22 Distribution of tensile stresses in the specimen (shadow optical investigation with a hole field)

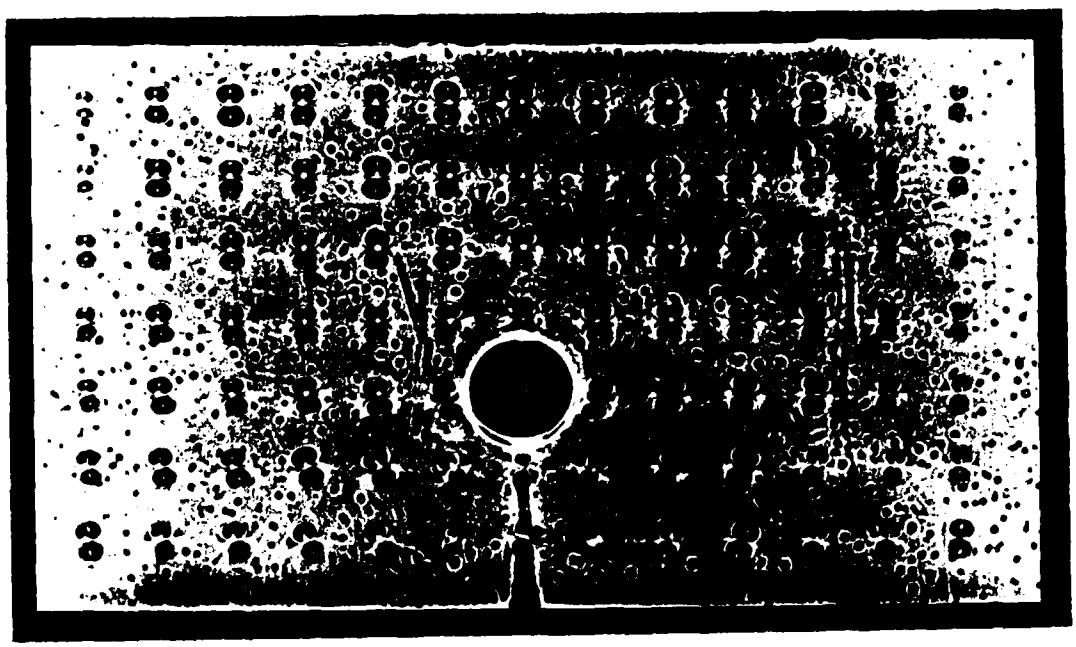

Fig. 23 Crack tip caustic and caustics of a hole field under tensile loading

The complete history of the crack tip stress intensification from the beginning of the impact procress on is shown in Fig. 24. A specimen with a sawed in initial notch has been utilized in the experiment. Since the surfaces of the notch cannot come into contact with each other during the compressive loading phase, a compressive stress intensification (negative stress intensity factor K_I) builds up first, as is indicated in frames No. 1 to 8. These compressive crack tip caustics then disappear when the tensile loading phase starts at 0 µs and change into tensile crack tip caustics.

The crack tip caustic observed in Figs. 23 and 24 are of good quality. Thus, any difficulties in analyzing these shadow patterns were not expected.

4.1.2 Crack Instability Experiments

A series of experiments had been performed to generate the first instability data and to find the appropriate impact parameters for the main investigations. Specimens with initial cracks of different lengths were prepared the following way: A notch of length less than the desired length has been sawed into the specimen. This notch was subsequently extended in length by precracking using a wedge loading device. In order to allow for an undisturbed passage of the compressive stress pulse across the crack, a plate of thickness equal to the width of the notch was inserted into the notch.

The results of a typical experiment are shown in Figs. 25 and 26. In Fig. 25 twelve frames of a series of 24 shadow optical pictures are reproduced. The camera has been delayed by an appropriate time to only analyze the shadow patterns under tensile loading. The frames No. 1 to 4 show the increase of the dynamic stress intensity factor at the tip of the stationary crack. At frame No. 5 the crack has become unstable. Frames No. 6 to 12 show the propagating crack. Due to the sudden acceleration of the crack tip, relief waves are radiated from the crack tip into the specimen which were visible in some of the photographs.

Fig. 26 shows quantitative data obtained according to eq. (1) from the shadow optical photographs. The dynamic stress intensity factor, K_I^{dyn}, and the momentary position of the crack tip, a, are plotted as functions of time. The a(t)-data give an indication of the time at which the crack became unstable. With this information the interesting parameters can be determined: the critical stress intensity factor for onset of rapid crack propagation, i.e. the dynamic fracture toughness, K_{Id}; the time to fracture, t_f; and the effective stress intensification rate, $\dot{K}_I^{dyn}$.

At velocities higher than about 40 m/s damage of the specimen under the contact area with the projectile was observed. The maximum allowable impact velocity for the direct loading arrangement, therefore, is in the range of 40 m/s. The stress intensification rate for specimens of the given size and material accordingly is of the order of 10^5 $MNm^{-3/2}s^{-1}$. The limiting velocity of course is considerably larger when steel specimens are investigated. Results of the main experiments with a systematic variation of test parameters are reported in Chapter 5.

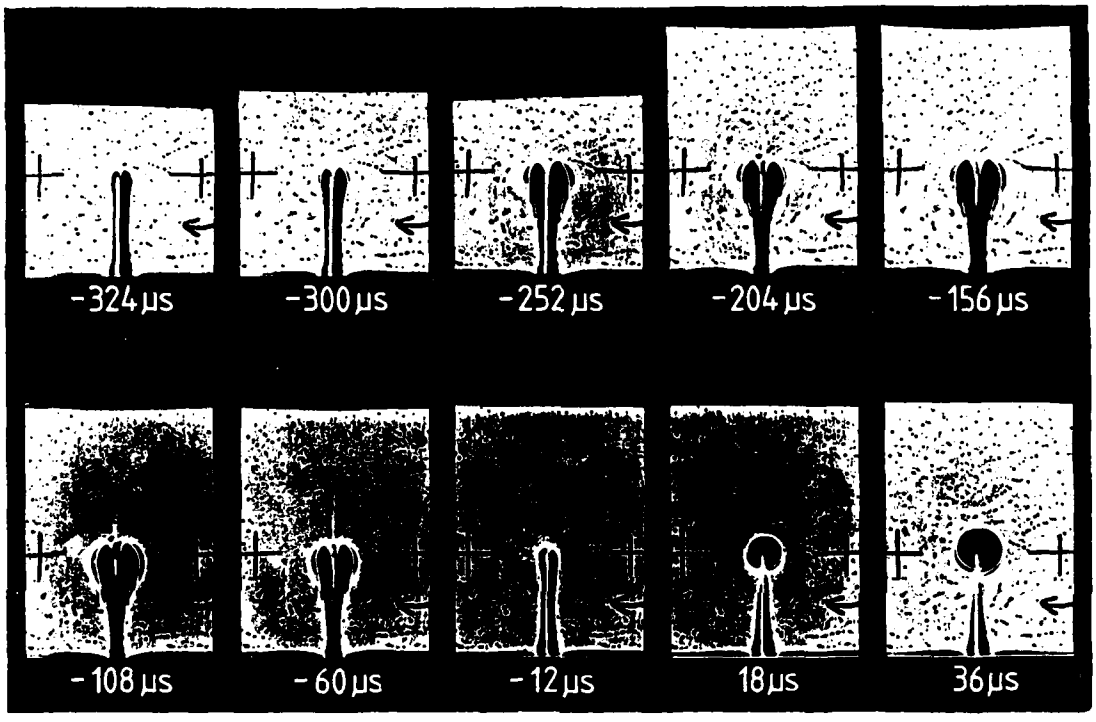

Fig. 24 Complete listing of compressive and subsequent tensile crack tip caustics

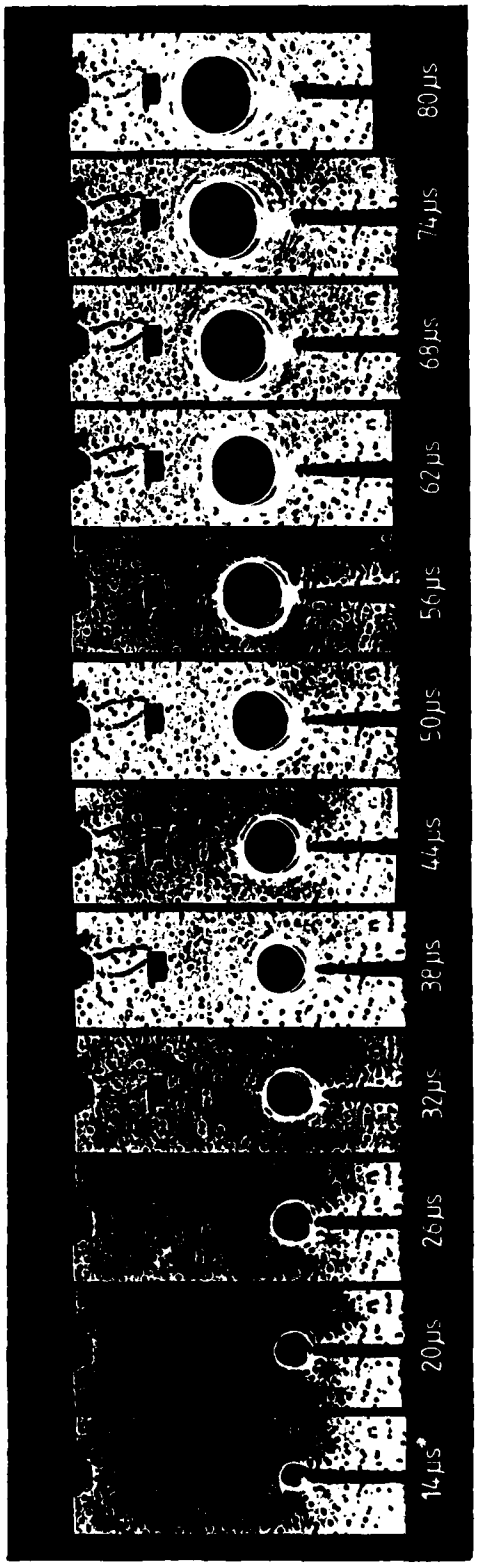

Fig. 25 Crack tip caustics, single crack under direct impact loading

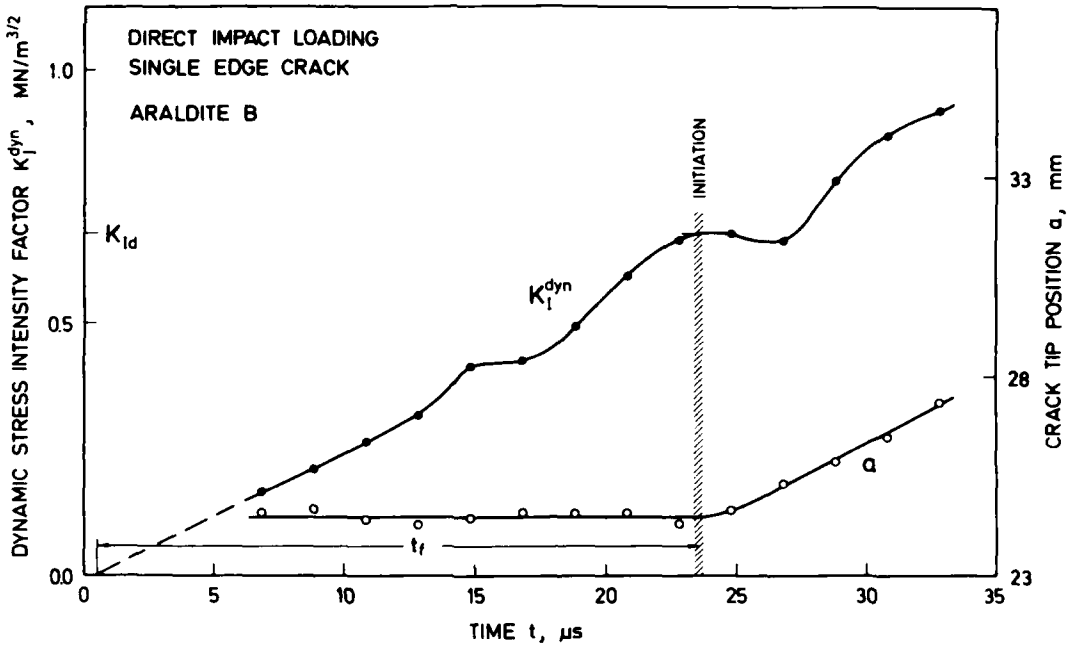

Fig. 26 Dynamic stress intensity factor and crack tip position, direct impact loading

4.2 Base Plate Loading

Since the stress distribution in the specimen under base plate loading conditions is much simpler than under direct impact conditions a detailed investigation of the distribution of stresses in the specimens has not been considered necessary. The loading arrangement has been tested by directly performing impact experiments with pre-notched or pre-cracked specimens.

To allow for a comparison with the direct impact data the specimen dimensions have been chosen the same as for the direct loading experiments, i.e. the specimens were 400 mm long, 100 mm wide and 10 mm thick Two specimens were simultaneously tested in the dual specimen loading fixture. Different crack configurations were utilized for the two specimens. Usually one of the specimens contained a single crack, whereas the other specimen contained a double crack configuration. The two specimens were fastened to a steel base plate (100 mm x 100 mm, 20 mm thick, 1.6 kg mass) which was impacted by steel projectiles of 50 mm diameter and different lengths.

Typical results are shown in Figs. 27, 28 and 29. Fig. 27 shows a series of shadow optical photographs. It shall be emphasized again that these pictures do not show one specimen with a configuration of three cracks, but two specimens, one with a single crack (i.e. the middle crack in the photographs) and another with a double crack configuration (i.e. the outer cracks in the photographs). The tensile stress pulse impinges on the cracks from the right hand side. The crack which is loaded the longest time exhibits the largest stress intensity factors. The shadow patterns of the middle crack and of the left hand crack are of pure mode-I type (at least at early times). The shadow pattern of the right hand crack shows a mixed mode loading from the very beginning on,since this crack is influenced by the left hand crack tip stress field. In frame No. 11, at 110 μs, the left hand crack becomes unstable and propagates through the specimen. Later on, at 150 μs, the center crack (i.e. the single crack in the other specimen) becomes unstable. The single crack propagates along its original direction without any deviation. The path of the left hand crack shows a slight deviation from the original crack direction, indicating a small superimposed mode-II loading. The observed experimental findings are in accordance with expectations.

Quantitative data for the single crack are shown in Fig. 28. The dynamic stress intensity factor, K_I^{dyn}, and the momentary crack length, a, are plotted as functions of time. As under direct loading conditions, the properties K_{Id}, t_f and K_I^{dyn} can be obtained from these plots. Fig. 29 shows quantitative results for the right hand crack of the double crack configuration of Fig. 27. The stress intensity factor K_I^{dyn} and the mode-II stress intenstiy factor K_{II}^{dyn} are plotted as functions of time. Since the crack did not become unstable, the crack tip position is not shown. Data of this kind give information on the mutual interaction of multiple cracks under dynamic loading condition.

Numerous experiments have been performed to study the reproducibility of

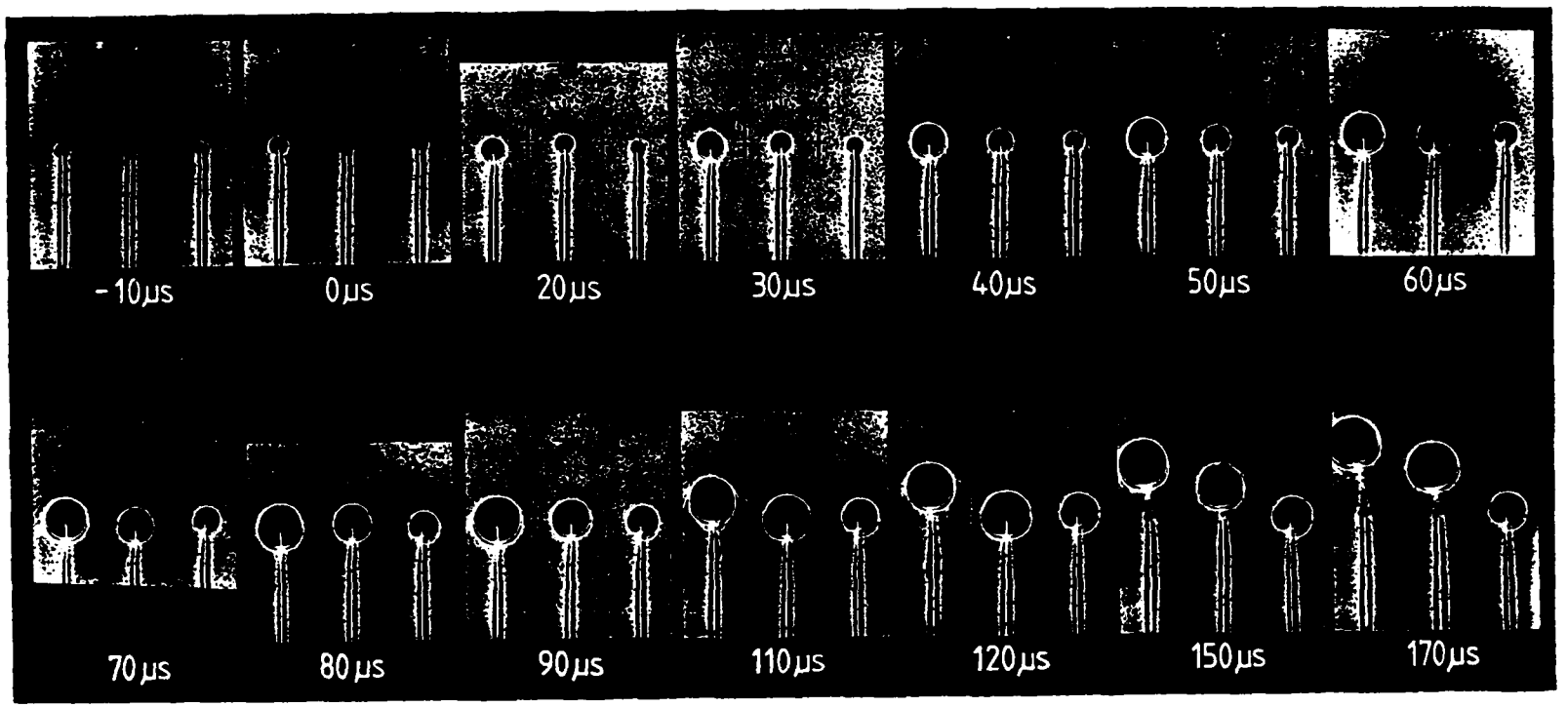

Fig. 27 Crack tip caustics, a single crack (inner) and a double crack configuration (outer cracks) under base plate loading

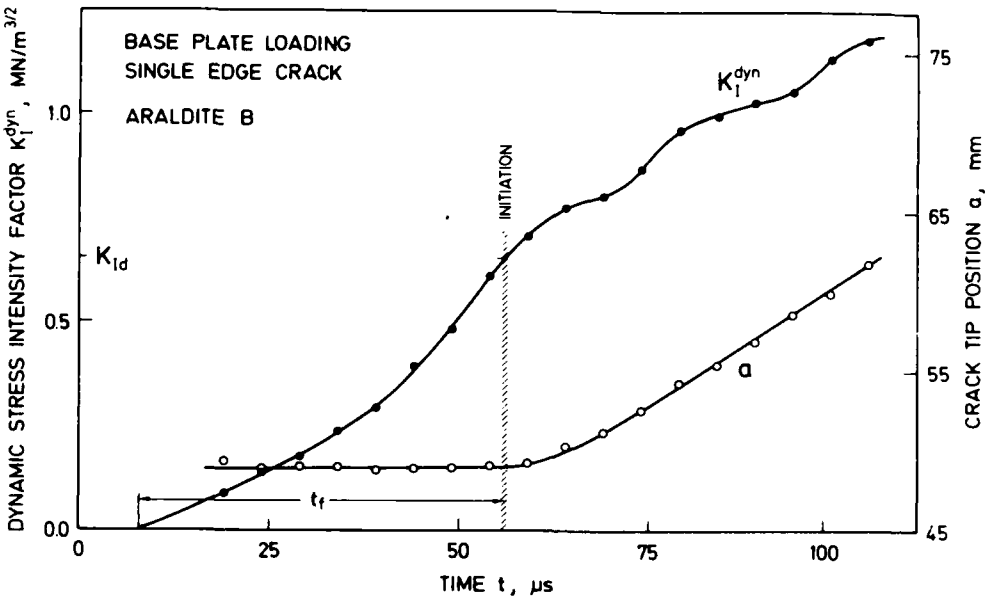

Fig. 28 Dynamic stress intensity factor and crack tip position, base plate loading

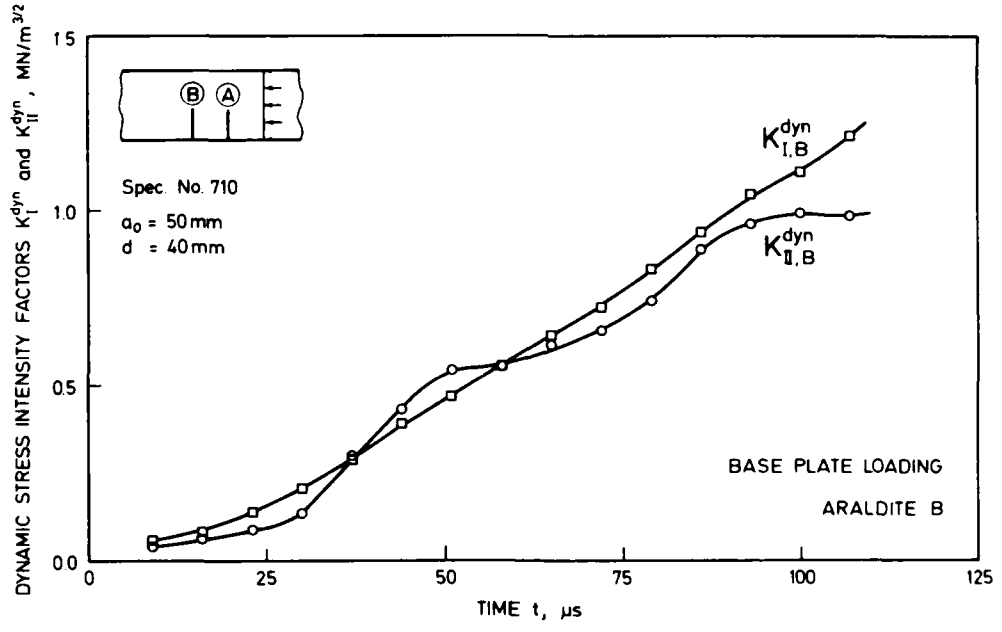

Fig. 29 Mode I and mode II stress intensity factors for a double crack configuration under base plate loading

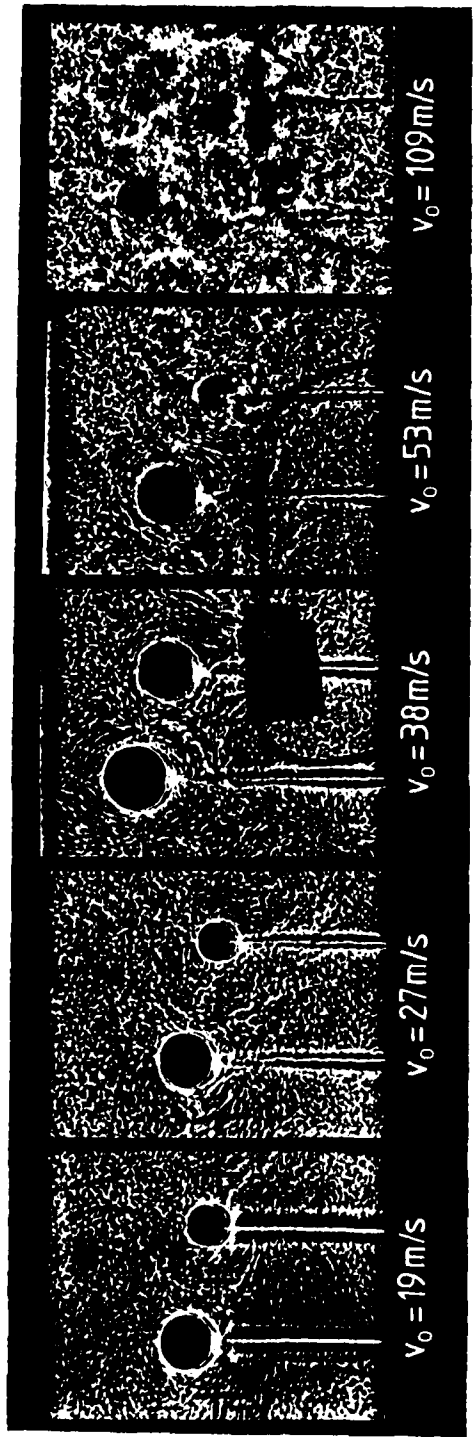

Fig. 30 Disturbance of caustics by air turbulence

the base plate loading arrangement. Early data indicate that the increase of the stress intensity factor with time was different although the impact conditions, in particular the impact velocities, were the same. More detailed investigations revealed a strong influence of the procedure how the specimens were fastened to the base plate. This difficulty was overcome by using fluted edges at the base plate and by fastening the specimens to the base plate in a controlled manner using a torque wrench.

A subsequent series of experiments has been performed by varying the impact velocity from about 10 m/s to 110 m/s. Fig. 30 shows the resulting shadow optical photographs. At higher impact velocities the pictures become disturbed by turbulences of the air following the projectile. Up to about 30 m/s this effect is of no influence. Up to 40 m/s the photographs can still be evaluated, but at higher velocitites it is not possible any more to derive reliable quantitative data. The base plate loading arrangement, therefore, is limited to a maximum impact velocity of about 40 m/s. The stress intensification rate then is of the order of 10^4 $MNm^{-3/2}s^{-1}$ when applied to Araldite B specimens. Results of the main experiments with a systematic variation of test parameters are reported in the next chapter.

5. DEPENDENCE OF IMPACT FRACTURE TOUGHNESS ON LOADING RATE

5.1 Experiments with Araldite B Specimens

Experiments with a systematic variation of test parameters have been performed to investigate the dependence of the impact fracture toughness K_{Id} on loading rate. Most impact fracture data reported so far in the literature have been measured at modest loading rates under drop weight loading or in pendulum type impact devices. Under these loading conditions the impact fracture toughness in general decreases with increasing loading rate, as already shown in Fig. 3. Experiments at higher loading rates allow to discriminate between the following behavior: a) a continuous decrease of the impact fracture toughness with increasing loading rate to zero values, b) the existence of a minimum fracture toughness which cannot be undergone even if the loading rate is increased, or c) a decrease of toughness followed by a final increase at very high loading rates. These different possibilities of the impact fracture toughness behavior are shown in the schematic representation of Fig. 31. Within this research project impact fracture toughness data at higher loading rates than under drop weight loading conditions are generated applying the two different techniques of directly impacting the specimen by a projectile (Section 4.1) or by loading the specimen in the base plate test arrangement (Section 4.2).

5.1.1 Results on Base Plate Loading Experiments

Precracked specimens made from the model material Araldite B have been dynamically loaded in the base plate loading arrangement (see Figs. 4b and 12). Details of the experimental procedure have been reported in Section 4.2 of this report. Some data that are necessary for the

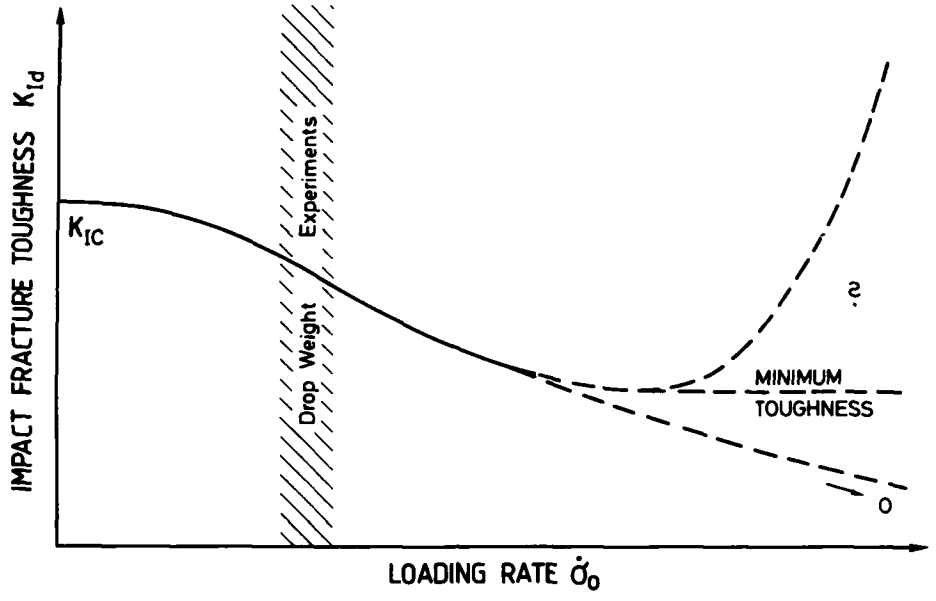

Fig. 31 Possible behaviour of impact fracture toughness on loading rate

following presentation of results shall be repeated here: The specimen dimensions are 400 mm x 100 mm x 10 mm. The specimens were precracked by a single edge crack. The crack length has been varied from 20 mm to 50 mm. Due to symmetry reasons two specimens were simultaneously tested in each experiment. In order to allow for an undisturbed observation of each individual caustic, the cracks of length less than 50 mm (i.e.half the specimen width) were inserted from opposite edges of the specimens. In the case of specimens containing crack lengths $>$ 50 mm specimens with double crack configurations have been used in the second test specimen. The results obtained from the double crack configuration are presented later in Chapter 6 "Dynamic Interaction of Multiple Cracks".

The two specimens are fastened at one end of the base plate (100 mm x 100 mm x 20 mm) made from a hardened steel (1.6 kg mass). The other ends are fastened to the muzzle of the gas gun. The base plate is accelerated by an impinging steel projectile of 50 mm diameter. Projectiles of different lengths, i.e. different masses, have been utilized in the experiments: 50 mm, 75 mm and 140 mm. The impact velocity has been varied from about 10 m/s to 40 m/s.

About 60 experiments have been performed. Several experiments failed due to experimental difficulties. A complete series of experiments showing very large uncontrolled scatter in the data had to be rejected since heavy work was simultaneously going on in the laboratory due to moving of heavy test equipment from one institute building into another. Data of successful experiments are summarized in Table 1. Presented are the specimen and projectile dimensions, the impact velocity, and data on the crack instability behavior, i.e. the time-to-fracture, t_f, and the impact fracture toughness, K_{Id}. When specimens with double crack configurations were simultaneously tested, these data are given here as well for completeness.

In Figs. 32 and 33 the obtained times-to-fracture t_f and the stress intensification rated $\dot{K}_I^{dyn}$ are plotted as functions of the impact velocity v_o. Most of the data were obtained from shots with projectiles of 75 mm length, i.e. 1 kg mass. Only some experiments have been performed with projectiles of different masses: 2 kg (140 mm length) and 0.5 kg (59 mm length). In accordance with expectations the time to fracture becomes smaller with increasing impact velocity and the stress intensification rate $\dot{K}_I^{dyn}$ accordingly increases with increasing impact velocity. The scatter of the data is rather high, in particular for the stress intensification rate. Changes in the results due to variations in the mass of the projectile were not significant. It is speculated that the large scatter is due to still existing slight variations in the process of how the specimens are fastened to the base plate (see Section 4.2).

In Figs. 34 and 35 the impact fracture toughness values K_{Id} are plotted as functions of the impact velocity v_o and the time-to-fracture t_f. The data show a scatter of about 10 to 20 % which is usual for toughness testing. Within the range of achieved loading rates the K_{Id} data do not vary. In Figs. 34 and 35 the data scatter around the value of 0.67 $MN/m^{3/2}$, which is almost the same as the static fracture

Spec. No.	Crack Length a_o, mm	Crack Distance d, mm	Crack Tip	Projectile			Time to Fracture t_f, µs	Impact Fracture Toughness K_{Id}, $MN/m^{3/2}$
				m, kg	l, mm	v_o, m/s		
670	50	0	b	1.02	75	10.7	-	-
(670	50	60	b	1.02	75	10.7	-	-)
674	50	0	b	1.02	75	10.1	-	-
(674	50	60	b	1.02	75	10.1	-	-)
677	50	0	s	2.01	139	9.6	-	0.664
(677	50	60	s	2.01	139	9.6	-	0.640)
687	50	0	s	1.02	74	9.9	-	-
(687	50	60	s	1.02	74	9.9	-	-)
688	50	0	s	1.02	74	10.1	52.0	0.600
(688	50	60	s	1.02	74	10.1	51.5	0.640)
689	50	0	s	1.02	74	9.3	52.5	0.640
(689	50	60	s	1.02	74	9.3	41.5	0.610)
690	50	0	s	1.02	74	8.9	-	-
(690	50	60	s	1.02	74	8.9	44.5	0.650)
691	50	0	s	1.02	74	31.9	39.0	0.670
(691	50	60	s	1.02	74	31.9	-	-)
692	40	0	s	1.02	74	9.4	38.0	0.650
692	40.5	0	s	1.02	74	9.4	-	-
693	40	0	s	1.02	74	9.4	-	-
693	40.5	0	s	1.02	74	9.4	12.5	0.640
694	40	0	s	1.02	78	31.9	-	-
694	40.5	0	s	1.02	78	31.9	-	-
695	40	0	s	1.02	78	31.8	-	-
695	40	0	s	1.02	78	31.8	16.0	0.770
696	40	0	s	1.02	78	31.4	-	-
696	40.5	0	s	1.02	78	31.4	17.8	0.650
697	40	0	s	1.02	78	31.4	32.3	0.640
697	40	0	s	1.02	78	31.4	24.3	0.505
698	40.5	0	s	1.02	78	31.8	28.3	0.580
698	40.5	0	s	1.02	78	31.8	28.8	0.710
699	30	0	s	1.02	78	31.3	23.5	0.660
699	30	0	s	1.02	78	31.3		

700	30	0	s	1.02	78	39.1	27.0	-
700	30	0	s	1.02	78	39.1	18.0	-
701	50	0	s	1.02	78	18.9	25.0	0.490
(701	50	60	s	1.02	78	18.9	27.0	0.650)
702	50	0	s	1.02	78	26.9	28.5	0.580
(702	50	60	s	1.02	78	26.9	31.5	0.600)
703	50	0	s	1.02	78	26.9	32.5	0.550
(703	50	60	s	1.02	78	26.9	29.0	0.650)
705	50	0	s	1.98	142	9.7	-	-
(705	50	60	s	1.98	142	9.7	45.0	0.650)
706	50	0	s	1.98	142	9.6	55.0	0.650
(706	50	60	s	1.98	142	9.6	47.0	0.700)
707	50	0	s	0.51	50	9.7	54.0	0.690
(707	50	60	s	0.51	50	9.7	45.5	0.660)
717	15	0	b	1.02	78	9.2	-	-
(717	15	20	b	1.02	78	9.2	-	-)

s = sharp, b = blunted

Table 1 Test conditions and results of base plate loading experiments, single edge cracks, Araldite B

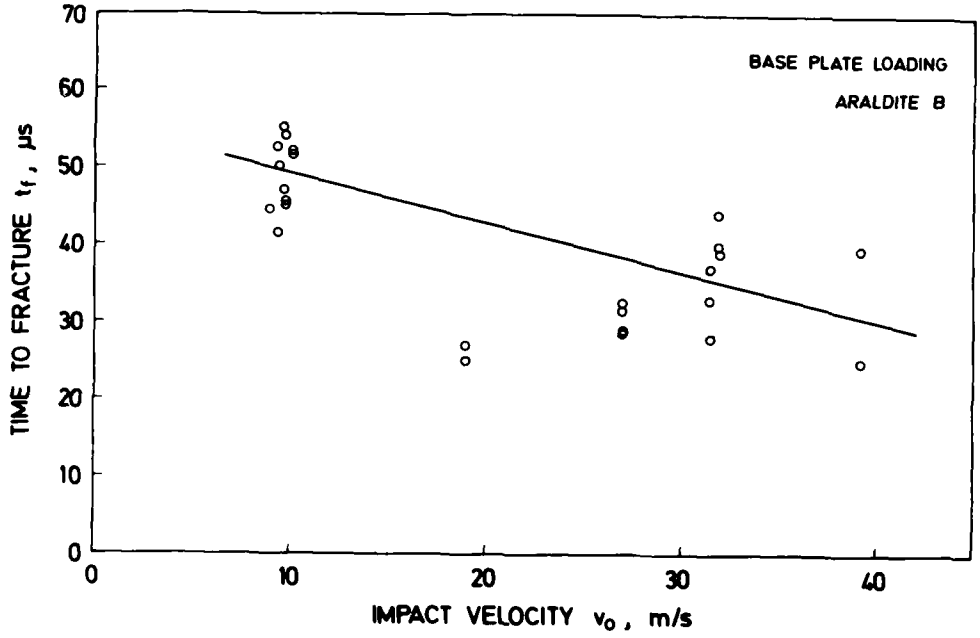

Fig. 32 Time to fracture versus impact velocity

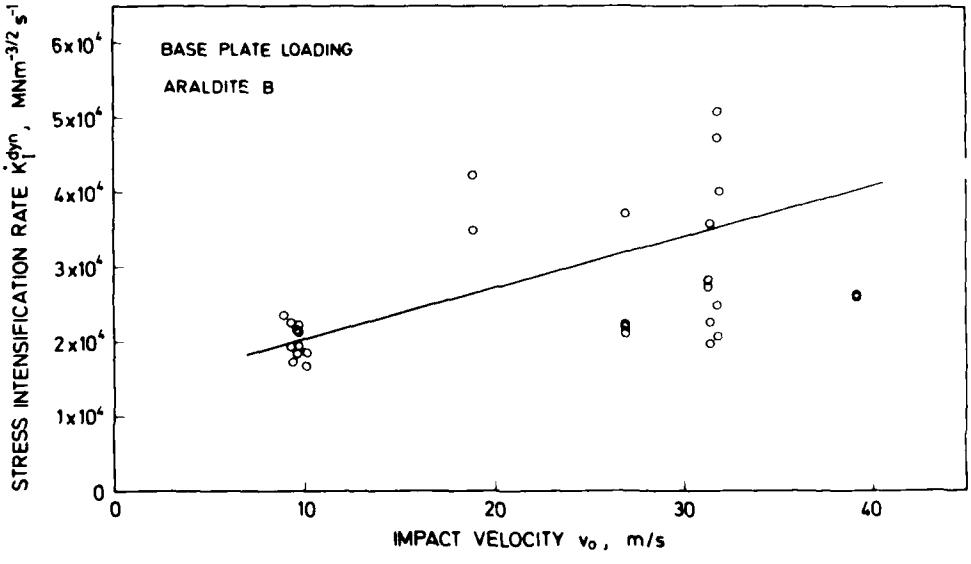

Fig. 33 Stress intensification rate versus impact velocity

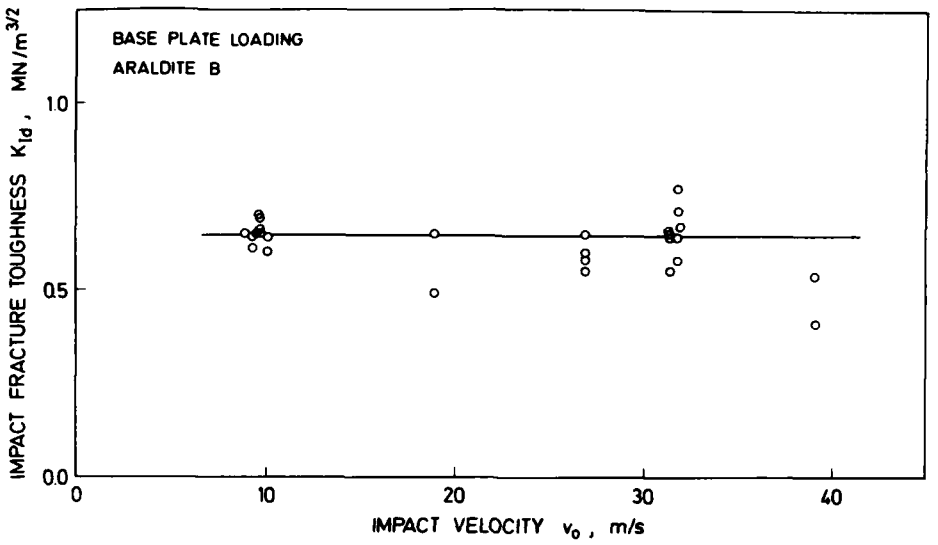

Fig. 34 Impact fracture toughness versus impact velocity

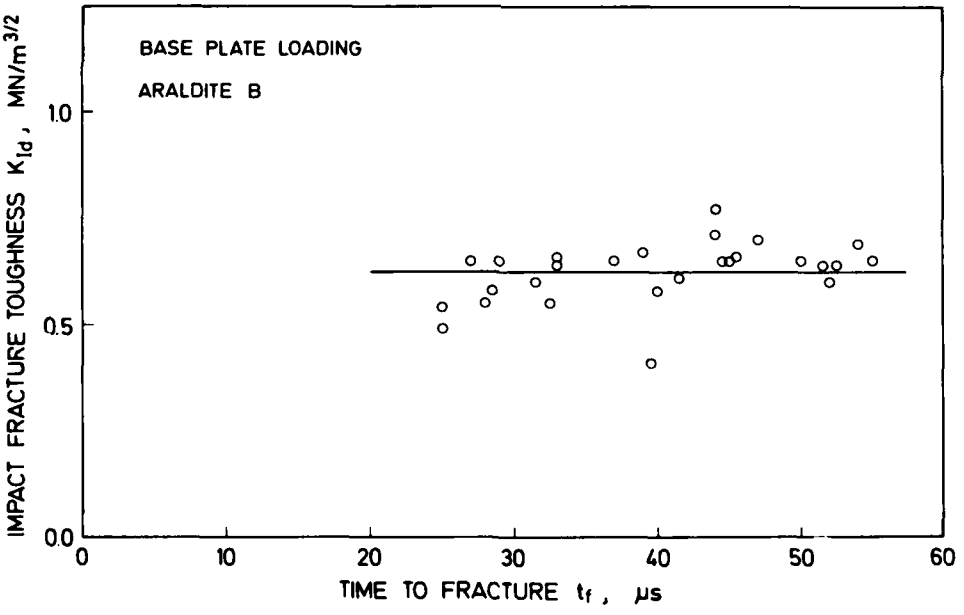

Fig. 35 Impact fracture toughness versus time-to-fracture

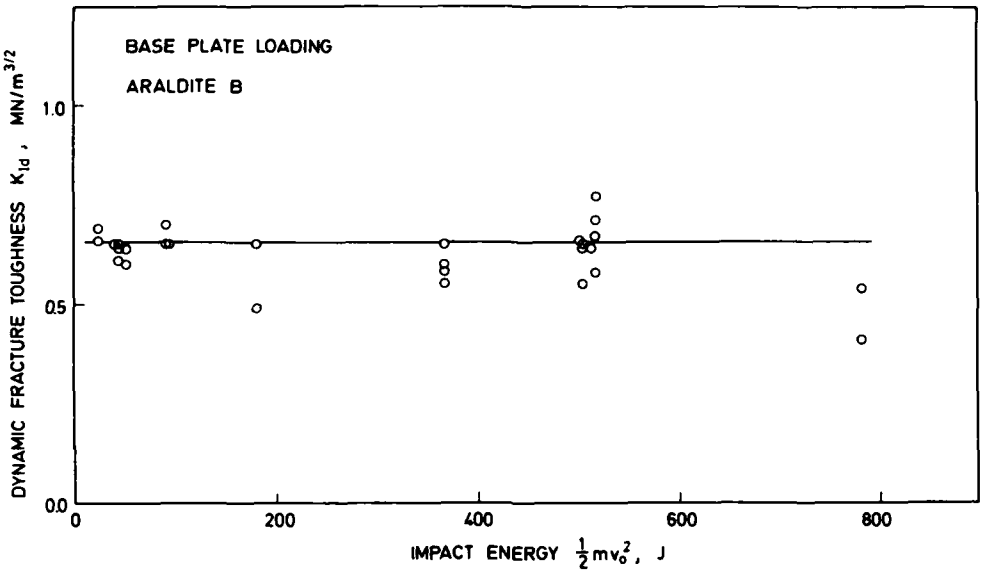

Fig. 36 Impact fracture toughness versus impact energy

toughness value $K_{Ic} = 0.7\ MN/m^{3/2}$. In Fig. 36 the impact fracture toughness data are plotted as a function of the kinetic energy of the projectile, $1/2\ m \cdot v_o^2$, where m is the mass of the projectile. As in the previous two diagrams a dependence of the impact fracture toughness is not observed.

It is speculated that the observation of constant fracture toughness data as a function of loading rate is due to two facts: First, Araldite B is a very brittle material and loading rate effects will have only little influence on the material behavior. Secondly, the times to fracture achieved in the experiments were still rather large, i.e. the maximum obtained loading rate was only modest.

5.1.2 Results of Direct Impact Loading Experiments

Similar specimens as tested in the base plate loading arrangement have been directly impacted by a projectile. As in the investigations discussed before the specimens were made from Araldite B, the dimensions were 400 mm x 100 mm x 10 mm. The length of the initial cracks was varied from 12 mm to 40 mm. Projectiles of 50 mm diameter and 200 mm length, machined from Araldite B, were utilized in these experiments. For further details of the experimental procedure see Section 4.1 of this report. The impact velocity in the experiments was varied from about 10 m/s to about 50 m/s.

About 100 experiments total have been performed. The results of successful experiments which have been utilized in the following graphs are summarized in Table 2.

In Figs. 37 and 38 the obtained times to fracture t_f and the stress intensification rates $\dot{K}_I^{dyn}$ are plotted as a function of the impact velocity v_o (full data points). For comparison the equivalent data obtained under base plate loading conditions (open data points) are shown in the same diagram. In accordance with expectations the times to fracture become smaller and the stress intensification rates are higher than for base plate loading conditions. The differences in loading rates are about a factor of 3 for the same impact velocity.

Fig. 39 shows the impact fracture toughness data K_{Id} as a function of the time to fracture (full data points) together with the data of the base plate loading experiments (open data points). The data from the direct impact experiments supplement the base plate data into the lower time to fracture regime. All data, however, fall within the same scatter band, indicating no influence of loading rate on the impact fracture toughness for the range of loading rates considered.

A strong increase of the fracture toughness with increasing loading rate, i.e. with decreasing time to fracture, was, however, observed by Ravi Chandar and Knauss [48] with Homalite-100 specimens loaded by electro-magnetic techniques (see Fig. 40). Obviously these two experimental findings are contradictions.

Spec. No.	Crack Length a_o, mm	Crack Tip	Projectile			Time to Fracture t_f, μs	Impact Fracture Toughness K_{Id}, $MN/m^{3/2}$
			m, kg	l, mm	v_o, m/s		
623	34.0	s	0.48	200	25.9	11.0	0.562
655	25.0	s	0.48	200	8.6	18.5	0.730
656	25.0	s	0.48	200	11.7	-	-
657	25.0	s	0.48	200	10.5	21.0	0.670
658	25.0	s	0.48	200	10.6	20.0	0.690
659	31.5	s	0.48	200	9.8	11.2	0.710
660	32.0	s	0.48	200	11.4	20.0	0.690
661	32.0	s	0.48	200	11.4	14.2	0.670
662	40.0	s	0.48	200	11.8	-	0.680
663	40.0	s	0.48	200	10.9	-	0.660
664	12.0	s	0.48	200	13.0	-	0.670
665	12.5	s	0.48	200	13.0	-	-
666	12.0	s	0.48	200	13.3	-	-
667	12.5	s	0.48	200	11.9	12.5	0.670
795	54.0	s	0.48	200	23.0	11.5	0.64
796	52.5	s	0.48	200	21.9	14.0	0.94
797	55.0	s	0.48	200	27.2	15.4	0.86
798	55.0	s	0.48	200	26.5	-	-
799	52.5	s	0.48	200	28.7	-	-
800	47.0	s	0.48	200	24.6	-	-
801	53.0	s	0.48	200	27.1	-	-
802	48.5	s	0.48	200	29.0	9.5	0.70
803	49.5	s	0.48	200	30.0	9.8	0.72
804	49.0	s	0.48	200	24.6	11.8	0.68
805	51.0	s	0.48	200	38.0	7.2	0.73
806	49.0	s	0.48	200	36.8	7.2	0.70
807	49.0	s	0.48	200	37.5	7.6	0.67

808	53.5	s	0.48	200	29.4	10.0	0.69
809	49.0	s	0.48	200	24.0	13.6	0.73
810	49.5	s	0.48	200	37.8	-	-
811	50.0	s	0.48	200	37.3	9.0	0.81
812	48.5	s	0.48	200	36.8	-	-
813	49.0	s	0.48	200	37.3	7.2	0.64
814	49.5	s	0.48	200	38.6	7.0	0.50
815	49.5	s	0.48	200	46.3	-	-
816	51.0	s	0.48	200	46.3	7.2	0.65
817	50.0	s	0.48	200	52.5	-	-
818	48.5	s	0.48	200	52.7	-	-
819	48.0	s	0.48	200	53.4	-	-
820	45.0	s	0.48	200	53.5	-	-
821	49.0	s	0.48	200	45.6	-	0.70
822	49.5	s	0.48	200	46.0	-	-

s = sharp, b = blunted

Table 2 Test conditions and results of direct impact loading experiments, single edge cracks, Araldite B

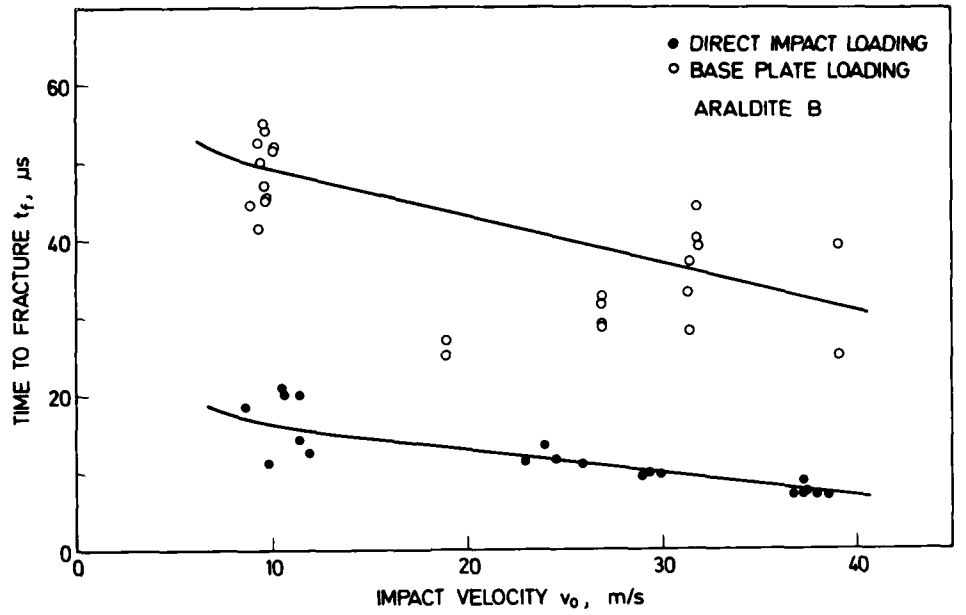

Fig. 37 Times-to-fracture versus impact velocity

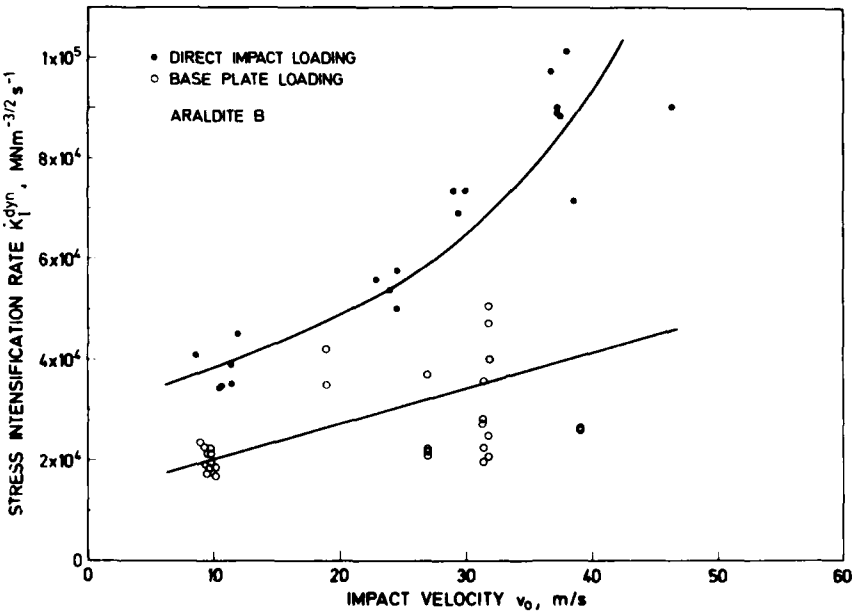

Fig. 38 Stress intensification rates versus impact velocity

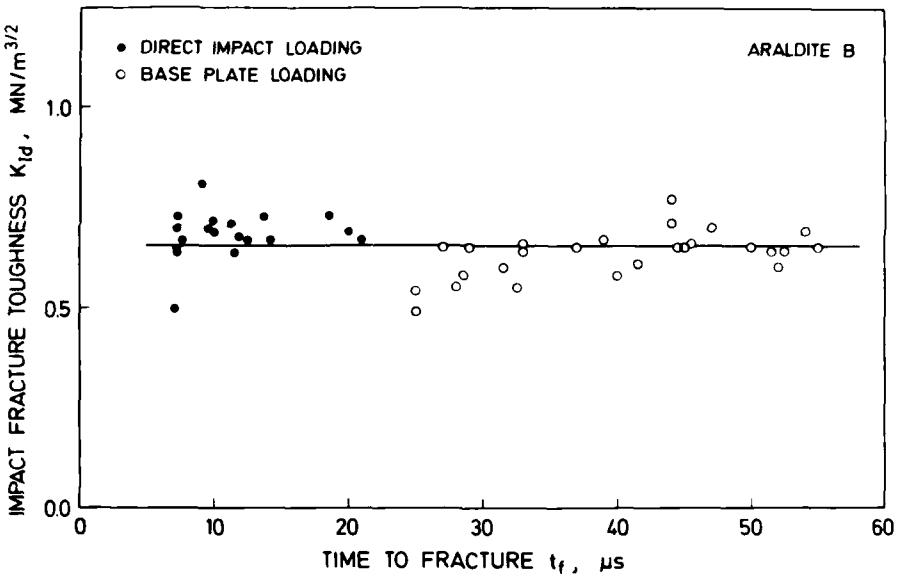

Fig. 39 Impact fracture toughness versus time-to-fracture

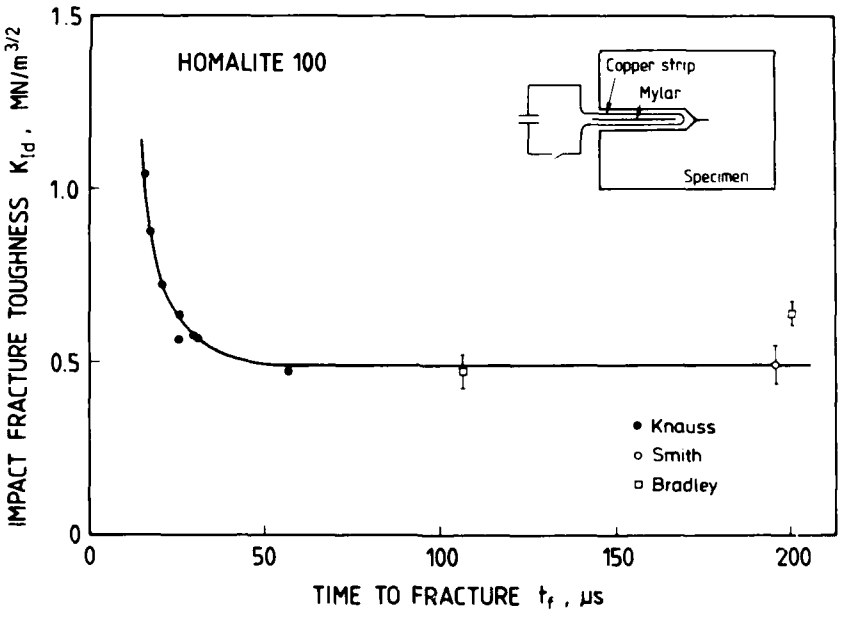

Fig. 40 Dependence of impact fracture toughness on time-to-fracture (after Ravi-Chandar, Knauss [48])

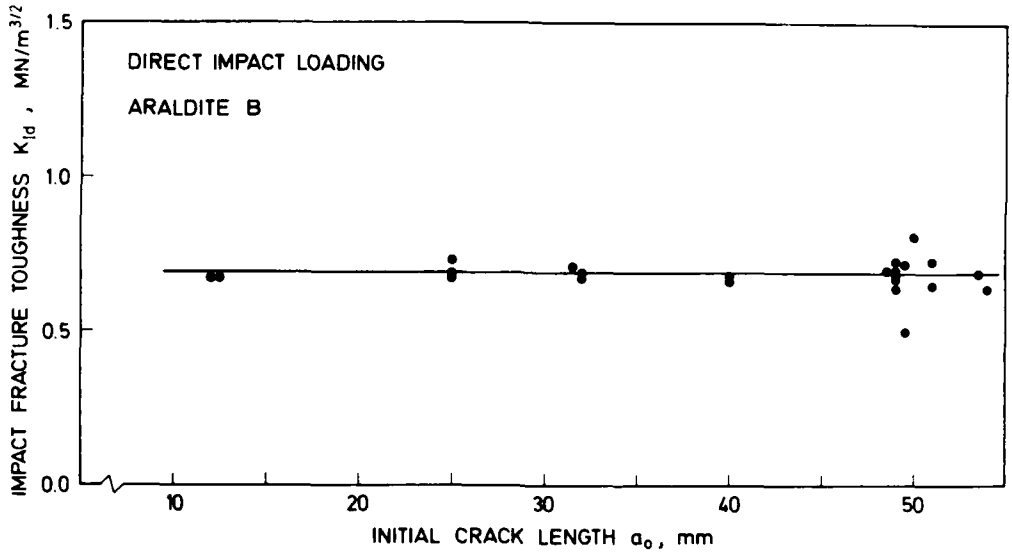

Fig. 41 Impact fracture toughness versus crack length

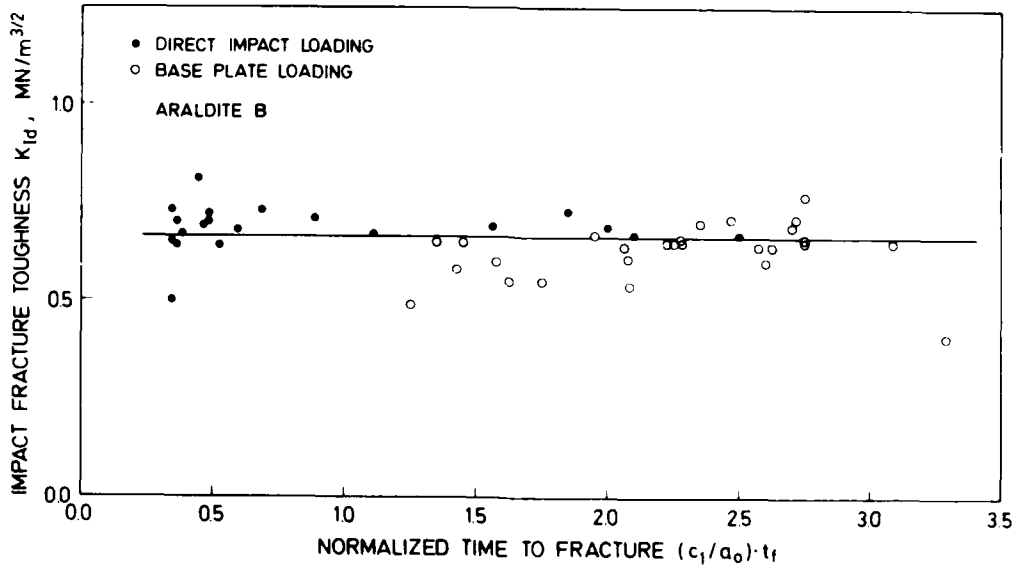

Fig. 42 Impact fracture toughness versus normalized time-to-fracture

Since it might also be possible that not the absolute time-to-fracture t_f but the ratio of the time-to-fracture to the crack length, t_f/a_o, influences the instability event the crack length has been varied in the experiments. Figs. 41 shows the measured impact fracture toughness data as a function of crack length. In Fig. 42 all data (obtained under base plate loading - and under direct impact loading) are plotted as a function of the dimensionless time $(c_1/a_o)t$, where c_1 is the longitudinal wave velocity. Also this plot does not show any trend in the data but a constant behavior.

5.2 Experiments with Steel Specimens.

After the investigations with Araldite B specimens had been finished an analogous research program has been carried through with steel specimens. The investigation of steel specimens is of greater practical relevance than of specimens made from the model material Araldite B: The wave propagation phenomena, in particular wave speed and attenuation of waves, and the failure mechanisms of the material are closer to those of possible cases of practical interest. Furthermore, steels behave in a less brittle manner than Araldite B and they are more strain rate sensitive, too. Thus, it is expected that more interesting results on the dependence of the impact fracture toughness K_{Id} with loading rate can be observed.

A special high strength maraging steel X2 NiCoMo 18 9 5 (HFX 760, produced by Stahlwerke Südwestfalen) has been chosen for these investigations (nominal composition: 18% Ni, 9% Co, 4.8% Mo and $<$ 0.03% C, heat treatment 480^{o}C for 4 hours in air). This steel is similar to the American designation 18 Ni maraging grade 300. The special steel X2 NiCoMo 18 9 5 has been chosen since it has been used before in the laboratory with other investigations and since it is very well suited for an application of the shadow optical method of caustics. The steel is very well characterized with regard to its mechanical parameters and fracture properties and the investigators are well familiar with this material. Thus, much preliminary research work had been avoided by selecting this steel for the research program.

Since the costs of material and in particular for specimen preparation are much higher with steel specimens than with Araldite B specimens, it was necessary to very carefully plan the experiments. Thus, the steel investigations had been performed only after sufficient knowledge and experience had been gathered with the Araldite B investigations, in particular with the loading technique and the shadow optical recording arrangement. Furthermore, the research program had been restricted to experiments with the direct loading arrangement only which had proven in the Araldite B investigations to be much faster than the base plate loading arrangement.

The specimen dimensions were almost the same as those of the Araldite B specimens: the width of the specimens was 100 mm, but the length of the specimens was only 260 mm instead of 400 mm to save material costs. Despite of the reduction in specimen length (see Section 4.1), the length of 260 mm has been found in pre-experiments to guarantee a

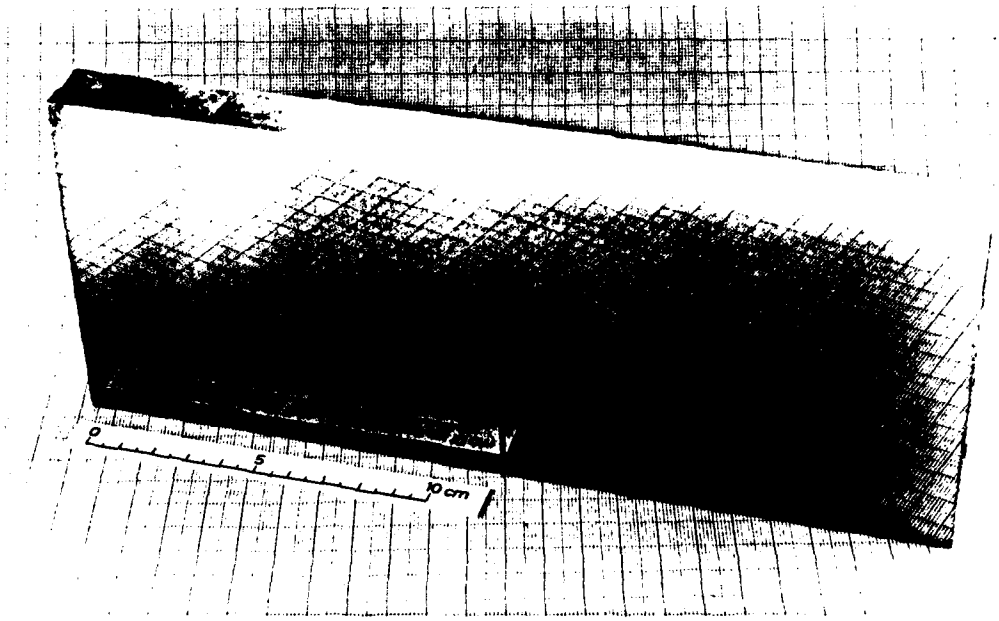

Fig. 43 Photograph of polished front surface of steel specimen

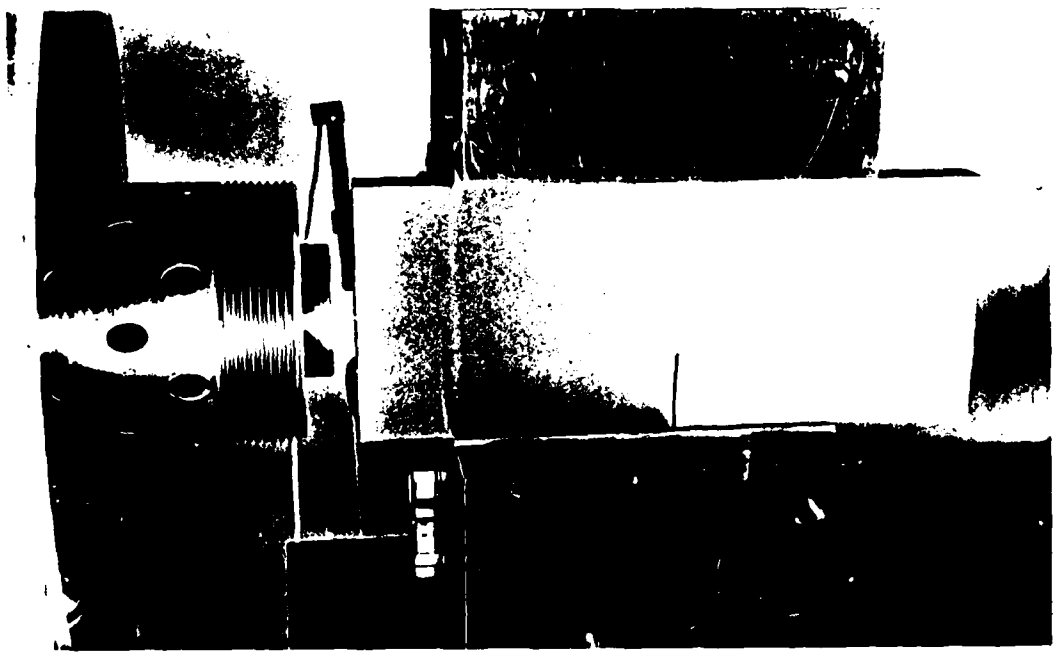

Fig. 44 Steel specimen in holding fixture

straight propagation of the crack through the specimen. The thickness of the specimen was about 20 mm. Similar to the Araldite B specimens, the steel specimens were prepared with a single-edge-notch (SEN) initial crack of about 50 mm, i.e. half the specimen width. In order to assure that the compressive stress pulse crosses the crack without any major disturbances the crack has been machined into the specimen over almost its entire length by fatigue loading. Special treatment was necessary to prepare one surface of the specimen that it could be used for shadow optical applications. In order to achieve a mirrored front surface of optical quality the specimen had been carefully ground and subsequently lapped and polished. In order to eliminate possible disturbances on the polished surface it often was necessary to perform the lapping process several times. Difficulties were often encountered since "dirt material" which was hidden inside the initial notch of the fatigue crack was set free by the lapping process then causing severe scratches on the specimen surface. The shadow optical method of caustics was applied in reflection with the steel specimens. The steel specimens were again impacted by projectiles made of the same material, i.e. steel, having a length of half the length of the specimens, i.e. 130 mm. Thus, the mass of the projectile was about 2 kg. Photographs of the specimen itself and of the specimen mounted in front of the muzzle of the IWM-gas gun are shown in Figs. 43 and 44.

Impact experiments have been performed with impact velocities ranging from about 10 m/s to 80 m/s. Some preliminary shots have been carried out in order to check the experimental set-up in combination with the steel specimens, in particular the loading arrangment and the shadow optical measuring technique when applied in reflection. No difficulties were encountered with the loading and the catcher arrangement. Despite of the considerably larger masses of both the specimen and the projectile the catcher tank was able to safely collect the moving parts after impact and to absorb the kinetic energy. Nevertheless it was necessary to replace certain parts of the catcher tank after several shots due to internal damage. Typical shadow optical photographs obtained for different impact velocities are shown in Fig. 45. It is recognized that undisturbed caustics are obtained for low impact velocities, i.e. 10 - 20 m/s. At higher impact velocities (e.g. 50 m/s), however, the shadow patterns are severely disturbed and do not allow a qualitative evaluation of caustics. Disturbances at high impact velocities have also been observed with Araldite B specimens loaded in the base plate arrangement (see Fig. 30) which then were caused by disturbances in the air from the gas gun following the projectile. The disturbances observed now with steel specimens under direct impact loading, however, are caused by Rayleighwaves which are excited on the surface of the specimen by the impinging projectile. In particular at high impact velocities the local deformations of the specimen surface were so large that the determination of a stress intensity factor became impossible. These Rayleighwave-disturbances restrict the allowable impact velocitiy to medium values of about 20 m/s. Further research work (see proposal for follow-on investigations) is necessary to eliminate or reduce the Rayleighwave-disturbances in order to make this technique of impact loading and shadow recording work at higher impact velocities and thus to achieve even higher loading rates.

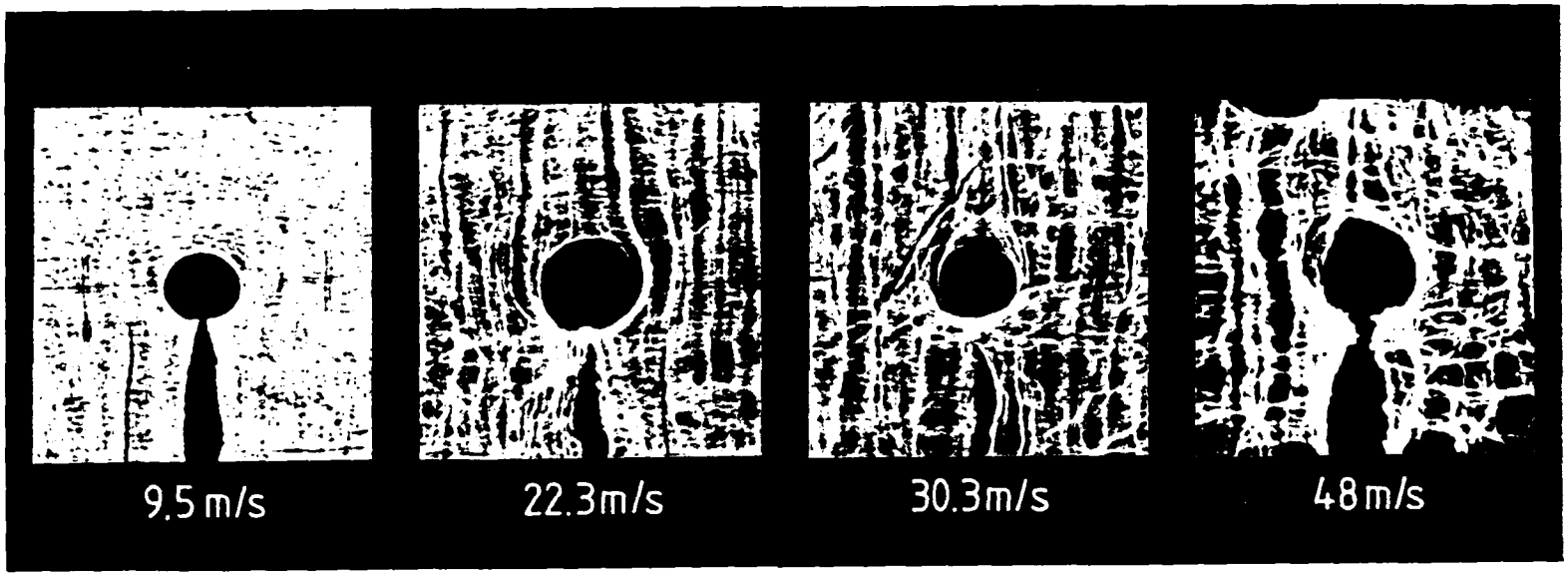

Fig. 45 Crack tip shadow patterns photographed in reflection with steel specimens. Disturbances due to Rayleigh waves at high impact velocities.

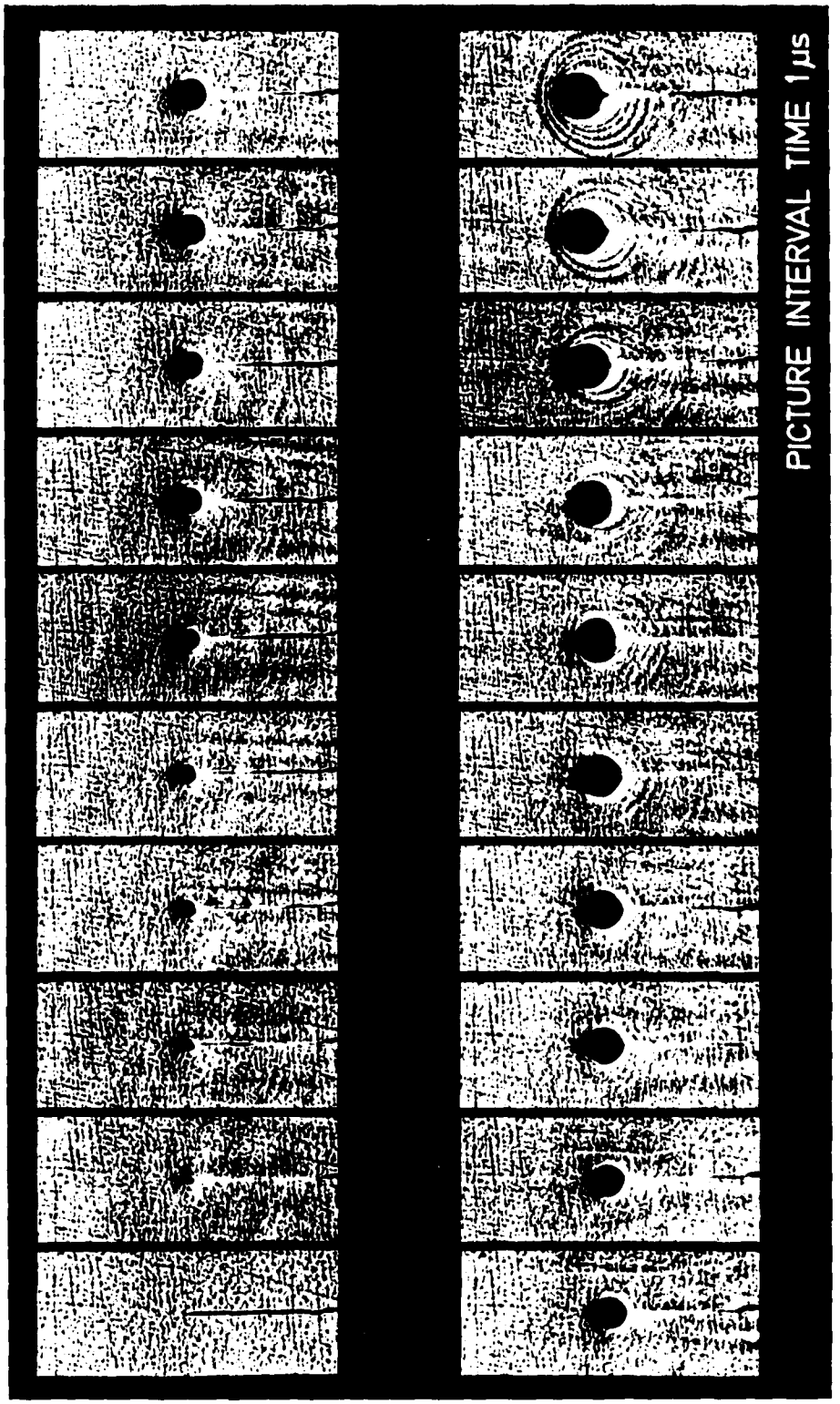

Fig. 46 High speed series of crack tip shadow patterns photographed in reflection with a high strength steel specimen

Spec. No.	Spec. Thickness t, mm	Crack Length a_o, mm	Crack Tip	Projectile			Time to Fracture t_f, μs	Impact Fracture Toughness K_{Id}, $Mm/m^{3/2}$	Remarks
				m, kg	L, mm	v_o, m/s			
780	17.5	49.0	b	1.93	125.0	7.3	–	–	P
781	17.5	49.0	b	1.93	125.0	7.3	–	–	P
782	17.5	50.2	b	1.93	125.0	48.0	–	–	P
783	17.5	49.0	b	1.91	124.6	8.3	–	–	P
784	17.5	49.0	b	1.91	124.6	9.5	–	–	P
785	17.5	49.0	b	1.91	124.6	15.0	–	–	P
786	17.5	50.0	b	3.11	200.0	9.8	–	–	P
787	17.2	50.0	b	3.11	200.0	9.9	–	–	P
788	17.2	50.0	b	3.11	200.0	9.8	–	–	P
789	17.2	50.0	b	3.11	200.0	15.0	–	–	P
790	17.2	50.0	b	3.05	200.0	20.1	–	–	P
791	17.2	50.0	b	3.05	200.0	30.3	–	–	P
792	17.5	48.5	b	1.90	124.0	7.9	–	–	P
793	17.5	48.5	b	1.90	124.0	7.0	–	–	P
794	17.5	48.5	b	1.90	124.0	22.3	–	–	P
824	19.0	45.0	b	1.90	124.0	20.3	–	–	P
825	17.2	0	b	1.90	124.0	19.1	–	–	P
826	17.2	0	b	1.90	124.0	20.1	–	–	P
827	7.7	45.0	b	1.90	124.0	20.6	–	–	P
828	7.7	45.0	b	1.90	124.0	21.3	–	–	P
829	19.0	45.0	b	1.90	124.0	19.1	–	–	P
836	19.0	45.0	b	1.90	124.0	21.4	–	–	P
837	19.0	45.0	b	1.90	124.0	29.9	–	–	P
840	7.7	45.0	b	1.87	123.6	21.5	–	–	P

852	17.0	51.0	s	1.90	125.1	19.6	—	—	M
853	18.2	51.0	s	1.90	125.1	19.7	6.3	50.0	M
854	16.8	50.5	s	1.90	125.1	19.5	7.1	45.0	M
855	17.3	49.7	s	1.90	125.0	19.8	7.5	42.0	M
856	16.8	50.3	s	1.90	125.0	9.6	13.9	42.0	M
857	18.4	50.3	s	1.90	125.0	27.8	6.5	55.0	M
861	18.5	51.2	s	1.90	125.0	47.0	5.7	91.5	M

s = sharp, b = blunt

P = Preexperiment, M = Mainexperiment

Table 3 Test conditions and results of direct impact loading experiments, single edge cracks, high strength steel X2 NiCoMo 18 9 5

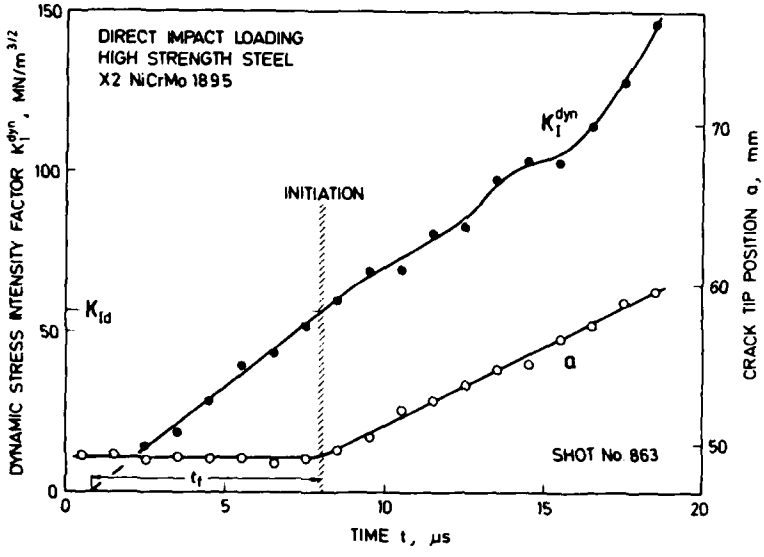

Fig. 47 Dynamic stress intensity factor and crack tip position, direct impact loading of steel specimen

Fig. 48 Fracture surface of high strength steel specimen X2 NiCoMo 18 9 5

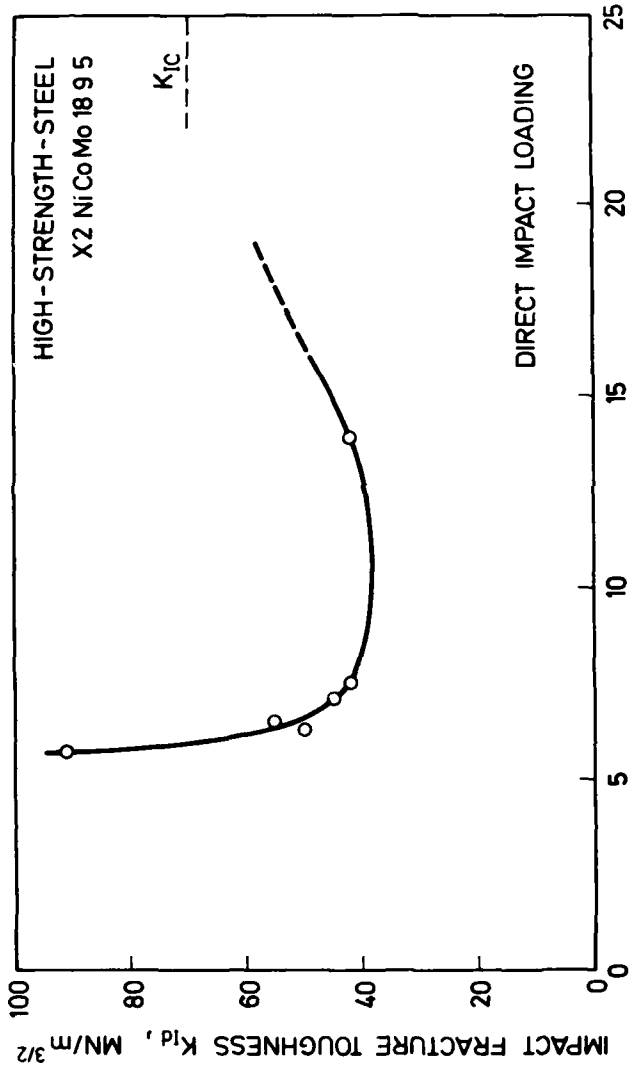

Fig. 49 Impact fracture toughness versus time-to-fracture

Results of one of the better shadow optical recordings are reported in Fig. 46. The complete loading phase and the instability of the crack, i.e. the start of the propagating crack, is shown. The picture interval time is 1 μs in the reproduced series of photographs. 22 of the total 24 frames are shown. At 11 μs after the beginning of the tensile loading phase the crack becomes unstable. Elastic waves emanate from the tip of the crack after the crack has become unstable. These waves are visible in the shadow photographs. Quantitative data obtained from the shadow optical photographs are shown in Fig. 47. The dynamic stress intensity factor, K_I^{dyn}, and the momentary position of the crack tip, a, are plotted as functions of time. Similar as for the Araldite B experiments the impact fracture toughness value, K_{Id}, the time-to-fracture, t_f, and the crack tip loading rate, $\dot{K}_I^{dyn}$, can be obtained from these plots. A photograph of the fractured surface of the specimen is shown in Fig. 48.

About 80 experiments total have been performed. The results of successful experiments are summarized in Table 3. Times-to-fracture in the range of 15 μs to about 6 μs have been obtained. It must be admitted, however, that due to the previously discussed phenomena the data points at low t_f values necessarily show larger scatter and thus are not as reliable as the data at larger t_f values. Fig. 49 shows a plot of the measured impact fracture toughnesses as a function of the time-to-fracture. It is interesting to recognize that the data show a very strong dependence on loading rate, respectively time-to-fracture. This observation is in absolute contradiction to the results found with Araldite B specimens. With steel specimens the impact fracture toughness K_{Id} obviously tends to increase when the time-to-fracture is decreased, at least in the range from 10 μs to 6 μs. Of course there are some uncertainties in the data due to the disturbances discussed above. Furthermore, the number of data points is very limited. In particular only one data point was measured at the very high toughness level so far (Shot No. 861). Nevertheless, this high value is supported by the trend of the data points at lower toughness levels (Shots No. 855, 854, 853, 857). It is believed therefore that the data are well out-side the range of experimental scatter and indeed reflect true material behavior.

5.3 Summary and Discussion

Projectile loading of precracked SEN-type specimens provides an appropriate experimental tool for achieving very high loading rates. An undistrubed mode I tensile loading of the cracks is obtained. Onset of rapid crack propagation is observed within loading times of a few microseconds only. For steel these times correspond to crack-tip loading rates $\dot{K}_I$ higher than 10^7 $MNm^{-3/2}s^{-1}$. The fracture toughness data measured with Araldite B and a high strength steel are summarized in Figs. 50 and 51. In addition to the high rate data results at lower loading rates and at quasi-static loading conditions are also shown. These data were measured by the author and his colleagues with drop-weight tests [49] utilizing the shadow optical method of caustics and with precracked Charpy tests applying the

authors' concepts of impact response curves [50].

The obtained results are quite different for the two materials investigated. Within the time range considered the impact fracture toughness data measured with Araldite B do not show a significant dependence on loading rate. The data are scattered around a value which is identical with the static fracture toughness K_{Ic} of the material. On the other hand, the impact fracutre toughness data for the steel X 2 NiCoMo 18 9 5 are strongly dependent on loading rate. For times-to-fracture in the range of 10 µs the measured fracture toughnesses are smaller than those at larger times-to-fracture. Furthermore, data measured at times-to-fracture below 10 µs show a sharply increasing trend. Impact fracture toughness values measured at 6 µs become even larger than the static fracture toughness value K_{Ic}. Although the data necessarily show a large scatter due to disturbances by Rayleighwaves and due to the limited time resolution of the high-speed camera (i.e. 1 µs) the trend in the shadow optical data is very pronounced and far beyond the expected uncertainties due to experimental scatter. At loading rates above a certain limit the impact fracture toughness of this steel obviously increases with inceasing loading rate.

Such an increase of the impact fracture toughness with decreasing time-to-fracture can be explained if the ususal static instability criterion is modified by assuming the existence of an incubation time, as is illustrated in Fig. 52: According to this assumption the crack tip would have to experience a supercritical stress intensity factor $K_I > K_{crit}$ for a certain minimum period of time before onset of rapid crack propagation can occur (see also [51]). This time interval is called the incubation time. It is very likely that this time is related to certain material processes and, therefore, would be different for different materials. If the stress intensity factor K_I^{dyn} increases slowly with time the delay in instability due to this incubation time is negligible. Consequently the critical stress intenstity factor for the onset of rapid crack propagation K_{Id} would be practically the same as the value K_{crit}. However, if the slope of the $K_I^{dyn}(t)$ curve is very steep then the stress intensity factor will increase significantly within the incubation time. Thus the critical stress intensity factor for the onset of rapid crack propagation, K_{Id}, would be considerably larger than the value K_{crit}. Consequently, impact fracture toughness values determined from measurements taken at the onset of rapid crack propagation would increase with decreasing time-to-fracture, i.e. with increasing loading rate. The data presented in Figs. 50 and 51 for the two materials investigated appear to indicate that the incubation time for Araldite B is considerably smaller than that for steel.

It should be emphasized that although the concept of the incubation time explains the experimental observations presented here, this does not necessarily imply that it is the only explanation. The existence of the incubation time is a hypothetical assumption. An explanation on the physical background of the incubation time is not presented. The

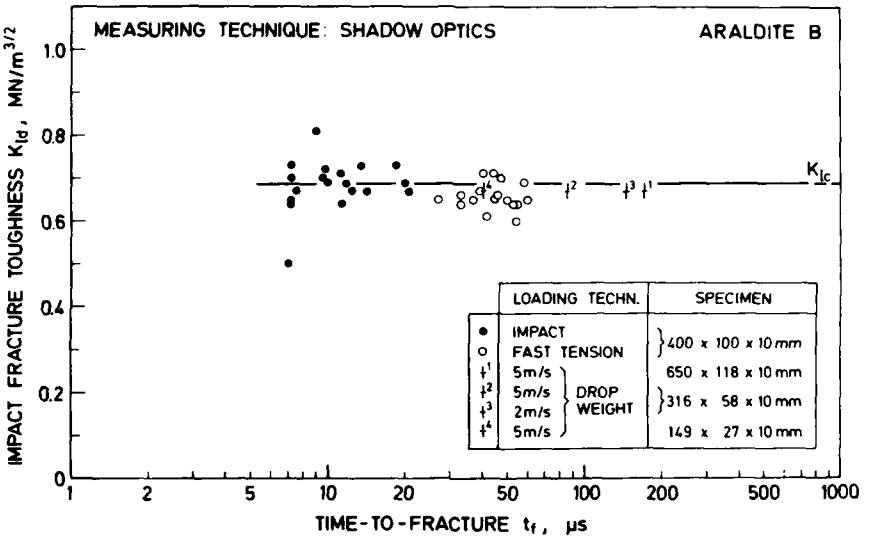

Fig. 50 Dependence of impact fracture toughness on time-to-fracture for Araldite B

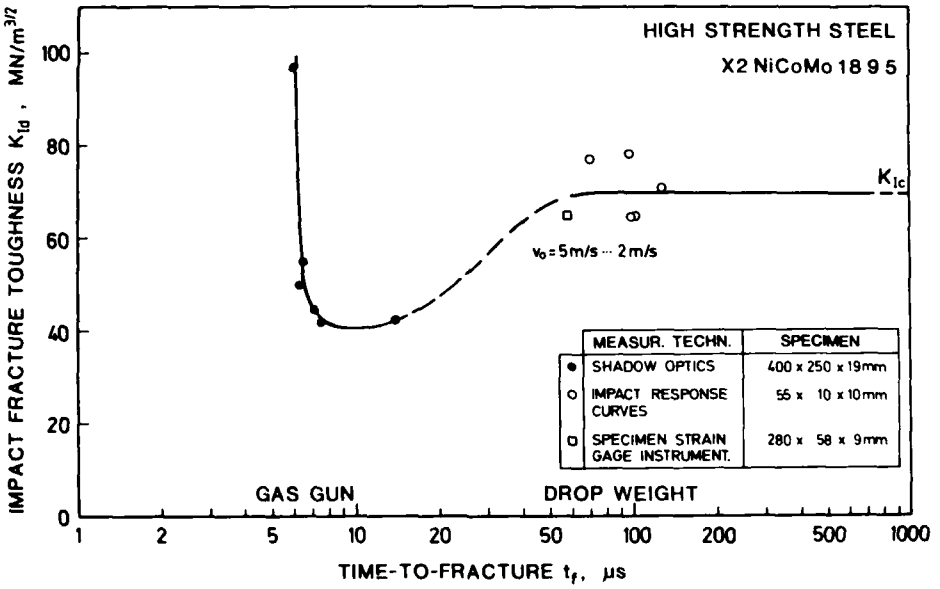

Fig. 51 Dependence of impact fracture toughness on time-to-fracture for the high strength steel X2 NiCoMo 18 9 5

validity of the concept must be tested through further experiments with a variety of materials and through theoretical modeling and analyses of the mateial and mechanicl processes that may occur near the crack tip at such high loading rates.

6 DYNAMIC INTERACTION OF MULTIPLE CRACKS

The fracture behavior of a structure which contains a configuration of multiple cracks is different from the one with only one crack: The stress fields of multiple cracks have a mutual influence on each other. Due to this interaction the stress intensity factors K_I^{dbl} of two parallel cracks under static loading condition are smaller than the stress intensity factor K_I^{sgl} for an equivalent single crack; in addition, a superimposed mode-II loading results. This is illustrated in Fig. 53. If the multiple crack configuration is hit by a tensile stress pulse the stress intensifications at the crack tips will become complicated functions of time. The experiments reported in this Chapter are aimed to study in detail the influences which control the interaction processes.

The base plate loading arrangement has been utilized to test specimens with double crack configurations. The cracks are oriented perpendicular to the impinging stress pulse. The test conditions were the same as reported in Chapter 4.2 "Base Plate Loading ". The crack length was varied from 15 mm to 50 mm, the distance of the two cracks was varied from 20 to 80 mm. The length of the two cracks in each experiment has been kept the same. The impact velocity has been varied from about 10 m/s to 30 m/s. Since it has not been the goal of these experiments to investigate the instability event, but the mutual interaction of the cracks as a function of time, blunted notches instead of sharp initial cracks have been utilized in these experiments. Thus, crack initiation was delayed and the interaction processes could be observed over longer time ranges. An overview on the test conditions of the successful experiments is given in Table 4.

A typical series of shadow optical photographs has already been shown in Fig. 27. The outer cracks represent the double crack configuration in one of the two specimens. These are the data which are of interest in this context. The center crack is the single crack in the other specimen (these data have been discussed already in Section 5.1 and are not considered here). The crack configuration is hit by a tensile stress pulse from the left side. The left hand crack is loaded the longest time and exhibits the largest stress intensity factor. The shadow pattern of the left hand crack is of mode-I type, at least for early times. The shadow pattern of the right hand crack is of mixed mode type from the very beginning on, since this crack is always influenced by the stress field of the left hand crack. In the frame No. 11, at 110 µs, the left hand crack becomes unstable and propagates through the specimen. The path shows a slight deviation from the original direction indicating a slight superimposed mode-II loading also for this crack at larger time For convenience the crack which is hit first by the stress pulse is denoted "crack A", the second crack which is hit afterwards is denoted "crack B".

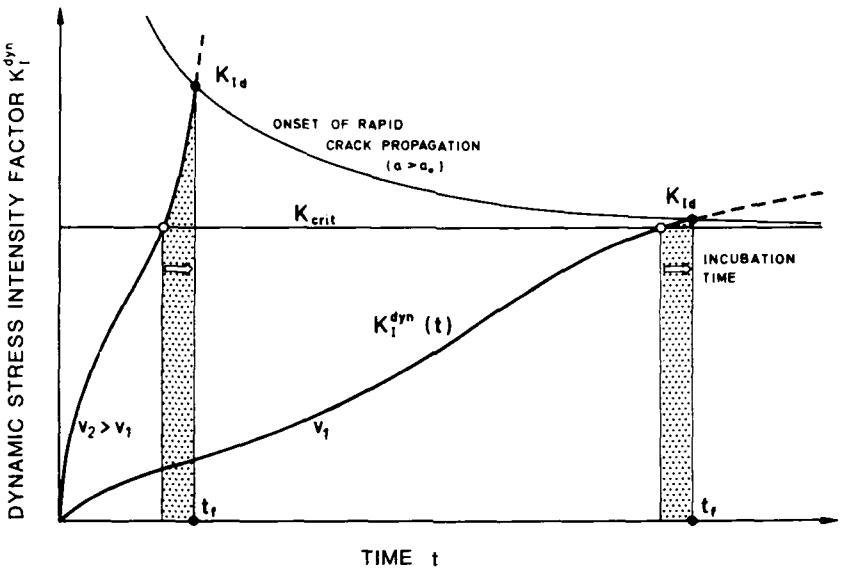

Fig. 52 Influence of incubation time on the impact fracture toughness

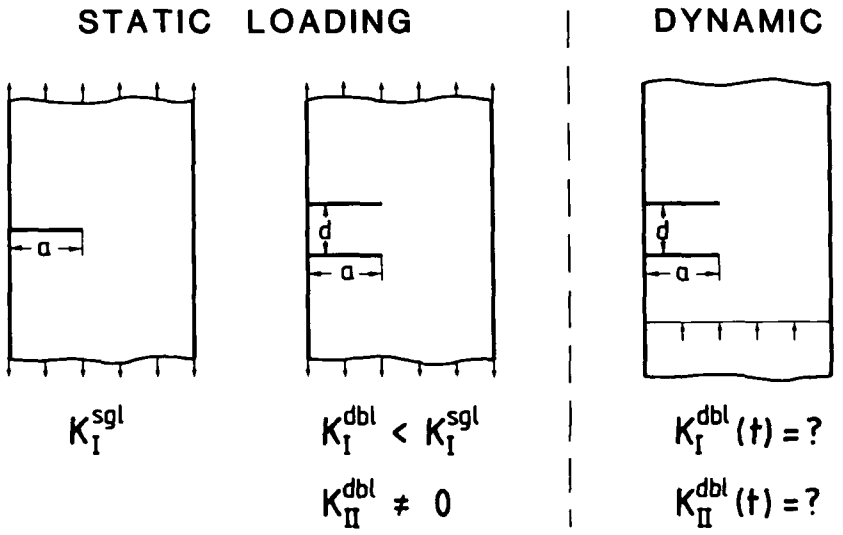

Fig. 53 Mutual interaction of multiple cracks, schematically

Spec. No.	Crack Length a_o, mm	Crack Distance d, mm	Crack Tip	Projectile			Time to Fracture t_f, μs	Impact Fracture Toughness K_{Id}, $MN/m^{3/2}$
				m, kg	l, mm	v_o, m/s		
670	50	60	b	1.02	75	10.7	-	-
(670	50	0	b	1.02	75	10.7	-	-)
674	50	60	b	1.02	75	10.1	-	-
(674	50	0	b	1.02	75	10.1	-	-)
677	50	60	s	2.01	139	9.6	-	0.640
(677	50	0	s	2.01	139	9.6	-	0.660)
687	50	60	s	1.02	74	9.9	-	-
(687	50	0	s	1.02	74	9.9	-	-)
688	50	60	s	1.02	74	10.1	51.5	0.640
(688	50	0	s	1.02	74	10.1	52.0	0.600)
689	50	60	s	1.02	74	9.3	41.5	0.610
(689	50	0	s	1.02	74	9.3	52.5	0.640)
690	50	60	s	1.02	74	8.9	44.5	0.650
(690	50	0	s	1.02	74	8.9	-	-)
691	50	60	s	1.02	74	31.9	-	-
(691	50	0	s	1.02	74	31.9	39.0	0.670)
701	50	60	s	1.02	78	18.9	27.0	0.650
(701	50	0	s	1.02	78	18.9	25.0	0.490)
702	50	60	s	1.02	78	26.9	31.5	0.600
(702	50	0	s	1.02	78	26.9	28.5	0.580)
703	50	60	s	1.02	78	26.9	29.0	0.650
(703	50	0	s	1.02	78	26.9	32.5	0.550)
705	50	60	s	1.98	142	9.7	45.0	0.650
(705	50	0	s	1.98	142	9.7	-	-)
706	50	60	s	1.98	142	9.6	47.0	0.700
(706	50	0	s	1.98	142	9.6	55.0	0.650)
707	50	60	s	0.51	50	9.7	45.5	0.660
(707	50	0	s	0.51	50	9.7	54.0	0.690)
709	50	80	b	1.02	78	9.0	-	-
709	50	20	b	1.02	78	9.0	-	-

710	50	40	b	1.02	78	10.3	-	-
710	25	20	b	1.02	78	10.3	-	-
711	50	20	b	1.02	78	10.3	-	-
711	25	20	b	1.02	78	10.3	-	-
713	15	20	b	1.02	78	9.5	-	-
713	25	20	b	1.02	78	9.5	-	-
715	15	20	b	1.02	78	10.8	-	-
715	15	20	b	1.02	78	10.8	-	-
717	15	20	b	1.02	78	9.2	-	-
(717	15	0	b	1.02	78	9.2	-	-)

s = sharp, b = blunted

Table 4 Test conditions and results of base plate loading experiments, double crack configurations, Araldite B

Fig. 54 shows results for cracks of 50 mm length with distances d = 20 mm, 40 mm, and 80 mm. In this figure only the mode-I stress intensity factors for both cracks are plotted as functions of time. The following behavior is deduced from these results: The cracks A exhibit the largest stress intensity factors and these stress intensity factors build up earlier than for cracks B, since cracks A are hit first. The time shift between the $K_I^{dyn}(t)$-curves for cracks A and cracks B increases with the distance d between the two cracks. The time shifts, however, are larger than one would expect due to a simple consideration of wave propagation times. Till about 60 µs the $K_I^{dyn}(t)$-curves for the cracks A are the same, regardless of the distance between the two cracks A and B. During the early time phase obviously the cracks A behave similar as a single crack and are not disturbed much by cracks B. For the narrow crack configuration (d = 20 mm) the interaction with cracks B then leads to a reduction of the crack-A-stress-intensity-factor for times larger than 60 µs. The crack-A stress-intensity-factors for wider crack configurations (d = 40 and 80 mm) still follow the same curve exhibiting a rather undisturbed single crack behavior.

The results for mode-II stress intensity factors of the experiments under consideration are shown in Fig. 55. For two crack configurations, d = 20 mm and 80 mm, the mode-II stress intensity factors are plotted as functions of time *). Data of other experiments have been omitted for clarity. The following trends can be recognized from the presented data: The stress intensity factors K_{II}^{dyn} of cracks B are larger than those for cracks A. This result is plausible since crack B is loaded by a stress pulse which is disturbed by crack A from the very beginning on. Crack A, however, for a long time behaves as a single crack, which is not disturbed by crack B. The stress intensity factors K_{II}^{dyn} of the crack A are larger for the narrow (d = 20 mm) configuration than for the wider (d = 80 mm) crack configuration. Again this result is plausible since the interaction for the narrow crack configuration starts earlier and is stronger than for the wider crack configuration. This result is also in accordance with the observed reduction of crack-A-stress-intensity-factors for the narrow crack configuration at $t > 60$ µs (see discussion before). Thus, the data show a behavior which is in accordance with expectations. The observed scatter in the K_{II}-data was larger than for pure mode-I data. This larger scatter is partly due to the evaluation procedure for determining the data from the asymmetry of caustics. The stress intensity factors are derived from the two longitudinal diameters D_{max} and D_{min} (see Fig. 7). Necessarily, however, the caustics are somewhat disturbed in the region where the caustic intersects the crack surfaces, i.e. where the asymmetry of the caustic is measured. The development of an improved evaluation procedure which takes unavoidable experimental disturbances of the caustic into account is planned.

Another series of experiments has been performed aimed to investigate the mutual interaction processes over a longer period of time. A further increase in crack tip bluntness, however, did not lead to larger obser-

---

*) The time scale relates to the one in Fig. 54

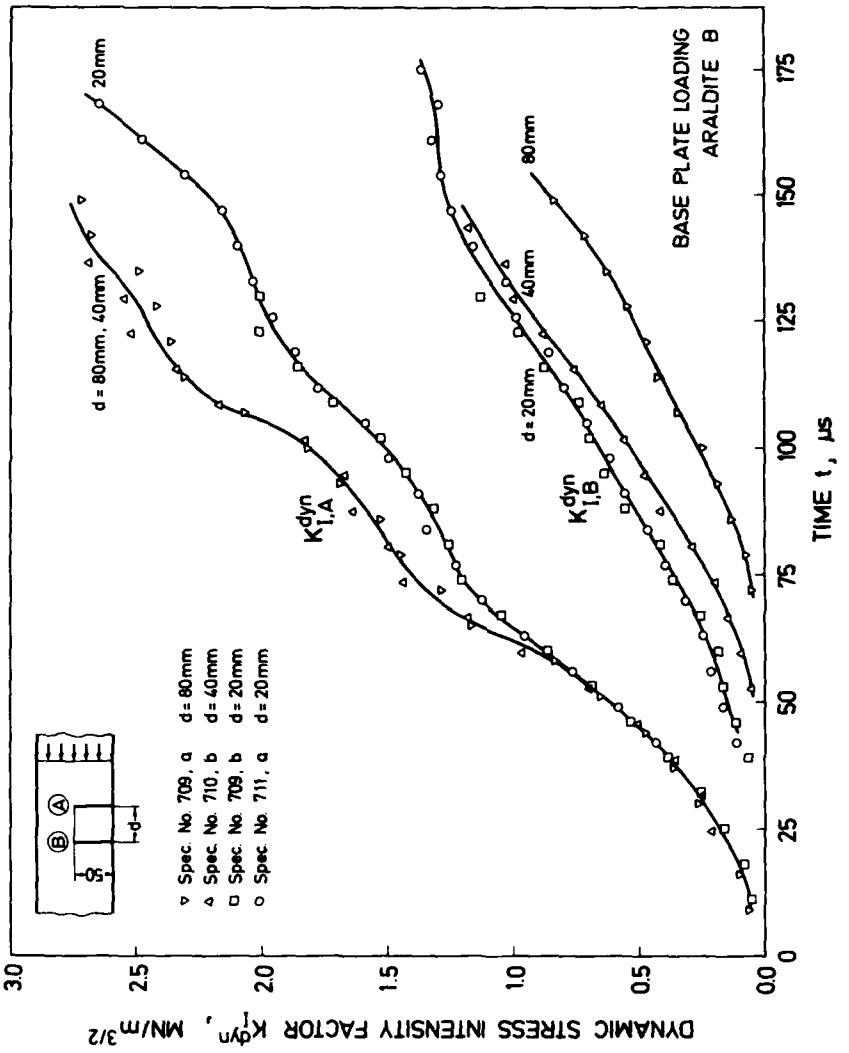

Fig. 54 Dynamic mode-I stress intensity factors for double crack configurations

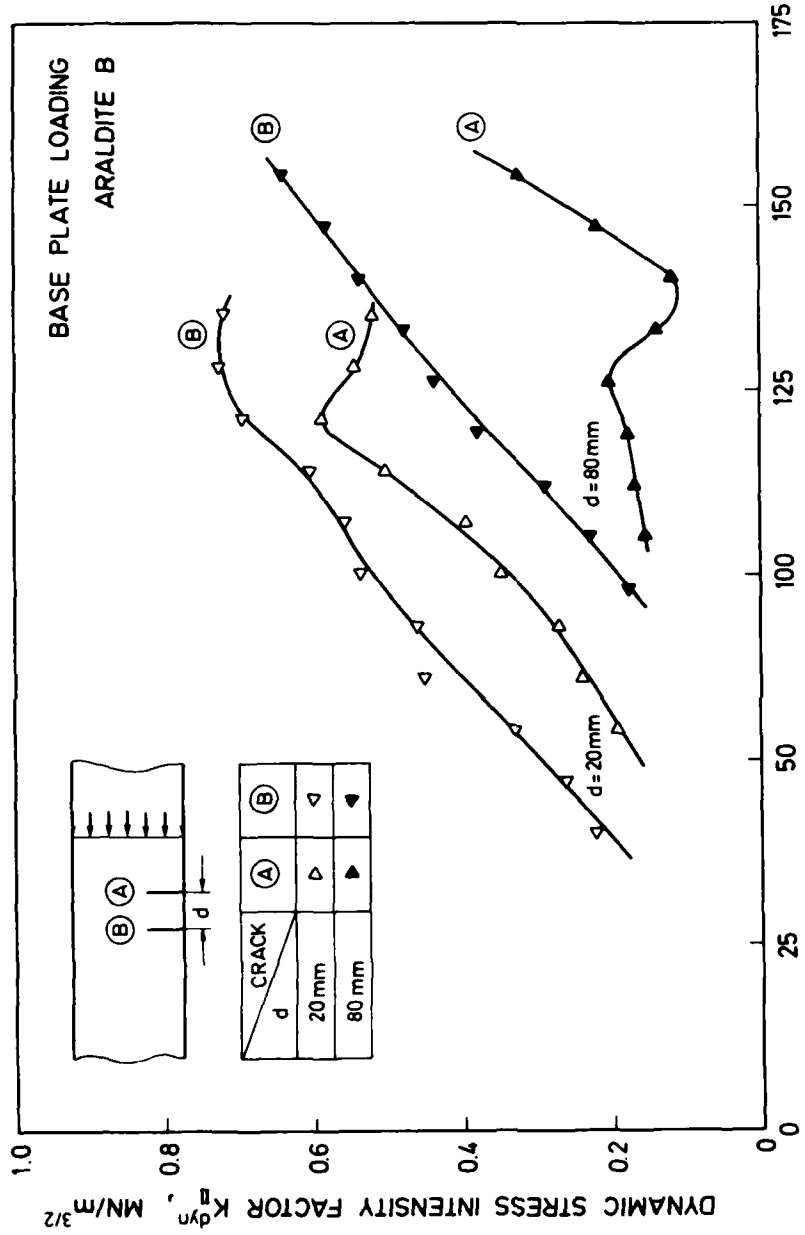

Fig. 55 Dynamic mode-II stress intensity factors for double crack configurations

vation times. For crack tip radii > 1 mm an initiation stress intensity factor of about 3 $MN/m^{3/2}$ was observed which could not be increased by a further increase in crack tip bluntness. Therefore, notches with reduced crack lengths have been utilized in order to reduce the stress intensity factor level.

A series of shadow optical photographs for a double crack configuration, d = 20 mm, a_o = 25 mm, is shown in Fig. 56. The tensile stress pulse impinges from the right side. For early times the crack-A-stress-intensity-factors are larger than the crack-B-stress-intensity-factors. This result is in accordance with the results discussed before. At later times, however, the situation changes. At 330 µs both caustics are of same size, i.e. the stress intensity factors are the same, and for larger times the situation is reversed and the crack-B-stress-intensity-factors are larger than the crack-A-stress-intensity-factors. Obviously an oscillation process takes place and the strain energy at the tip of one crack is transferred to the other.

Quantitative data for the crack configuration d = 20 mm, a_o = 15 mm are shown in Fig. 57. The stress intensity factors for crack A and crack B are shown as functions of time. In addition the behavior of an equivalent single crack is shown. At early times the crack A shows a similar behavior as the single crack, and crack B is only less loaded. Some time later (at 95 µs), however, the situation has changed and crack B exhibits the larger stress intensity factor. Data at larger times show that this process varies periodically. At very large times the average stress intensity factor of the two parallel cracks is smaller than the one of the single crack, similar as in the static case.

These data show that predicitons on dynamic fracture processes on the basis of simplified static analyses can only be considered as reasonable approximations for times which are considerably large. In the transient regime the situation is much more complex and static predictions can be very misleading.

7 SUMMARY

During the starting phase of the research project the necessary experimental set-up has been built up for investigating the fracture behavior under impact conditions of high rates of loading. The existing IWM gas gun has been modified for this purpose. A Cranz-Schardin camera operated in a shadow optical recording arrangement has been aligned to the gas gun. High speed recordings of the shadow optical caustics determine the crack tip loading condition $K_I^{dyn}(t)$. Furthermore, holding fixtures have been designed and built to load the specimens under both direct and base plate loading conditions. The complete set-up has been successfully tested under the different impact conditions. In particular the load pulse history in the specimen has been studied. In serveral series of pre-experiments the parameters for the main investigations have been specified. Considerably higher loading rates were achieved under the conditions of direct impact loading than under

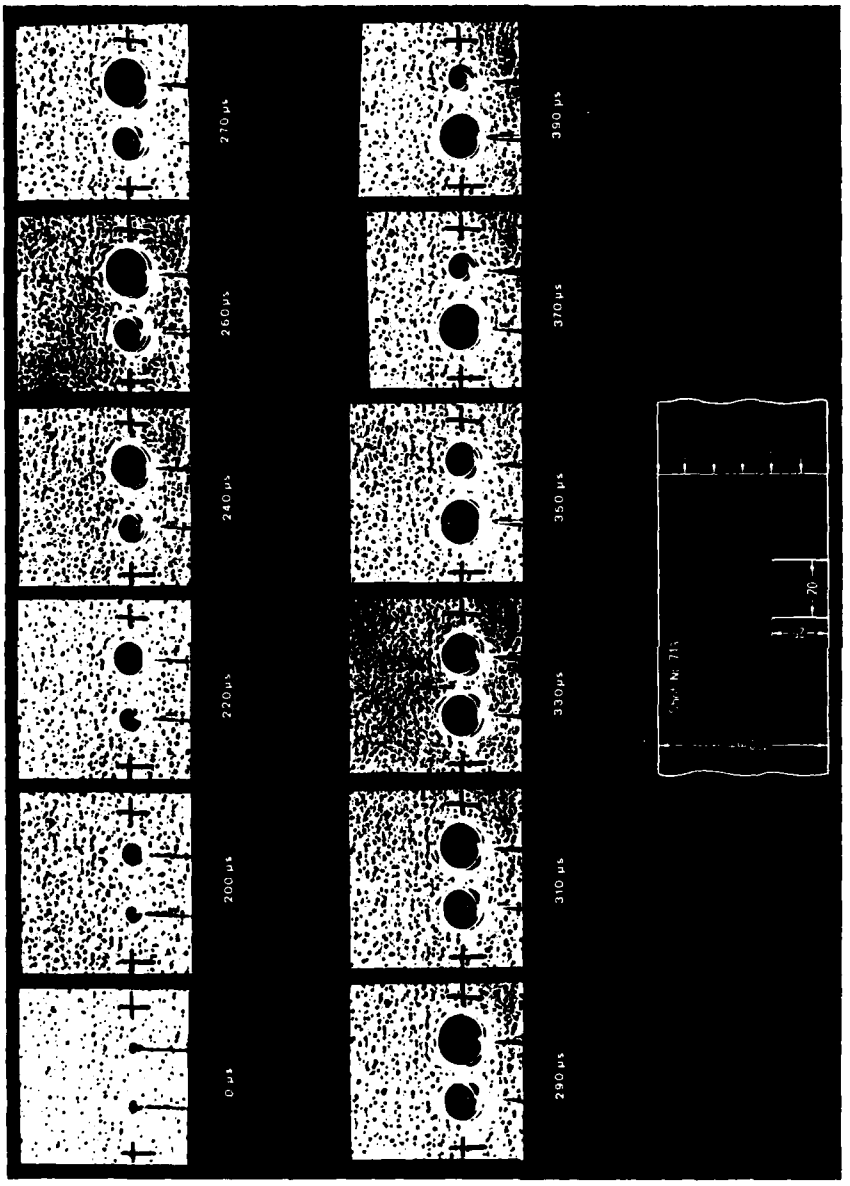

Fig. 56 Dynamic interaction of a double crack configuration

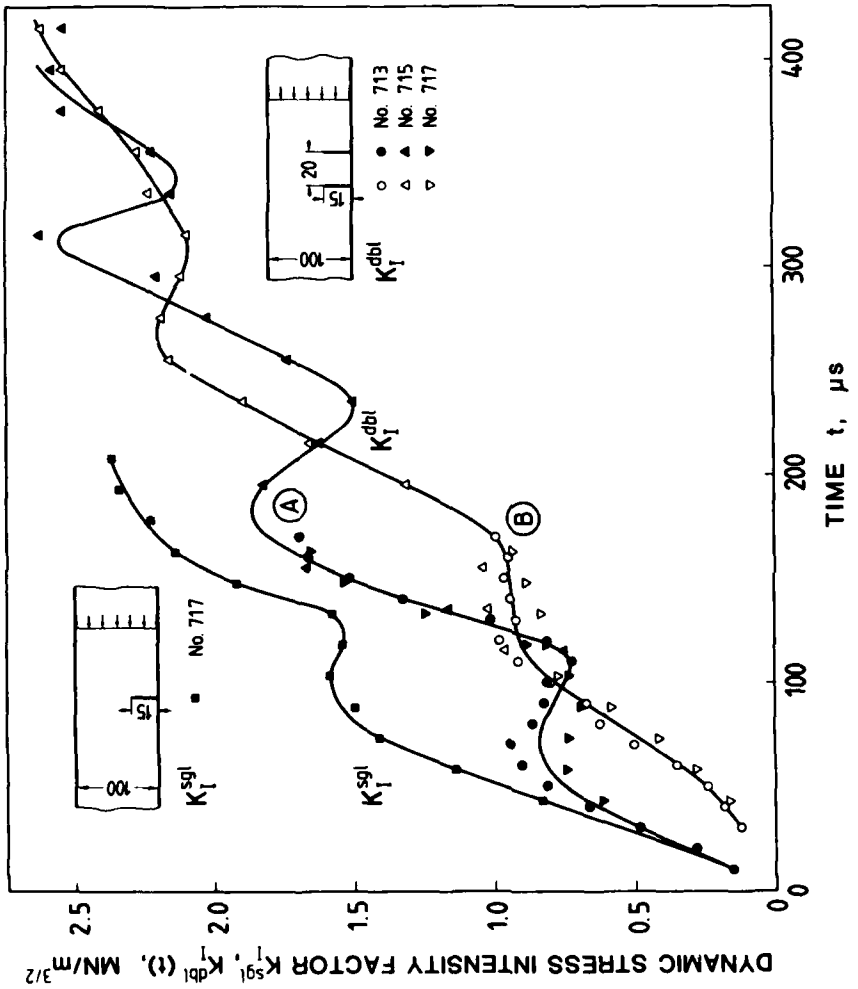

Fig. 57 Dynamic stress intensity factors for a double crack configuration in comparison to an equivalent single crack

base plate loading. The highest crack tip loading rates achieved were in the range of $\dot{K} = 2 \times 10^7$ $MNm^{-3/2}s^{-1}$.

In the middle and the end phase of the research project the main experiments have been performed with a systematic variation of test parameters. Most of the research work was concentrated on measuring the impact fracture toughness K_{Id} on loading rate. First, specimens made from the model material Araldite B with single edge cracks have been tested under both base plate and direct impact loading conditions. Times-to-fracture down to 6 µs have been achieved. Within this range of loading rates the observed impact fracture toughness data K_{Id} did not show a dependence from loading rate.

Subsequent experiments with specimens made from a high-strength-steel, however, resulted in a strong dependence of K_{Id} from loading rate. As with the Araldite B specimens times-to-fracture down to about 6 µs have been reached. With regard to the static fracture toughness K_{Ic} these data first show a reduced toughness in the time-to-fracture range of 50 µs to 10 µs, but a very rapid increase in toughness if the time-to-fracture is decreased further down to 6 µs. The dynamic toughnesses then become even larger than the static ones. The observed experimental findings are explained on the basis of a novel instability criterion which is based on the existence of an incubation for a crack to start propagating. This incubation time is believed to be a material-dependent property.

Furthermore, the dynamic interaction of multiple crack configurations under asymmetric impact loading conditions was studied. Due to cost reasons these experiments have only been performed with specimens made from the model material Araldite B. The experiments showed a rather complex time dependent stress intensity factor history. Due to transient effects the early time behavior is very different foom the static behavior. In general, much larger asymmetric mode II (in-plane shear) contributions were observed in the local crack tip loading fields than under equivalent static conditions. In particular, with a double crack configuration a periodic exchange of the crack tip strain energy from one crack to the other takes place. Only for long times after impact the overall situation became similar to the one under static loading conditions.

As supplementary work the stress intensity factor histories for cracks of different lengths under impact loading has been measured. The data do not show an influence of crack length on the crack tip loading when early times after impact are considered. Only at later times the larger crack exhibits a larger stress intensity factor, as one expects from static considerations. Obviously, in this regime of small ratios of "time" to "crack length" the parameter "time" is the only parameter which controls the fracture behavior and not the length of the crack, as is the case in static considerations.

It is planned to continue this research work at the Fraunhofer-Insitut für Werkstoffmechanik. Some complimentary investigations are envisaged

to extend the data bases for $K_{Id}(\dot{\sigma}_0)$ by performing additional experiments with high-strength-steel specimens, by investigating the material Homolite 100 in order to solve the discrepancy with the Caltech-results, by trying to decrease the times-to-fracture to even lower values, and to improve the accuracy of the shadow optical recording technique at high rate impact conditions. Most of the research work of the follow-on investigations, however, will be aimed to extend the research work performed within this project to shear loading conditions. The shear impact fracture toughness K_{IId} will be measured at exptremely high loading rates and compared to that behavior found so far under tensile (mode I) loading. Due to the practical relevance of shear loading conditions further valuable knowledge on the load carrying capacity of structures subjected to impact conditions is anticipated.

8 APPENDIX

Independence of the Stress Intensity Factor From Crack Length

Stress intensity factor histories for cracks of different lengths which were impacted under similar conditions have been measured and compared with each other. In order to allow for an easy survey and to avoid a consideration of too many parameters only the results of single edge cracks are discussed here. Fig. 58 shows data for cracks 50 mm and 15 mm long, loaded in the base plate arrangement (see Chapter 3) at about 10 m/s. The stress intensity factors K_I^{dyn} are plotted as functions of time. It is recognized that the stress intensity factors for the two cracks of different length are indentical till about 80 µs Only for longer times the larger crack shows a larger stress intensity factor as one would expect from static considerations. In the early time regime, however, the stress intensity factors are obviously independent of crack length. This experimental result is in accordance with earlier theoretical predictions. Sih et at. [6,10], Achenbach [7,8] and Freund [9] calculated the stress intensity factor histories for cracks under step function loads (see Fig. 2) and showed that the stress intenstiy factors should increase according to a square root of time relationship, independent of crack lengths for $t \leq a_0/c_1$ (see also Chapter 1). In their minimim time fracture criterion, Kalthoff and Shockey [15-18] state that cracks which are loaded by stress pulses of finite durations T_0 should show instability stresses which are independent of crack length if $T_0 < 2a_0/c_1$. Only for $T_0 > 30\ a_0/c_1$ static preditions would be applicable. The data reported in Fig. 58 indicate an independent stress intensity factor behavior for times $t < 80$ µs, i.e. $13\ a_0/c_1$. It is interesting to recognize that this value is in the range of the above mentioned theoretical predictions although the loading conditions in the reported experiments were different from the ones considered in the theoretical analyses and thus do not allow for a direct comparison of data.

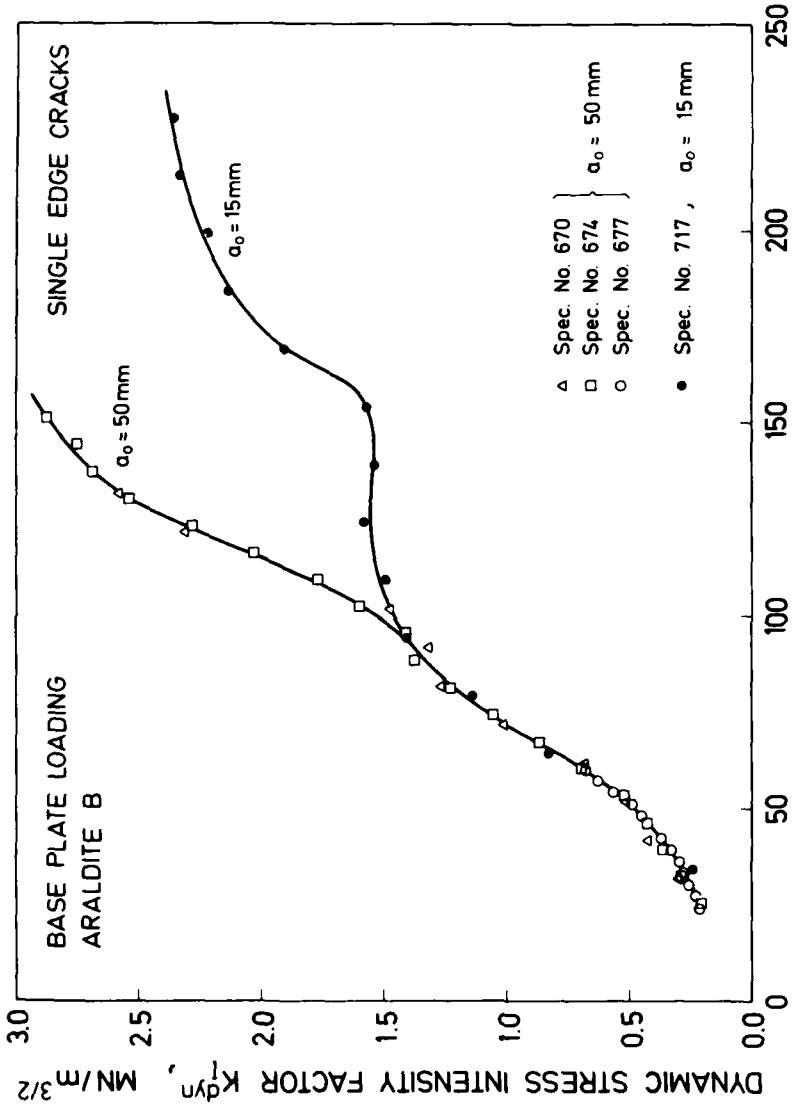

Fig. 58 Dynamic stress intensity factors for cracks of different lenghts

9 REFERENCES

[1] ASME Boiler and Pressure Vessel Code, The American Society of Mechanical Engineers, New York, N.Y., U.S.A.

[2] ASTM Book of Standards, Part 10, American Society for Testing and Materials, Philadelphia, Pa., U.S.A.

[3] ASTM E 24.03.03, "Prosposed Standard Method of Tests for Instrumented Impact Testing of Precracked Charpy Specimens of Metallic Materials", Draft 2c, American Society for Testing and Materials, Philadelphia, Pa., U.S.A., 1980

[4] Kalthoff, J.F., Böhme, W., Winkler, S., and Klemm, W.: "Measurements of Dynamic Stress Intensity Factors in Impacted Bend Specimens", CSNI Specialist Meeting on Instrumented Precracked Charpy Testing, EPRI, Palo Alto, Calif., U.S.A., Dec. 1980

[5] Kalthoff, J.F., "Time Effects and their Influences on Test Procedures for Measuring Dynamic Material Strength Values", Plenary Lecture, Int. Conf. on Application of Fracture Mechanics to Materials and Structures, Eds. G.C. Sih, S. Sommer W. Dahl, Fraunhofer-Institut für Werkstoffmechanik, Freiburg, June 20 - 24, 1983, Martinus Nijhoff Publishers, 1984, 107 - 136

[6] Sih, G.C.: "Some Elastodynamic Problems of Cracks", Int. J. Fract. Mech. 4, 1968, 51-68

[7] Achenbach, J.D.: "Brittle and Ductile Extension of a Finite Crack by a Horizontally Polarized Shear Wave", Int. J. Eng. Sci. 8, 1970, 947-966

[8] Achenbach, J.D.: "Dynamic Effects in Brittle Fracture", Mechanics Today, Vol. 1, 1972, ed. by Nemat-Nasser, Pergamon

[9] Freund, L.B.: "Crack Propagation in an Elastic Solid Subjected to General Loading - III. Stress Wave Loading", J. Mech. Phys. Solids 21, 1973, 47-61

[10] Sih, G.C.: "Handbook of Stress Intensity Factors", Institute of Fracture and Solid Mechanics, 1973, Lehigh University, Bethlehem, Pa., U.S.A.

[11] Steverding, B., Lehnigk, S.H.: "Response of Cracks to Impact", J. Appl. Phys. 41, 1970, 2096-2099

[12] Steverding, B., Lehnigk, S.H.: "Collision of Stress Pulses with Obstacles and Dynamics of Fracture", J. Appl. Phys. 42, 1971, 3231-3238

[13] Lehnigk, S.H.: " A Macroscopic Dynamic Theory of Stability and Instability of Cracks Under Impulsive Loading", Dynamic Crack

Propagation, ed. by G.C. Sih, Noordhoof-Groningen, 1973, 333

[14] Steverding, B.: "Fracture and Dislocation Dynamics", Dynamic Crack Propagation, ed. by G.C. Sih, Noordhoff-Groningen, 1973, 349

[15] Kalthoff, J.F.; Shockey, D.A.: "On the Dynamic Instability of Cracks Loaded by Tensile Stress Pulses of Short Duration", Poulter Laboratory, Technical Report 001-75, 1974, Stanford Research Institute, Menlo Park, California

[16] Shockey, D.A., Kalthoff, J.F.: "Stability of Cracks Under High Rate Loads", Joint JSME-ASME Applied Mechanics Western Conf., 24 - 27 March 1975, Waikiki Beach, Honolulu, Hawai

[17] Kalthoff, J.F., Shockey, D.A.: "Instability of Cracks Under Impulse Loads", Journ. Appl. Phys. 48, 1977, 986-993

[18] Shockey, D.A., Kalthoff, J.F., and Ehrlich, D.C.: "Evaluation of Dynamic Crack Instability Criteria", Int. J. Fracture, Vol. 22, 1983, 217-229

[19] ASTM SPT 466 "Impact Testing of Metals", American Society for Testing and Materials, Philadelphia, Pa., 1974, U.S.A.

[20] ASTM STP 563 "Instrumented Impact Testing", American Society for Testing and Materials, Philadelphia, Pa., 1974, U.S.A.

[21] Shoemaker, A.K., Rolfe, S.T.: "The Static and Dynamic Low-Temperature Crakk Toughness Performance of Seven Structural Steels", J. Eng. Fract. Mech., Vol. 2, 1971, 319-339

[22] Loss, J.F., Hawthorne, J.R., Griffis, C.A.: "Fracture Toughness of Light Water Reactor Pressure Vessel Materials", Naval Research Laboratory Memorandum Report 3036, 1975

[23] Proc. Int. Conf. Dynamic Fracture Toughness, London, July 5-7, 1976

[24] Costin, L.S., Duffy, J., and Freund, L.B.: "Fracture Initiation in Metals Under Stress Wave Loading Conditions", ASTM STP 627, Fast Fract. and Crack Arrest, American Society for Testing and Materials, Philadelphia, Pa., U.S.A., 1977, 301

[25] Costin, L.S., Server W.L., Duffy, J.: "Dynamic Fracture Initiation: A Comparison of Two Experimental Methods", to be published in ASME, J. of Eng. Materials and Technology

[26] J.R. Klepaczko, Applications of the Split-Hopkinson Pressure Bar to Fracture Dynamics", in Proc. 2nd Conf. Mech. Prop. High Rates of Strain (J. Harding, ed.), pp. 201-204. Oxford. The Institute of Physics, Conf. Ser. No. 45, Bristol, London (1979) and
J.R. Klepaczko, Loading Rate Spectra for Fracture Initiation in

Metals. Theoretical and Applied Fracture Mechanics, 1, 181-191 (1984).

[27] Shockey, D.A., Curran, D.R.: "A Method for Measuring K_{Ic} at Very High Strain Rates", ASTM STP 536, American Society for Testing and Materials, Philadelphia, Pa., U.S.A., 1973, 297

[28] Homma, H., Shockey, D.A., and Muragama, Y.: "Response of craccs in Structural Materials to Short Pulse Loads", submitted to J. Mech. Phys. Solids

[29] Shockey, D.A., Kalthoff, J.F., Homma, H., and Ehrlich, D.C.: "Response of Cracks to Short Pulse Loading", Workshop on Dynamic Fracture, Ed. W.G. Knauss, California Institute of Technology, Pasadena, Ca., U.S.A., February 17-18, 1983

[30] Kalthoff, J.F., Shockey, D.A., and Homma, H.: "Short Pulse Fracture Mechanics", Proc. 3rd Conf. Mech. Prop. High Rates of strain, (J. Harding, ed.) Oxford, 1984, Inst. Phys. Conf. Ser., Bristol, No. 70, 205-211

[31] Ravi-Chandar, K., and Knauss, W.G.: "Dynamic Crack-Tip Stresses under Stress Wave Loading - A Comparison of Theory and experiment" to appear in Int. Journ. of Fracture

[32] Eftis, J., Krafft, J.M.: " A Comparison of the Initiation with the Rapid Propagation of a Crack in a Mild Steel Plate", J. Basic Eng., 1965, 257

[33] Manogg, P.: "Anwendung der Schattenoptik zur Untersuchung des Zerreißvorgangs von Platten", Dissertation, Universität Freiburg, Germany, 1964

[34] Manogg, P.: "Schattenoptische Messung der spezifischen Bruchenergie während des Bruchvorgangs bei Plexiglas", Proceedings, International Conference on the Physics of Non-Crystalline Solids, Delft, The Netherlands, 1964, pp. 481-490

[35] Theocaris, P.S.: "Local Yielding Around a Crack Tip in Plexiglas", J. Appl. Mech., Vol. 37, 1970, pp. 409-415

[36] Rosakis, A.J., Freund, L.B.: "Optical Measurement of the Plastic Strain Concentration at a Tip in a Ductile Steel Plate", Journ. Eng. Mat. Tech. 104, 1982, 115-125

[37] Beinert, J. and Kalthoff, J.F.: "Experimental Determination of Dynamic Stress Intensity Factors by Shadow Patterns" in Mechanics of Fracture, Vol. 7, Ed. G.C. Sih, Martinus Nijhoff Publishers, The Hague, Boston, London, 1981, pp. 281-330

[38] Kalthoff, J.F.: "Stress Intensity Factor Determination by Caustics", Int. Conf. Experimental Mechanics, Society for Experimental Stress Analysis and Japan Society of Mechanical Engineers, Honolulu, Maui, Hawaii, U.S.A., May 23-28, 1982

[39] Kalthoff, J.F.: "The Shadow Optical Method of Caustics", Chapter 9 in: Handbook on Experimental Mechanics (A. S. Kobayashi, ed.), Pentice Hall, Englewood Cliffs, N.J. (to appear in 1986)

[40] Kalthoff, J.F., Beinert, J., and Winkler, S.: "Measurements of Dynamic Stress Intensity Factors for Fast Running and Arresting Cracks in Double-Cantilever-Beam-Specimens", ASTM STP 627 - Fast Fracture and Crack Arrest, American Society for Testing and Materials, Philadelphia, U.S.A., 1977, pp. 161-176

[41] Kalthoff, J.F., Beinert, J., Winkler, S., and Klemm, W.: "Experimental Analysis of Dynamic Effects in Different Crack Arrest Test Specimens", ASTM STP 711 - Crack Arrest Methodology and Applications, American Society for Testing and Materials, Philadelphia, U.S.A., 1980, pp. 109-127

[42] Kalthoff, J.F., Beinert, J., Winkler, S.: "Analysis of Fast Running and Arresting Cracks by the Shadow Optical Method of Caustics", Symposium on Optical Methods of Mechanics of Solids, International Union of Theoretical and Applied Mechanics (IUTAM), Poitiers, Fancs, Sept. 1979

[43] Kalthoff, J.F., Böhme, W., and Winkler, S.: "Analysis of Impact Fracture Phenomena by Means of the Shadow Optical Method of Caustics", VIIth Int. Conf. Experimental Stress Analysis, Society for Eyperimental Stress Analysis, Haifa, Israel, Aug. 23-27, 1982

[44] Kalthoff, J.F., Winkler, S., Böhme, W. and Klemm, W.: "Determination of the Dynamic Fracture Toughness K_{Id} in Impact Tests by Means of Repsonse Curves", 5th Int. Conf. Fracture, Cannes, March 29 - April 3, 1981, Advances in Fracture Research, Ed. D. Francois et al., Pergamon Press, Oxford, New York, 1980

[45] Theocaris, P.S.: "Complex Stress-Intensity Factors at Bifurcated Cracks", J. Mech. Phys. Solids 20, 1972, 265-279

[46] Seidelmann, U.: "Anwendung des schattenoptischen Kaustikenverfahrens zur Bestimmung bruchmechanischer Kennwerte bei überlagerter Normal- und Scherbeanspruchung", IWM-Report 2/76, Fraunhofer-Institut für Werkstoffmechanik, Freiburg, 1976

[47] Beinert, J., Kalthoff, J.F., Seidelmann, Ul, and Soltész, U.: "Das schattenoptische Kaustikenverfahren und seine Anwendung in der Bruchmechanik", VDI-Berichte Nr. 207, pp. 15-25, VDI-Verlag, Düsseldorf, 1977

[48] Ravi-Chandar, K., and Knauss, W.G.: "An Experimental Investigation into Dynamic Fracture: I. Crack initiation and arrest". Int. J. Fracture 25, 247-262 (1984)

[49] Böhme, W., and Kalthoff, J.F.: "Der Einfluß der Probengröße auf dynamische Effekte bei der K_{Id}-Bestimmung im Kerbschlagbiege-

test, Report W3/83 on the Project Ka 443-3-6-7 prepared for Deutsche Forschungsgemeinschaft, Fraunhofer-Institut für Werkstoffmechanik, Freiburg (1983)

[50] Kalthoff, J.F.: "The Concept of Impact Response Curves", in: Dynamic Fracture Testing, Metals Handbook, Vol. 8, Mechanical Testing. American Society for Metals, Metals Park, Ohio (to appear), 1985

[51] Kalthoff, J.F.: "On Some Current Problems in Experimental Fracture Dynamics", Workshop on Dynamic Fracture, sponsored by NSF and ARO, W.G. Knauss, Ed., Calif. Inst. of Technology, Pasadena, Ca., Feb. 17-18, 1983

END

12-86

DTIC